UNIVERSIDADE DE LISBOA
FACULDADE DE CIÊNCIAS
DEPARTAMENTO DE QUÍMICA E BIOQUÍMICA


# Biochemistry of Tau aggregation and interactions in Alzheimer's disease

Guilherme Gil Da Silva Veríssimo Moreira

**Mestrado em Bioquímica**
Especialização em Bioquímica Médica

Dissertação orientada por:
Professor Doutor Cláudio M. Gomes

2018

# Acknowledgments

First, I would like to thank Professor Cláudio Gomes for his reception in his team at his laboratory, for all his patience, support, perfectionism and motivation, not forgetting the opportunity he has given me, for which I feel very grateful.

A special thank you to all my friends and colleagues at the Protein folding and Misfolding Laboratory, even those who left the Lab but who always remained in our conversations and thoughts.

To Joana Cristóvão for her guidance, availability, sharing of scientific tips and most importantly for her patience and insistence. Also, to Mariana Romão, Rodrigo David, Joana Ferreira and Maria Joana for the good times that we shared, the jokes, the dinners and the spirit of brotherhood.

I would like to thank Prof. Mário Rodrigues and Dr. Ana Carapeto from the BioISI Magnetic Nanosystems Group and FCUL Department of Physics for the AFM bioimaging and analysis.

I would like to thank Prof. Isabelle Landrieu, University of Lille, for sharing of expression plasmids and Tau purification protocols.

I would like to express my gratitude to my mother, my father, my brother and my friends for their support and companionship during this work, for their concerns and attention.

Last but not the least, I would like to express my deep gratitude to Rita for her patience, help, advices and unconditional support.

Thank you all.

# Abstract

Alzheimer's disease (AD) is characterized by neuroinflammation, amyloidogenesis and disturbance of metal homeostasis. In this neurodegenerative disorder, the accumulation of highly phosphorylated Tau protein in neurofibrillar tangles constitutes one causative agent of the disease. Regardless of intense research, the mechanisms underlying pathological aggregation of Tau remain unclear and no disease-modifying therapies are available. Interestingly, important neuronal components such as pro-inflammatory cytokines and transition metal ions levels are consistently deregulated with aging, which is the most prominent risk factor for AD. In particular, the S100B pro-inflammatory cytokine is upregulated in AD and is known to promote β-amyloid (Aβ) precursor protein overexpression, modulate Aβ aggregation and promote Tau hyperphosphorylation. It was also discovered intercellular co-localization of S100B and Tau neurofibrillary plaques in AD patients brain tissue; however no clear mechanistic relationship between S100B and Tau has been established.

The goal of this work was to investigate the interaction between Tau and S100B and to determine if this interaction influences Tau aggregation. Since metal ions are deregulated in AD and both proteins have metal binding properties, we have investigated how calcium and zinc influence protein structure, interactions and Tau aggregation. The work employs several advanced biochemical and biophysical methodologies, including recombinant protein expression and purification using protein chromatography, circular dichroism (CD), attenuated total reflectance Fourier transform infrared (ATR-FTIR), thioflavin-T (ThT) fluorescence spectroscopy and atomic force microscopy (AFM) imaging.

The results obtained suggest that recombinant full-length human Tau (hTau441) and S100B interact and form a stable complex, as assessed by a size exclusion chromatography (SEC) assay. We demonstrate that this interaction involved protein secondary structure changes leading to loss or relaxation of α-helical structure of S100B, and that the interaction is strongly favored by $Ca^{2+}$ binding to S100B, as evaluated by CD and ATR-FTIR. In the presence of $Zn^{2+}$-bound S100B, a greater loss of α-helical structure is observed, concomitantly to an increase of β-sheets, which could be explained by the onset of hTau441 amyloidogenic aggregation. Furthermore, we determined that hTau441 heparin-induced aggregation, followed by ThT fluorescence, can be modulated by NaCl, $Ca^{2+}$ and $Zn^{2+}$ and also by the S100B protein. We set the concentration of NaCl at 50mM since it is the best pro-aggregation concentration. Interestingly, both $Ca^{2+}$ and $Zn^{2+}$ enhanced the aggregation propensity of hTau441. $Ca^{2+}$ reduces up to 4-fold the lag phase compared to the apo hTau441 aggregation and $Zn^{2+}$ that markedly accelerates the lag phase, greatly reducing the time of lag phase. In the presence of apo S100B, hTau441 aggregation was delayed (from ~5h to ~20h), albeit the aggregation velocity was slightly increased. In the presence of Ca-S100B, hTau441 aggregation was completely inhibited at protein equimolar concentrations and above. Even at substoichiometric levels, Ca-S100B was able to substantially delay the time of lag phase up to 8 times. However, Zn-S100B does not have an effect on hTau441 aggregation kinetics. AFM topographic imaging of aggregates at end-time points of hTau441 aggregation showed amyloid fibril formation in all conditions, except in the condition with S100B and $Ca^{2+}$, in which non-amyloid aggregates were mostly observed.

Altogether, the results from this work contributed to unravel the mechanism of hTau441 aggregation in the presence of $Zn^{2+}$ and $Ca^{2+}$, as well as to elucidate the contribution of S100B in the aggregation of hTau441 and fibril formation. We expect that these findings will open new avenues for further investigations of the roles of protein-protein interactions, neuroinflammation and neurometals in AD physiopathology.

**Keywords**: Alzheimer's disease, Tau, protein aggregation, metal ions

# Resumo

A doença de Alzheimer é a doença neurodegenerativa mais comum no mundo e tem características patológicas específicas tais como avanço progressivo e incessante, afetando áreas cerebrais como o hipocampo e o córtex cerebral. Esta doença degenerativa afeta as células neuronais do cérebro resultando na perda de memória, raciocínio, alterações na linguagem e mudança de comportamento nos doentes. A doença de Alzheimer é também caracterizada por neuroinflamação, amiloidogénese e distúrbios da homeostase de iões metálicos, entre outros processos celulares afetados nesta doença neurodegenerativa, a agregação do péptido β-amilóide (Aβ) em placas amilóide e a acumulação da proteína Tau anormalmente fosforilada em emaranhados neurofibrilares constituem agentes característicos causativos da doença. Apesar de pesquisa intensa, o mecanismo subjacente à agregação patológica da proteína Tau continua pouco claro e não existem terapias capazes de alterar ou mitigar a progressão da doença. O envelhecimento é o fator de risco mais proeminente para a doença de Alzheimer. Curiosamente, componentes neuronais importantes tais como os níveis de citocinas pro-inflamatórias e iões metálicos de transição como zinco, cobre e ferro encontram-se desregulados com a progressão da idade. Uma das biomoléculas alteradas nesta doença é a citocina pro-inflamatória S100B que tem os níveis proteicos elevados e é conhecida por promover a expressão aberrante da proteína precursora da β-amilóide, modular a agregação do Aβ e promover a híper-fosforilação da proteína Tau, o que exacerba as suas características amiloidogénicas. Contudo, não está reportado nenhum mecanismo claro que interliga as proteínas S100B e Tau.

Este trabalho teve como objetivo investigar a interação entre a Tau e a S100B e determinar se daí decorre algum efeito regulatório da S100B sobre o processo de agregação da proteína Tau. Dado que ambas proteínas ligam cálcio e zinco, investigou-se também o envolvimento destes iões metálicos no processo de fibrilação da proteína Tau. Para o efeito procederam-se a estudos detalhados de bioquímica estrutural de proteínas e ensaios cinéticos de agregação proteica, complementados com estudos de imagem de fibras. Neste estudo utilizamos um conjunto vasto de técnicas bioquímicas e métodos biofísicos, que incluíram expressão e purificação de proteínas recombinantes recorrendo a processos cromatográficos, análise espectroscópica por dicroísmo circular no UV longínquo (UV-CD), espectroscopia no infravermelho por transformada de Fourier com refletância total atenuada (FTIR-ATR), espectroscopia de fluorescência e microscopia de força atómica (AFM).

Na primeira fase do estudo foi necessário otimizar os protocolos de purificação proteica, nomeadamente da proteína Tau humana intacta com 441 resíduos (hTau441). O processo envolveu a realização de culturas celulares de *E. coli* transformadas com plasmídeo para expressar hTau441. Subsequentemente ao crescimento bacteriano e expressão proteica, seguiu-se a lise celular. O lisado obtido foi incubado a 75°C para precipitação diferencial das proteínas contaminantes do hospedeiro, uma vez que a hTau441 é termoestável mantendo-se solúvel. Uma vez que o nosso objetivo era purificar a forma monomérica da hTau441com um elevado grau de pureza, procedeu-se à realização de uma série de cromatografias (troca catiónica e exclusão molecular) em várias condições distintas, tendo-se identificado a melhor condição experimental (7.6M de ureia e 50mM de ditiotreitol) para cromatografia de exclusão molecular (SEC), da qual resulta o melhor rendimento e obtenção de proteína Tau humana monomérica com elevado grau de pureza (>95%).

Para avaliar a interação entre as proteínas hTau441 e S100B verificou-se se a sua co-incubação resultaria na formação de um complexo estável. Para isso utilizou-se a técnica de SEC que permite distinguir as proteínas pela sua massa molecular. O resultado obtido evidenciou a formação de um complexo entre as duas proteínas, sendo, contudo inconclusivo relativamente à estequiometria do complexo formado. Este

resultado levou-nos a investigar esta possível interação, avaliando agora as principais alterações conformacionais da estrutura secundária de ambas as proteínas, tirando partido da sensibilidade de espectroscopia de CD, uma das técnicas espectroscópicas de excelência para determinar interações proteína-proteína. De facto, a titulação da proteína S100B (rica em hélices-α) com hTau441 (desordenada) evidenciou uma série de alterações conformacionais (perda de hélices-α) indicativas de uma interação. Verificamos que a ligação de cálcio à proteína S100B favorece a sua associação com a proteína Tau. Também foi avaliada a alteração de estrutura secundária na presença de $Zn^{2+}$, o que revelou uma ainda maior perda da estrutura de hélices-α, mas também um aumento da contribuição de folhas-β, que pode ser explicado pela alteração conformacional subjacente ao começo de agregação amilóide da hTau441, com formação de oligómeros ricos em folhas-β cruzadas, característicos de amilóides. Conclui-se assim que as duas proteínas interagem fisicamente e que dessa interação resultam alterações conformacionais em ambas. Não foi contudo, possível determinar a constante de ligação do complexo Tau:S100B.

De seguida, e para determinar se a proteína S100B influencia a agregação da proteína Tau, realizaram-se estudos de cinética de agregação da hTau441 induzida por heparina, um modelo de estudo bem estabelecido e caracterizado para estudo do processo de fibrilação da proteína Tau. A formação de agregados foi seguida pela fluorescência de tioflavina-T (ThT), um fluoróforo repórter da formação de agregados amilóides com estruturas β-cruzadas, no qual a ThT se intercala tornando-se fluorescente. Usando esta abordagem, foi possível observar que a agregação de hTau441 pode ser modulada por NaCl, $Ca^{2+}$ e $Zn^{2+}$ e também pela presença da proteína S100B. Num estudo inicial foram testadas várias condições por forma a identificar aquela que seria a melhor condição para a agregação de hTau441 (0.5mg/mL de heparina e 50mM de NaCl). Após esta definição, estas concentrações foram usadas em todas as experiências de agregação. No estudo sobre o efeito de $Ca^{2+}$ e $Zn^{2+}$ (testados a 1.1mM) concluiu-se que ambos promovem a agregação de hTau441, reduzindo o tempo da fase de latência do processo de agregação. O efeito do $Zn^{2+}$ (1.1 mM) na agregação de hTau441 (0.5-50 μM) foi muito superior do que o efeito do $Ca^{2+}$, quase eliminando a fase de latência. Posteriormente analisou-se o efeito da S100B sobre a agregação da hTau441 em condições apo (S100B sem metais ligados), na presença de $Ca^{2+}$ (Ca-S100B) e na presença de $Zn^{2+}$ (Zn-S100B). Na presença de apo-S100B, a agregação de hTau441 foi atrasada (aumento do tempo da fase de latência de ~5h para ~20h) sendo que, contudo, a velocidade de agregação aumentou ligeiramente. No entanto, a presença de Ca-S100B resulta na completa inibição da agregação de hTau441, a partir de concentrações proteicas equimolares. Mesmo em condições subestequiométricas ([Tau] >> [S100B]), verifica-se um atraso no tempo da fase de latência. Curiosamente, utilizando o mesmo procedimento experimental, mas com Zn-S100B, não houve qualquer efeito sobre a cinética de agregação de hTau441, quando comparada com os controlos contendo apenas hTau441 e $Zn^{2+}$. Conclui-se, portanto, que a proteína S100B modula a agregação de hTau441 e que este efeito é passível de regulação por associação de cálcio, mas não zinco, à proteína S100B.

Com o intuito de caracterizar e identificar as estruturas amilóides formadas durante o processo de agregação da proteína Tau nas condições acima descritas, recorreu-se à técnica de microscopia de força atómica para analisar a topografia dos agregados formados. Este estudo permitiu determinar que em condições apo, na presença de $Ca^{2+}$ e na presença de $Zn^{2+}$, houve formação de fibras amilóides. Apenas na condição na presença de Ca-S100B não ocorreu a formação de fibras hTau441, tendo-se, contudo, constatado a formação de agregados não amilóides, provavelmente devido à interação entre S100B na presença de $Ca^{2+}$.

No seu conjunto, os resultados deste trabalho contribuíram para um melhor entendimento de processos bioquímicos passíveis de regularem a agregação da proteína Tau, com impacto na compreensão

de processos fisiopatológicos subjacentes à Doença de Alzheimer. De facto, sabe-se que nesta patologia a proteína S100B está substancialmente aumentada, assim como a proteína Tau monomérica. Especificamente, este estudo contribuiu para desvendar o mecanismo de agregação da hTau441 na presença de $Zn^{2+}$ e $Ca^{2+}$, bem como a contribuição da S100B na cinética de agregação da hTau441 e a consequente formação de fibras. Espera-se que este estudo permita abrir novos caminhos para a investigação futura das funções das interações proteína-proteína na doença de Alzheimer, processo de neuroinflamação e influência de iões metálicos.

**Palavras-chave**: Doença de Alzheimer, Tau, agregação proteica, iões metálicos.

# Contents

# List of figures

# List of tables

# Abbreviations

| | |
|---|---|
| **$Abs_{280nm}$** | Absorbance at 280nm |
| **Aβ** | Amyloid-β |
| **AD** | Alzheimer's disease |
| **AFM** | Atomic force microscopy |
| **ANS** | 1-anilinonaphethalene-8-sulfonic acid |
| **APP** | Amyloid precursor protein |
| **ATR** | Attenuated total reflectance |
| **$Ca^{2+}$** | Calcium ion |
| **CD** | Circular dichroism |
| **CEX** | Cation exchange chromatography |
| **CDK5** | Cyclin-dependent kinase 5 |
| **Cryo-EM** | Cryo-electron microscopy |
| **$Cu^{2+}$** | Copper ion |
| **DIAD** | Dominant inherited Alzheimer's disease |
| **DLDH** | Dementia lacking distinctive histopathology |
| **DTT** | Dithiothreitol |
| **EDTA** | Ethylenediamine tetraacetic acid |
| **FRET** | Förster resonance energy transfer |
| **FTD** | Frontotemporal dementia |
| **FTDP-17** | Frontotemporal dementia with parkinsonism linked to chromosome 17 |
| **FTIR** | Fourier transform infrared |
| **GSK3** | Glycogen synthase kinase 3 |
| **HD** | Huntington's disease |
| **hTau441** | Recombinant full-length human Tau |
| **IDP** | Intrinsically disordered protein |
| **IFN** | Interferon |
| **IL** | Interleukin |
| **IPTG** | Isopropyl β-D-1-thiogalactopyranoside |
| **IR** | Infrared |
| **JNK** | c-Jun N-terminal kinase |
| **Kd** | Dissociation constant |
| **$K_{app}$** | Apparent aggregation velocity |
| **LTD** | Long-term depression |
| **MAP1A** | Microtubule-associated protein 1A |
| **MAPT** | Microtubule-associated protein Tau |
| **MBD** | Microtubule binding domain |
| **NaCl** | Sodium Chloride |
| **NF-κB** | Nuclear factor kappa B |
| **NFT** | Neurofibrillary tangle |
| **NMR** | Nuclear magnetic resonance |
| **$OD_{600nm}$** | Optical density at 600nm |

| | |
|---|---|
| **PD** | Parkinson's disease |
| **Phe** | Phenylalanine |
| **PHF** | Paired helical filaments |
| **PMSF** | Phenylmethylsulfonyl fluoride |
| **PS** | Presenilin |
| **RAGE** | Receptor for advanced glycation end products |
| **ROS** | Reactive oxygen species |
| **SDS-PAGE** | Sodium dodecyl sulfate–polyacrylamide gel electrophoresis |
| **SEC** | Size exclusion chromatography |
| **SF** | Straight filaments |
| **SV** | Synaptic vesicles |
| **ThT** | Thioflavin T (4-(3,6-dimethyl-1,3-benzothiazol-3-ium-2-yl)-N,N-dimethylaniline chloride) |
| $\mathbf{t_{lag}}$ | Lag phase time |
| **TNF** | Tumor necrosis factor |
| **Trp** | Tryptophan |
| **Tyr** | Tyrosine |
| **UV** | Ultraviolet |
| **Zn** | Zinc |

# I. INTRODUCTION

The introduction of this dissertation is divided in three parts. The first part overviews Alzheimer's Disease (AD) and the particular contribution of Tau, outlining its structure, function and pathogenicity (aggregation and neurotoxicity). The second part focuses on the neuroinflammatory S100B protein, overviewing its structure and biological functions in the brain. Finally, the last section addresses the protein structural analysis and biophysical technics used in this work.

## 1.1 Alzheimer's disease and Tau protein

### 1.1.1 Alzheimer's disease

Alzheimer's disease (AD) is the most common neurodegenerative disorder in the world and it has specific features such as progressiveness and unremitting advancement, affecting cerebral areas like hippocampus and cerebral cortex. In the brain, the initial abnormalities related to the formation of plaques and neurofibrillary tangles are normally detected in the frontal and temporal lobes and slowly advance to other areas such as the neocortex with a progression that varies between individuals (figure 1.1, C). This degenerative disorder affects the brain's neurons, resulting in loss of memory, cognition, language skills and behavioral changes in the patients [1]. AD also causes a large loss in brain weight and volume and affects some brain regions and neuronal populations more than others. Although AD clearly causes loss of number of neurons in specific brain areas like pyramidal cells in lamina II of the entorhinal cortex and in the CA1 region of hippocampus, much of the overall loss of brain volume appears to be due to the shrinkage and loss of neuronal processes [2].

The duration of illness ranges from 8 to 10 years. However, before the symptomatic phases, the preclinical and prodromal stages (from the initial symptoms to the full development of disease) can span for over two decades. Sporadic AD is the most common type, with patients developing symptoms from 65 years old onwards, with a peak at around 80 years old. For yet unclear reasons, the incidence of the disease is higher in women than in men. Less than 1% of AD patients suffer from the autosomal dominant inherited AD (DIAD) form that is characterized by an early age of disease onset (≈45 years). However, the disease is just confirmed postmortem by observing amyloid plaques and neurofibrillary tangles (NFTs) in the brain [1]. At this moment the diagnosis of AD is based on clinical observations and cognitive testing such as neuropsychological testing [3].

Major risk factors for AD are ageing, gender and traumatic brain injury. However, AD is promoted by pathogenic mutations in genes encoding for the amyloid precursor protein (APP), presenilin 1 (PS1) and presenilin 2 (PS2), that result in an overproduction or formation of aberrant amyloid-β (Aβ).

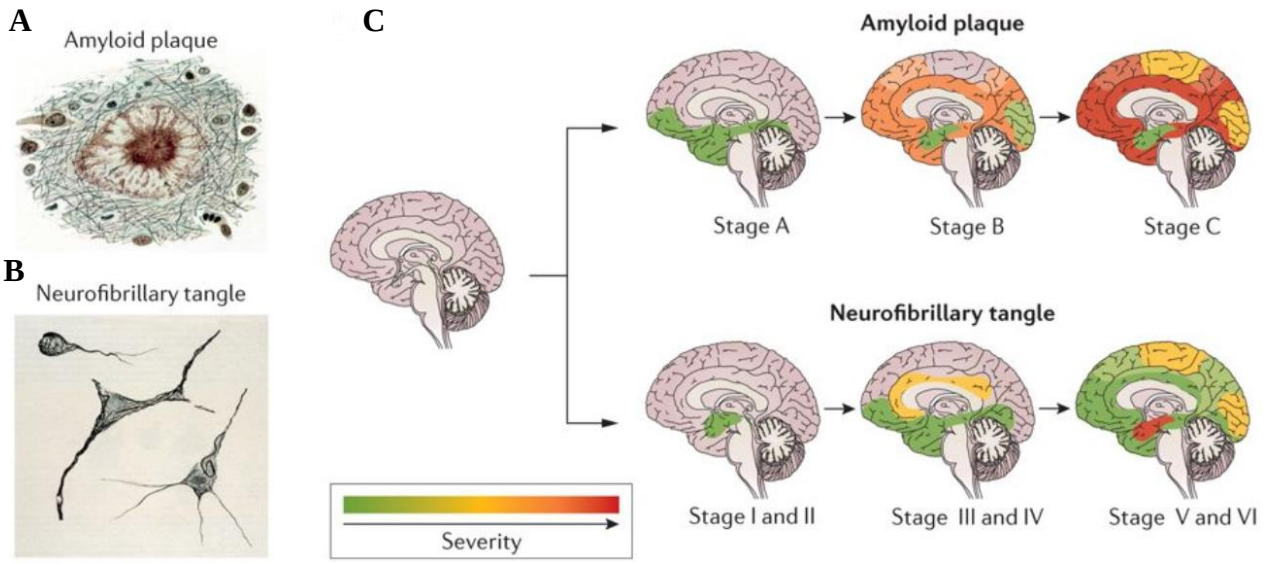


**Figure 1.1: Alzheimer's disease brain Braak stages**. Histology of AD brain sections showing a plaque (**A**) and NFT (**B**); **C** – Sites of initial formation and spreading of amyloid deposits (Aβ) and neurofibrillary tangles (Tau) in the AD brain along disease progression. The degree of AD pathology is accessed by the so called Braak staging that correlates disease severity with molecular and histological features in the affected brain. Adapted from [4].

AD shares numerous molecular characteristics with other neurodegenerative diseases, like Parkinson's disease (PD), prion disorders, Huntington's disease (HD) and frontotemporal dementias (FTD). The most striking common characteristic of these diseases is the formation of amyloidogenic aggregates. In the case of the AD, the proteins that are involved in aggregation cascades are the Aβ peptide and Tau protein. Aggregation of these proteins leads to the formation of histological hallmarks of AD: extracellular senile plaques, composed by Aβ peptides, and intracellular NFTs, composed of hyperphosphorylated Tau protein (figure 1.1, A and B).

Senile plaques form as a result of enzymatic (mis)cleavage of APP resulting in the formation and release of Aβ peptides with multiple lengths. From these, the Aβ(1-40) and Aβ(1-42) are the most aggregation prone and cytotoxic ones (Aβ42 >> Aβ40) which engage into the aggregation cascades with the downstream formation of toxic oligomers and subsequently fibrils that constitute the plaques. APP processing involves several secretases (α-, β- and γ- secretases [1, 5]), but only the combined action of β- and γ- secretases leads to the formation and release of Aβ monomers (figure 1.2). NFTs are composed of paired helical filaments (PHF), which are build-up of hyperphosphorylated insoluble and aggregated forms of Tau protein [6]. These NFTs cause atrophy of nerve cells, therefore damaging the synaptic connected axons. The properties and physiopathology of Tau is discussed in the following section.

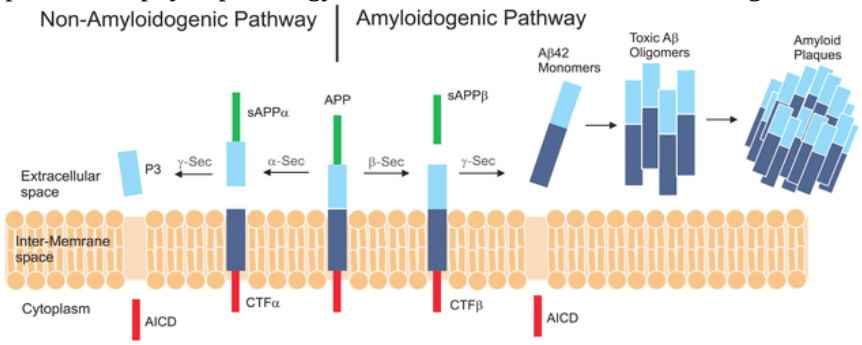


**Figure 1.2: Schematic representation of amyloid- β pathway that leads to AD pathology**. Extracted from [7].

### 1.1.2 Tau isoforms and structure

Human Tau protein is encoded by the microtubule-associated protein Tau (MAPT) gene localized on chromosome 17 whose alternative splicing generates multiple Tau isoforms (figure 1.3) [8]. The alternative splicing of MAPT gene results in six molecular isoforms of Tau that differ in containing three (3R Tau) or four (4R Tau) microtubule binding repeats (R) of 31-32 amino acids at the carboxy terminal half and one (1N) or two (2N), or zero (0N) amino terminal inserts of 29 amino acids each. The extra repeat in 4R Tau is the second repeat (2R) in the microtubule binding domain (MBD). The combination of these isoforms results in three 3R Tau (0N3R, 1N3R and 2N3R) and three 4R Tau proteins (0N4R, 1N4R and 2N4R). The 2N4R Tau isoform is the longest human Tau expressed in the brain, with a total of 441 amino acids (hTau441); the smallest is the 0N3R Tau isoform that lacks both the two amino terminal inserts and the extra repeat in the MBD, being only 352 amino acids long (hTau352). The longest isoform contains 80 Serine or threonine residues, 56 negative residues (asparagine or glutamine) 58 positive residues (lysine or arginine) and 8 aromatic residues (5 tyrosine and 3 phenylalanine, but no tryptophan). hTau352 is the only form that is expressed in fetal human brain [9]. The levels of 3R and 4R forms are roughly equal, and their imbalance is sufficient to cause neurodegeneration and dementia [10].

Tau is a so called intrinsically disordered protein. Native unfolded Tau isoforms are all highly hydrophilic and heat stable, and show a limited tendency to aggregate, although this propensity increases as a result of its phosphorylation [11]. Despite its disordered character, the Tau molecule has been proposed to have a preference for changing its global conformation to form a “paperclip” shape, in which both of the terminals and the MBD approach each other [12], which seems to protect Tau from aggregation.

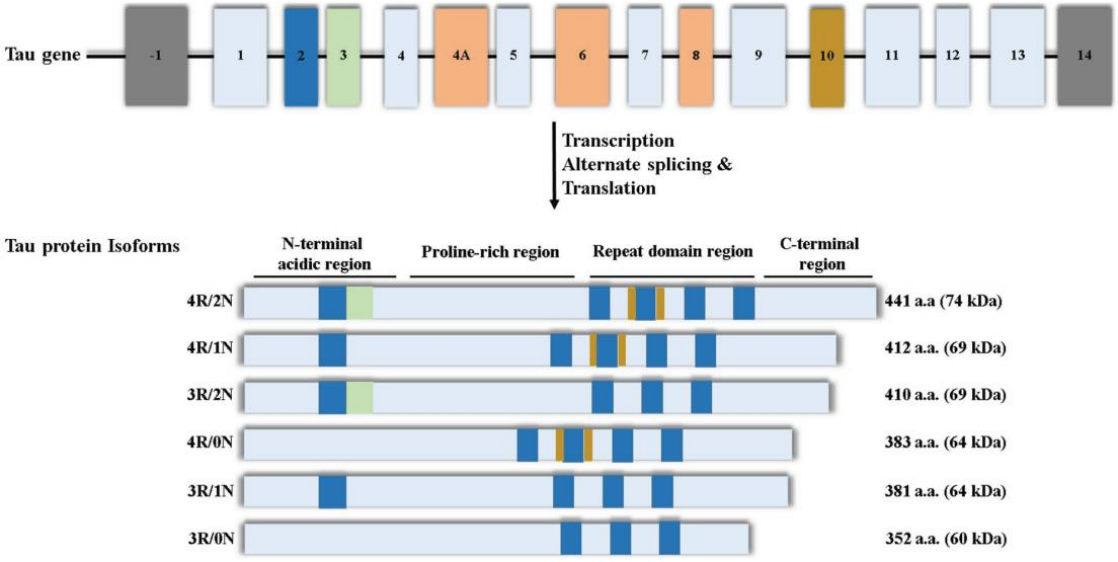


**Figure 1.3: Tau gene, protein isoforms, and domain structure**. Extracted from [13].

The assessment of Tau's structure has been a very difficult task to the scientific community and the progress in understanding Tauopathies in general has been hampered by the lack of atomic structures of Tau filaments from brain samples. The major difficulty lies in the fact that Tau is an intrinsically disordered protein that does not possess a defined native structure, thus impairing conventional structural analysis by nuclear magnetic resonance or x-ray crystallography. However, in the fibrillar form, Tau is more amenable to structural studies. Recent advances in cryo-electron microscopy (cryo-EM) have however allowed for a major breakthrough which the resolution of an atomic structure of Tau fibrils [14]. These structures were determined from Tau present in straight filaments (SF) and in paired helical filaments (PHF), isolated from samples of the cerebral cortex of a patient with a neuropathologically confirmed diagnosis of Alzheimer's disease (figure 1.4) [14].

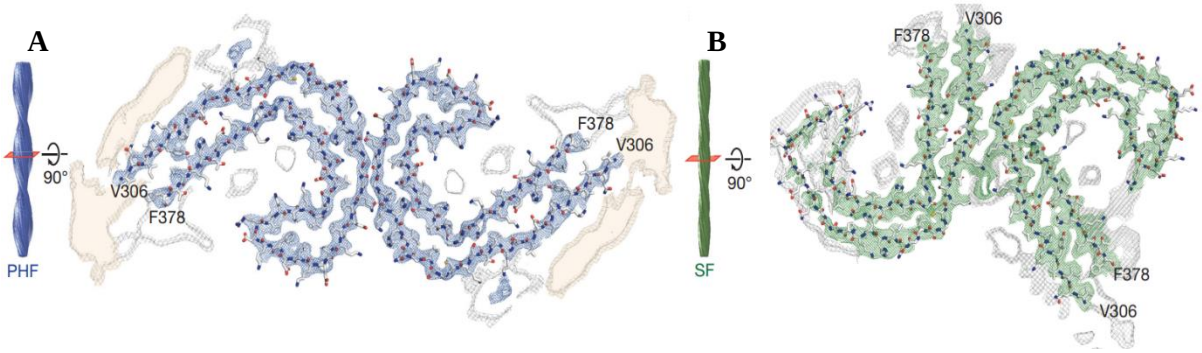


**Figure 1.4: Cryo-EM Tau structure in PHF and SF. A** – cross-section of PHF; **B** – cross-section of SF. Extracted from [14].

### 1.1.3 Tau function and phosphorylation

Until recently the only established physiological function of protein Tau protein was the promotion of the assembly of α- and β-tubulin into microtubules and consequent stabilization of their structure [15]. Recent studies revealed that cytosolic Tau protein is also involved in other physiological processes, including neural polarization, axonal transport, axonogenesis, and regulation of synaptic function and neuronal signaling [16-19]. Microtubules are critical for cellular function, especially for neurons, which require microtubule assembly from tubulin building blocks for the growth and integrity of axons and dendrites [20] and for the transport of molecular cargos between the cell body and distant synapses [21]. The distribution of Tau in mature neurons has been described as being mainly present in the axon [22], although a small proportion might be present in the somatodendritic compartment [23]. In a normal mature neuron, tubulin is present in over a tenfold excess over Tau. The normal neuronal Tau concentration is 2μM [24, 25] where it binds to microtubules at high affinity, with a dissociation constant ($K_d$) of 100nM [26]. Therefore, practically all Tau is probably bound to microtubules in neurons, and recently a near-atomic model of microtubule-Tau interactions has been obtained (figure 1.5) [27]. Alternative splicing also affects the biological activity of Tau: both the extra repeat in 4R Tau and the amino terminal insert N1 and N2 enhance binding of Tau to tubulin which makes the 2N4R Tau isoform as the relatively most effective in promoting microtubule assembly. Tau has also been found in the nucleus [28] where it is postulated to play a role in DNA protection [29] and in the regulation of the cell cycle [30].

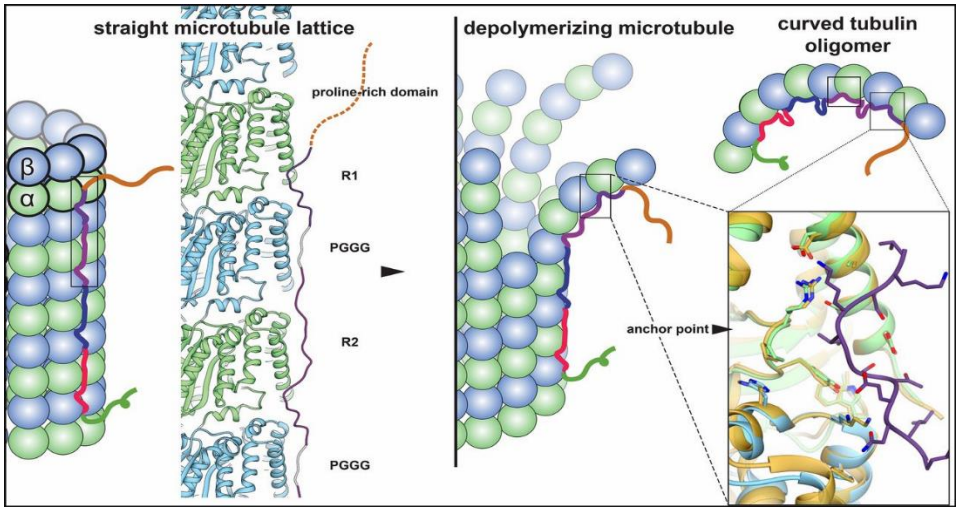


**Figure 1.5: Model of full-length Tau binding to microtubules and tubulin oligomers**. Extracted from [27].

Tau protein can be phosphorylated and the degree of phosphorylation regulates its biological activity (polymerization of tubulin) (figure 1.5) [31, 32]. The optimal ratio for Tau interaction with tubulin and microtubule assembly in neuronal cells is 2-3 moles of phosphate per mole of Tau protein [33]. It is the kinases and phosphatases that modulate the degree and pattern of the Tau molecule's phosphorylation [34]. It has been widely accepted that Tau is a phosphoprotein that can be modified by many different protein kinases, such as proline-directed protein kinases like glycogen synthase kinase 3 (GSK3) or cyclin-dependent kinase 5 (CDK5). The modification of Tau by these and other kinases appears to decrease its affinity for microtubules [35]; through this mechanism the destabilized microtubules disintegrate and the cytosolic concentration of free Tau rises (figure 1.6). Overall, Tau phosphorylation at different sites likely affects not only its interaction with microtubules, but also its capacity to aggregate or interact with other proteins.

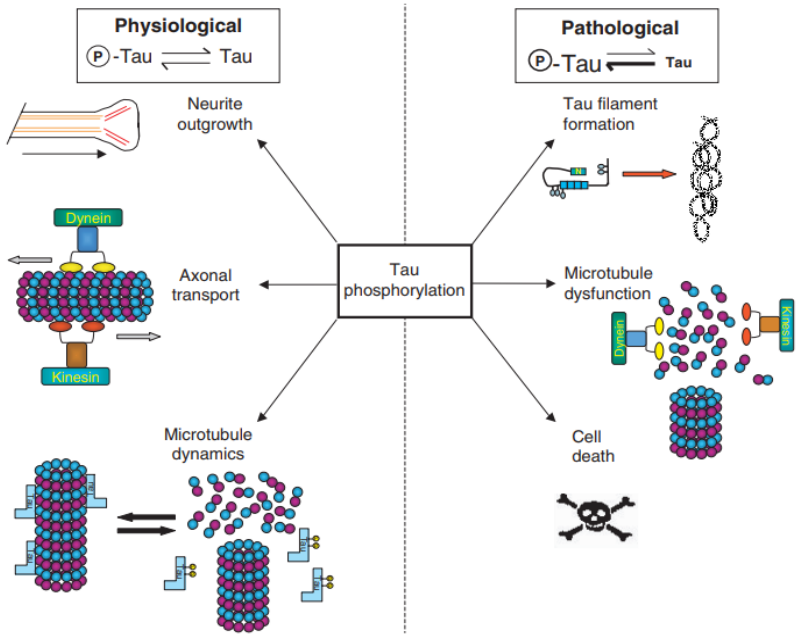


**Figure 1.6: Scheme of Tau physiological and pathological roles by Tau phosphorylation modulation**. Extracted from [36].

### 1.1.4 Tau mutations and disease

Tau is abnormally hyperphosphorylated and aggregated into bundles of filaments in several neurodegenerative diseases, collectively designated as Tauopathies [34]. Apart from AD, this group comprises for example supranuclear palsy, corticobasal degeneration, Pick's disease, and frontotemporal dementias with parkinsonism liked to chromosome 17 (FTDP-17). The understanding of the role of aberrant Tau in neurodegenerative diseases has advanced when Tau mutations were discovered to be associated with FTDP-17 and also by being specifically and only characterized by Tau pathology [37].

Initially identified mutations cluster in and around the regions encoding the microtubule-binding domains, suggesting that they may compromise microtubule binding. FTDP-17 mutations provided clear evidences that changes in Tau alone could cause neurodegeneration and strongly suggested that aberrant Tau plays a pathogenic role in other Tauopathies, including AD. To date, at least 37 mutations associated with FTDP-17 (figure 1.7) or related disorders have been identified [38]. These are either missense mutations, mutations that affect splicing, or both, and almost all are localized at the C-terminal coding region or at an intervening sequence near exon 10. C-terminal missense mutations all appear to impair Tau binding to microtubules and the ability of Tau to promote microtubule assembly. Most of phenotypical silent mutations increase the 4R/3R ratio by modulating alternative splicing of exon 10.

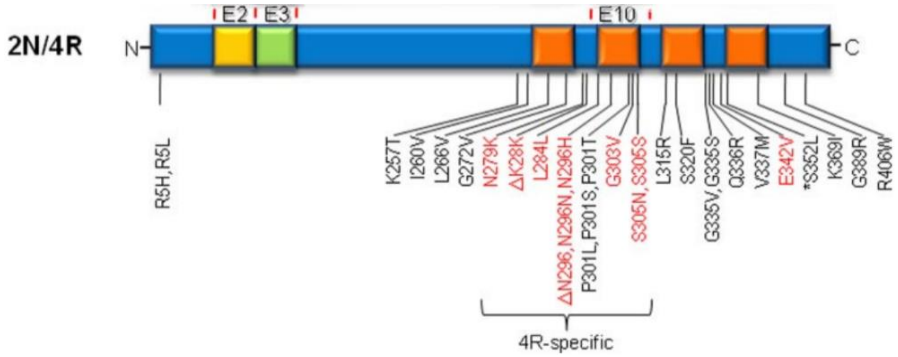


**Figure 1.7: Scheme of missense mutations that are associated with familial FTDP-17 and related disorders**. Extracted from [39].

Since consistent Tau deposition occurs in all familial cases, the observation that complete knock-out of Tau in mice does not lead to neurodegeneration and the fact that all but one of the disease associated mutations [40] are dominant, strongly suggests a gain of a toxic function. Indeed, it has been suggested that missense mutations may directly confer the ability of Tau to form filaments. Some studies show for instance that a wide range of missense mutants (R5L, K257T, I260V, G272V, K280, P301L, P301S, G335V, Q336R, V337M, and R406W) promote *in vitro* the formation of filaments in the presence of polymerization-inducing agents such as heparin and arachidonic acid [41]. Interestingly, ultrastructural differences in Tau filaments from brain tissue have also been observed in correlation with different Tau mutations: while some mutations correlate with twisted helical filaments, others favor paired helical filaments (similar to what is seen in AD), and others generate straight filaments [37]. However, it has not yet been proven that a single mutation on MAPT can develop or even increase the pathogenicity of AD, albeit a Tau deletion mutation (K280) has been found in an AD case [42].

### 1.1.5 Tau pathology in Alzheimer's disease

The aggregation of Aβ triggers a cascade of disease-causing processes such as inflammation, tau-tangle formation, synapse dysfunction and cell death. Tau pathology is triggered Aβ aggregates by yet unclear mechanisms (figure 1.8 - A) and results from the formation of intraneuronal neurofibrillary tangles of paired helical filaments (PHF) occasionally admixed with straight filaments (SF). Aggregates of abnormally hyperphosphorylated filaments are also seen in dystrophic neurites surrounding the Aβ plaque core, and in the neuropil as neuropil threads [43]. In AD the cognitive symptoms are correlate with the number and location of tau tangles more than with amyloid-β plaques (figure 1.8 – B), and this has led to the proposal that Tau may be the effective toxic agent in AD.

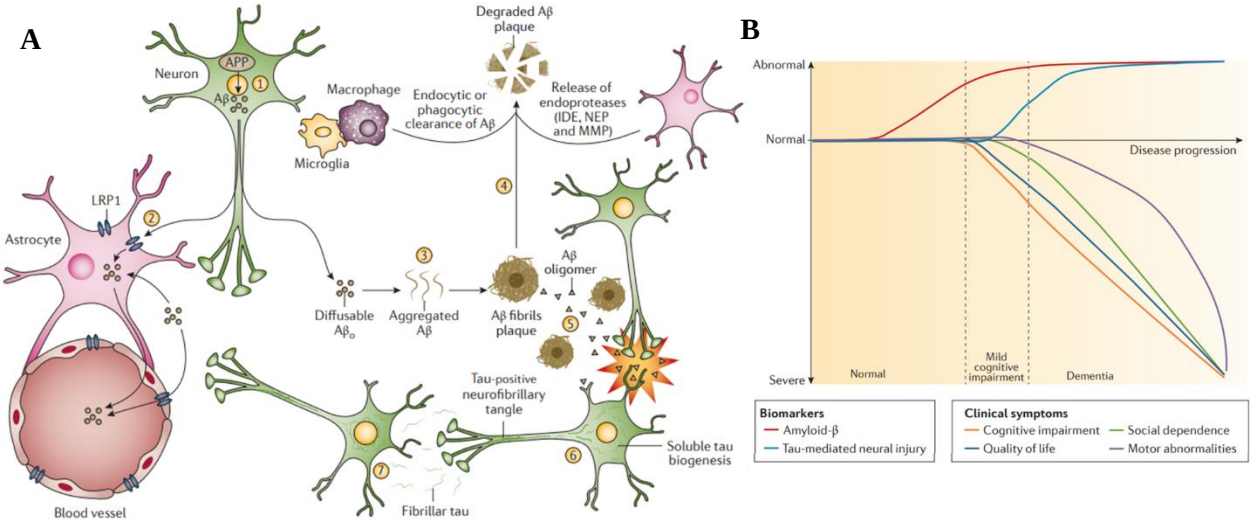


**Figure 1.8: Pathways and disease progression focused on Tau and Aβ pathological molecular contribution**. **A** –Pathways leading to plaques and tangles form the basis of the Aβ theory of Alzheimer's disease; **B** – Quality of life of patients with Alzheimer's disease. Extracted from [4].

#### 1.1.5.1 Tau amyloid aggregation

Tau intra-cellular aggregation is a hallmark of several neurodegenerative disorders; however, it is a natural event in aging as observed in aged brains that contained Tau aggregates. By observing the natively disordered unfolded nature of Tau, its aggregation into highly structured aggregates and periodic fibrils is expected to have a low probability to occur. Nevertheless, the two short hexapeptide motifs VQIINK and VQIVYK at the beginning of R2 and R3, respectively, are prone to form β-sheet structures and are essential for Tau aggregation, even if only part of these sequences are involved [44]. The motif VQIVYK has been shown to suffice for the formation of fibrils containing interdigitated β-sheets; also, Tau aggregation onset seems to involve by this motif, whose unmasking allows β-sheet stacking. Disruption of these motifs abrogates the tendency for Tau to aggregate, while the enhancing of β-structure formation in these same motifs, promotes Tau aggregation [45]. When Tau is bound to microtubules, it does not fold into a globular structure (see figure 1.5), but some residues containing the hexapeptide motifs can form a local hairpin conformation. This suggests that stabilization of the Tau microtubule-bound conformation delays its aggregation [46].

Tau aggregation can be accelerated by inducers such as polyanions that compensate for the repulsive positive charges of Tau. One of the most used *in vitro* Tau aggregation inducers is heparin, which presumably acts by stabilizing an aggregation-prone conformation of Tau [47].

Post-translational modifications, notably phosphorylation also affect Tau aggregation propensity. Indeed, it has been observed in AD patients that this modification precedes Tau aggregation and that Tau hyperphosphorylation has indeed been observed in patients with AD or other Tauopathies [48]. Yet, Tau aggregation can be efficiently induced *in vitro* by polyanionic cofactors, regardless of phosphorylation.

Truncated Tau fragments that contain the repeat domain have a higher tendency to aggregate, probably due to disruption of Tau's "paperclip" structure. These truncations can result in Tau fragments that induce neurodegeneration independently of Tau aggregation.

*In vitro* studies show that Tau aggregation follows a nucleation-elongation mechanism. Experimentally, the nucleation rate-limiting can be circumvented by using external seeds from preformed PHFs, accelerating the overall assembly. *In vivo*, Tau aggregation may follow the same mechanism, as preformed PHFs can seed Tau aggregation in cultured cells and *in vivo* [44].

As happens for all amyloid diseases, specific proteins can undergo aggregation through specific conformational changes that lead to the formation of highly ordered cross-β-sheet structures that are formed by stacking of structurally altered β-sheet segments. The experimentally observed cellular toxicity of Tau is associated with the self-assembly process in which free Tau monomers are converted to into Tau amyloid fibrils. Therefore, it is of great importance to understand the amyloid formation process in terms of the underlying molecular events that define its mechanism. There are specific steps during this aggregation that can be followed *in vitro* for instance, by thioflavin-T (ThT) fluorescence that shows increased fluorescence emission when is bind to the cross-β-sheet structures and excited at 440nm.

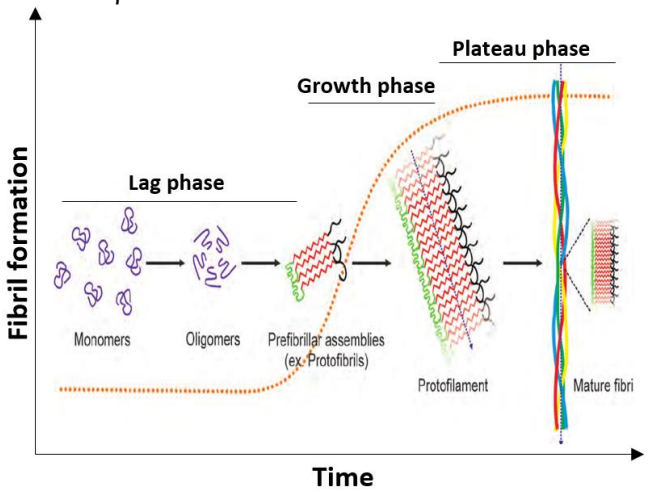


**Figure 1.9: Amyloid protein aggregation kinetics steps**. Adapted from [49].

The kinetics formation of fibrils *in vitro* typically follows one sigmoidal growth curve (figure 1.9). The first step is the lag phase (or nucleation phase), where monomers of the protein (for example Tau) are organized in multimers and oligomers that does not give any signal once there was not formed yet ThT reactive species. Between the lag phase and growth phase some prefibrillar assemblies start to emerge and exhibiting cross-β-sheet structures. In the growth phase (elongation phase) monomers are added to

protofilaments and protofibrils contributing prompting exponential growth of the fibril. Finally, the plateau phase represents the end point of this reaction which is determined by the exhaustion of all monomeric protein and the system reaches an equilibrium (figure 1.9). One important feature of this nucleation-dependent polymerization reaction is that small amounts of pre-formed fibrils are able to accelerate (seed) the reaction, significantly reducing the time of the lag phase (figure 1.10) [50].

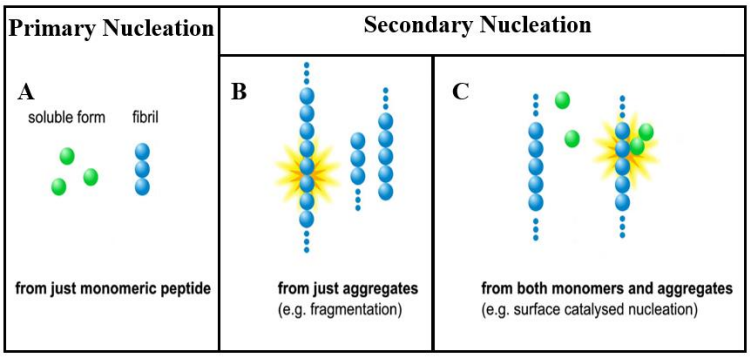


**Figure 1.10: Amyloid protein aggregation mechanisms**. **A** – Primary nucleation consist in the addition of monomers to aggregates. **B** – Fragmentation is one way of secondary nucleation by generating 2 aggregation "templates". **C** – Secondary nucleation by addition of aggregates with other aggregates. Adapted from [50].

### 1.1.5.2 Effects of metals in Tau aggregation

Alteration of metal ion homeostasis is a characteristic feature in AD. Indeed, it is well established that the intra and extracellular levels of metals such as calcium, zinc, copper and iron are deregulated during disease progression with implications in for example in aggregation propensity and oxidative stress [51, 52]. In particular, Tau aggregation is known to be modulated by metal ions (figure 1.11).

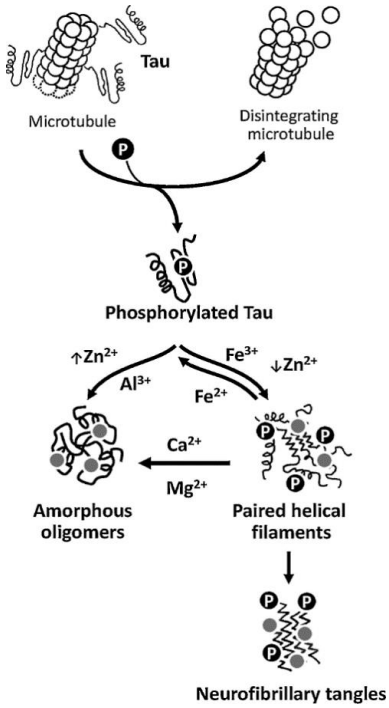


**Figure 1.11: Modulation of tau aggregation by metal ions**. Extracted from [51].

The formation of PHF through intracellular Tau aggregation and the subsequent assembly to form NFT is a process which is strongly dependent of metal ions [51]. Metal binding to Tau is almost exclusively associated with misfolding and initiation of amorphous aggregation or fibrillization. Tau can bind several metal ions like $Al^{3+}$, $Fe^{3+}$, $Cu^{2+}$, $Zn^{2+}$, $Cd^{2+}$ and $Hg^{2+}$, and all have modulatory effects over Tau aggregation, with the exception of $Cu^{2+}$ [51].

With special interest to this work, binding of $Zn^{2+}$ to Tau has been shown to induce faster fibrillization [53]. $Zn^{2+}$ can bind Tau promoting its hyperphosphorylation [54] and also induces fibril formation via disulfide cross-linking. Interestingly, the effect of at low micromolar concentrations $Zn^{2+}$ accelerates Tau fibril formation whereas at higher concentrations granular aggregates are formed [55].

$Fe^{3+}$ binds to hyperphosphorylated Tau and induces its aggregation towards PHF. However, the reduction of $Fe^{3+}$ into $Fe^{2+}$ reverses Tau aggregation [56]. Excess of iron ions is accumulated in NFT which can be a generating site of reactive oxygen species (ROS), due to Fenton reaction, contributing to oxidative stress and perpetuating Tau hyperphosphorylation [52].

The role of $Cu^{2+}$ is controversial in Tauopathies. While there are studies suggesting that Tau binds $Cu^{2+}$ leading to inhibition of its aggregation *in vitro*, there is evidences that it promotes Tau hyperphosphorylation in hippocampal neurons [57].

As above described binding of metal ions have a great impact in the pathological pathway as well as *in vitro* Tau aggregation. In this work, among the effect of other interactions, it is also assessed the effects of $Zn^{2+}$ and $Ca^{2+}$ of *in vitro* hTau441 aggregation.

#### 1.1.5.3 Neurotoxicity of Tau

In previous studies, Tau was discovered not to be essential to mice survival, as its function can be partly compensated by other proteins (microtubule-associated proteins, such as MAP1A). However, the behavioral impairments observed in aged Tau-knockout mice unraveled that Tau is necessary for normal neuronal and brain activity [58]. One of the human diseases featuring low levels of Tau in brain is dementia lacking distinctive histopathology (DLDH), the most common pathological variant of sporadic FTD.

Normally loss of Tau function has been ascribed to aggregation and hyperphosphorylation. The pathological pathway of Tau hyperphosphorylation starts when phosphorylation of the repeat domain lowers its affinity to microtubules leading to microtubule disassembly, culminating in axonal transport deficits (figure 1.12).

It was recently discovered that Tau is involved in other functions beyond microtubule stabilization. Tau's proposed novel functions include iron transport, neurogenesis, long-term depression (LTD) and neuronal DNA protection; therefore, loss of function of Tau may also lead to neurodegeneration by impairment of these processes. For example A152T mutation may cause the loss of Tau function [59].

In what concerns the neurotoxic gain of Tau function it is known that the regional distribution of NFTs in the AD brain correlates well with the severity of cognitive deficits. Therefore, NFTs have initially been considered to be the main players in Tau-mediated toxicity. Meanwhile, several other studies provided evidences that NFT formation by itself is not necessary nor sufficient for neurodegeneration. For example,

it reported that tangle-bearing neurons in AD have long survival times, a finding confirmed by several transgenic mouse models. Therefore, neuronal loss is not correlated with tangle formation, as many dying neurons do not contain NFTs and some neurons with tangles can survive and function normally [30].

Therefore, NFT formation by itself is not the cause of synapse loss and cognitive deficits in Tau transgenic mice. In several studies using transgenic mice that overexpress wild-type or mutant human Tau, synapse loss, impaired synaptic function and cognitive deficits occur before or without any eventual NFT formation, suggesting that soluble Tau species are the main cause of neurodegeneration. Therefore, some authors have proposed that the formation of PHFs or NFTs rather than being toxic, may actually be part of a protective pathway. For instance, these structures might scavenge toxic Tau species (monomers or oligomers) that would otherwise trigger toxic downstream processes such as oxidative stress and mitochondrial dysfunction.

It is known that the NFTs themselves are inert, but a question remains: what are the intermediary soluble species that are neurotoxic? Several studies are concordant with the amyloid cascade hypothesis, which proposes that soluble oligomers are the main agents causing neurodegeneration in AD, once that in these studies Tau oligomers are suggested as toxic species and its levels are increased in AD brains [60]. Nevertheless, so far, the role of Tau oligomers in Tauopathies remains a matter of debate, as Tau oligomers have not been well characterized. However, recent studies proved that the ability of Tau to aggregate is necessary for toxicity, by using 2 Tau mutants, one pro- and another anti-aggregant and observing that the neurotoxicity was only present when using the pro-aggregant mutant [61].

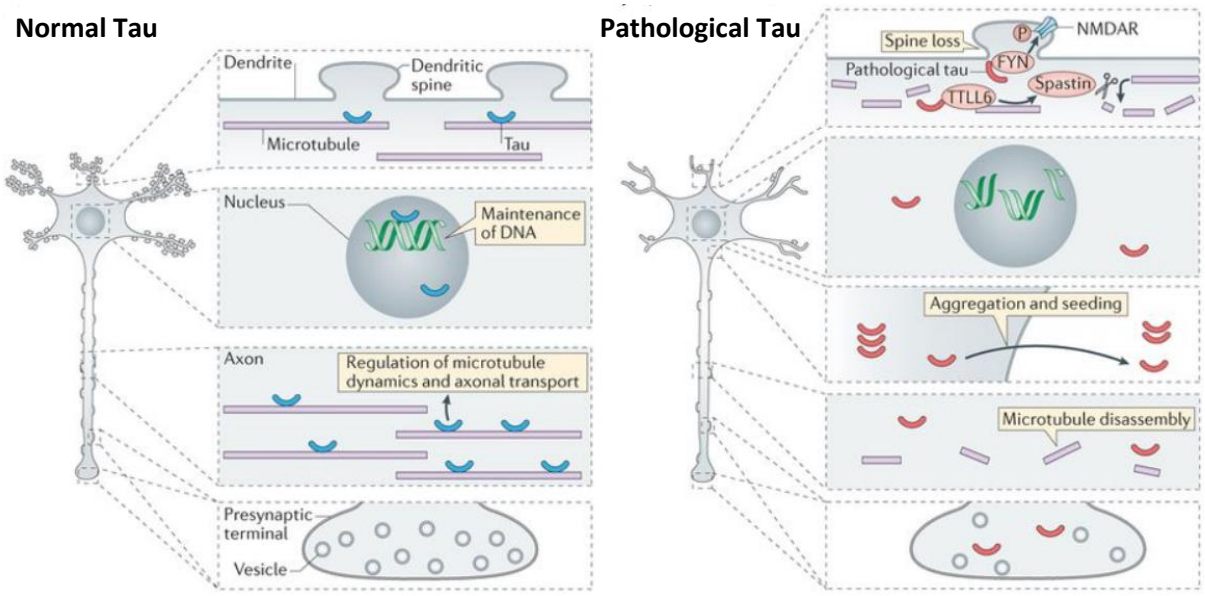


**Figure 1.12: Normal/physiological functions and pathological functions/disfunctions of normal and pathological Tau**. Extracted from [11].

In normal neurons there are low levels of Tau localized in the dendritic compartment, when in AD or other Tauopathies cases happens the opposite, Tau levels rises in dendritic compartment and this is one of the first and most evident pathological abnormalities. The hyperphosphorylation, mutations and overexpression of Tau can drive the mislocalization of Tau into postsynaptic spines, culminating in synaptic dysfunction [62].

### 1.1.5.4 Seeding and spreading of pathological Tau

The proposed factors that determine the pattern of pathological Tau spreading are still debated, however there are evidences that neuronal vulnerability factors (inadequate myelination, elevated metabolic rates and vulnerability to toxins), neuronal and regional connectivity and processes independent of Tau transmission (such as spread of neuroinflammation) are some of the factors involved in spread pattern.

The new thinking that Tau can be transmitted between neurons alongside with the emerging evidences that supports the neuronal network, both ideas may account for the pathology spreading. In experiences involving AD brains or mice transgenic models and injection of synthetic Tau fibrils or Tau aggregates from these, induces time-dependent spread of Tau pathology from the inoculation site to synaptically connected brain regions in wild-type mice [63]. Although knowing these evidences, there is still a matter of debate which Tau species are transmitted among neurons and what are the underlying mechanism of transmission.

Growing evidences allowed the establishing of presumable actions in those Tau transmission mechanisms. It is known that the degeneration of presynaptic neurons can cause the leakage of this part of the membrane, allowing presynaptic Tau seeds to diffuse throw the synaptic cleft. Then, Tau seeds can be released from the presynaptic terminal via exocytosis (figure 1.13, mechanism 1) or via exosome (figure 1.13, mechanism 2) or via synaptic vesicles (SV) (figure 1.13, mechanism 3). After release, Tau seeds can be taken up by postsynaptic neuros and subsequently initiate Tau aggregation.

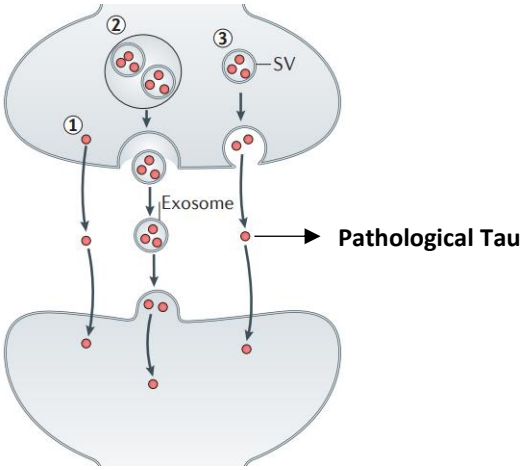


**Figure 1.13: Seeding and neuronal spreading of Tau pathology**. **1** – Via exocytosis; **2** – Via exosome; **3** – Via synaptic vesicles (SV). Extracted from [11].

## 1.2 The neuroinflammatory S100B cytokine

Neuroinflammation is another downstream process occurring in AD, which implies the release of inflammatory mediators by astrocytes and microglia as a response to plaque formation and toxicity. The S100 proteins are among the different cytokines which are substantially upregulated during this process. In particular, the intra and extracellular levels of S100B, the most abundant protein of this family in the human brain are particularly elevated along AD progression. Interestingly this protein is constitutively expressed in prodromal AD and has been recently proposed to play a housekeeping role as anti-aggregation chaperone [64], in addition to its pro-inflammatory activities. This work will explore the interaction between Tau and S100B and therefore a brief introduction to this important protein of the human brain is due.

### 1.2.1 S100B structure and function

S100B is expressed in varying abundance in a restricted number of cell types such as astrocytes, maturing oligodendrocytes, kidney epithelial cells, neural progenitor cells, certain neuronal populations, adipocytes and dendritic cells, among others. Also, S100B expression is enhanced in several tumors arising from cell types normally expressing the protein as well as in the aging brain and in the brain of patients affected by AD, chronic epilepsy and other brain pathological conditions. Other proinflammatory cytokines such as interleukin (IL)-1β and Aβ, upregulate S100B expression in astrocytes. On the other hand, epidermal growth factor, interferon (IFN)-γ, were shown to downregulate S100B expression in astrocytes and microglial cells.

S100B is a member of S100 family which consists of small (~10 KDa) $Ca^{2+}$-binding proteins of the EF-hand type comprising about 25 members. The name of this family is derived from the fact that these proteins are 100% soluble in ammonium sulfate at neutral pH. The human gene encoding S100B is present in chromosome 21q22.3 with consequent overexpression of the protein in Down syndrome, since this disease is caused by a trisomy of the chromosome 21. Like the other members of the family, S100B harbours two $Ca^{2+}$-binding sites in an EF-hand (a helix-loop-helix motif), interconnected by a hinge region, and a C-terminal extension [7]. Like other members of the family, S100B exists *in vivo* as a homodimer in which the two subunits are held together by non-covalent bonds and are disposed in an anti-parallel conformation (figure 1.14). S100B is one of the S100 proteins that contains secondary metal binding sites, namely a promiscuous zinc/copper binding site located at the dimer interface. In this site S100B can coordinate $Zn^{2+}$ ions (two per dimer) in a symmetric manner by His15/His25 of one S100B subunit and His85/Glu89 of the other subunit [65]. The role of this additional metal binding site is not clear although it is likely involved in the regulation of S100B conformation. Interestingly, S100 proteins and S100B in particular have been shown to be able to undergo amyloid-type self-assembly due to aggregation prone segments present at dimer interfacial helices [66].

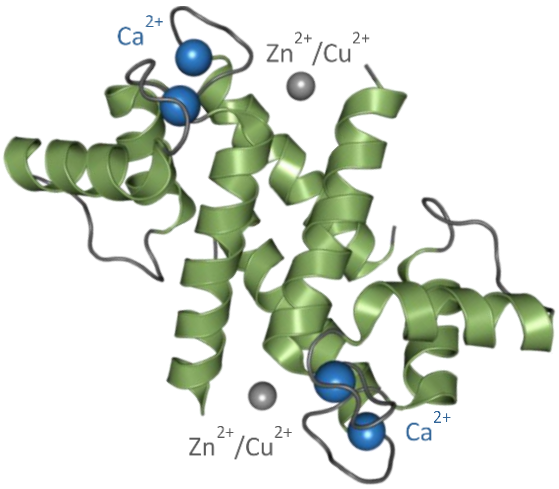


**Figure 1.14: Dimer structure of S100B protein**. Structure of S100B dimer (green) harboring $Ca^{2+}$ (blue) and $Zn^{2+}$ (gray) in specific coordination sites. Structure from PDB - 3D0Y.

S100B localizes in the cytoplasm, centrosomes, microtubules and intermediate filaments [67]. Inside cells S100B acts as a $Ca^{2+}$ sensor protein. Upon binding with $Ca^{2+}$, helix III of individual S100B monomers becomes more perpendicular to helix IV, causing the hinge region to move apart. This conformational change lead to exposure to the solvent of several hydrophobic residues in hinge region, helices III and IV and the C-terminal extension. These residues and others from helix I of the opposite monomer define a hydrophobic cleft through which dimeric S100B binds to target proteins. Nevertheless, other regions of the S100B dimer have been involved in recognition of some target proteins within cells, and S100B-target protein interactions may not be $Ca^{2+}$-dependent in some cases [68]. In other cases, can be $Zn^{2+}$-binding dependent. Alignment of structures of human $Ca^{2+}$–$Zn^{2+}$–S100B with $Ca^{2+}$–S100B showed that $Zn^{2+}$ binding only slightly change the conformation of the C-terminal classical EF-hand inducing a more open $Ca^{2+}$-S100B conformation, promoting by this way target binding proteins. Sole $Zn^{2+}$ binding to S100B leads like $Ca^{2+}$ binding to an exposure of hydrophobic patches to the solvent and can mediate $Ca^{2+}$-independent interactions with target proteins [69].

In any case, S100B apply its biological function by interacting with other proteins thereby affecting their activities. Thus, S100B is involved in cell proliferation regulation, cell differentiation and shape, $Ca^{2+}$ homeostasis, protein phosphorylation, transcription, microtubules dynamics, enzyme activity and metabolism. Other reasons that make possible the interaction of S100B with many target proteins, is its relatively high abundance and its cytoplasmic localization.

However, S100B has a great importance in extracellular processes. S100B is actively secreted by astrocytes, adipocytes, and maybe other cell types. Moreover, S100B release by astrocytes can be elevated upon stimulation with the proinflammatory cytokine, tumor necrosis factor (TNF)-α and during metabolic stress. Other stimulators include such diverse agents as high levels of cytosolic $Ca^{2+}$ or natural anti-oxidants.

Several results have suggested that active S100B release might be dependent on the presence and activation of receptor for advanced glycation end products (RAGE) on the cell surface, and that S100B might stimulate its own release via the same engagement. On the other hand, the active secretion of S100B can be reduced in primary astrocytes and Schwann cells treated with high glucose [70].

Whatever is the source of extracellular S100B or the mechanism of its release, extracellular S100B can reach local concentration enough to affect cellular activities by acting in a paracrine, autocrine and endocrine fashion. There is evidence of S100B and RAGE V-domain binding, that the non-reducing and high $Ca^{2+}$ conditions found extracellularly favors the formation of multimers, and these cause RAGE dimerization or stabilization of preformed RAGE oligomers, important for RAGE activation [71].

### 1.2.2 S100B in Alzheimer's Disease

Some studies have proved that S100B have neurotrophic properties on neurons stimulating the neurite outgrowth and regeneration *in vitro* and *in vivo*, and in fact S100B is expressed primarily by astrocytes and is one of the most abundant soluble proteins in the brain (0.5%) [72]. The neurotrophic property was involved in enhancing survival of neurons during development and after injury, and preventing motor neuron degeneration in newborn mice after sciatic nerve section [73].

S100B seems to be involved in protection of the neurons when there is a toxic stimulus, by leading the upregulation of the anti-apoptotic factor, Bcl-2, via engagement of RAGE and activation of nuclear factor kappa B (NF-κB) pathway (figure 1.15) [74]. The neuronal protection effect of S100B may also be indirect, such as protein stimulating uptake of the neurotoxic glutamate by astrocytes, reduction of neurotoxin-dependent activation of microglia and astrocyte, and reduction of neuronal and glial cytotoxicity under hypothermic conditions [75].

Several studies have data suggesting that S100B might have protective, neurotrophic effects during brain development, at early stages of brain insult and during regeneration of injured peripheral nerves. But the most important feature of these neurotrophic effects is that they are observed at nanomolar levels of S100B, such as those at the extracellular space under normal conditions. At levels >250nM S100B seems to activate a RAGE/ROS pathway leading to lipid peroxidation and caspase-3 activation causing neuronal apoptosis (figure 1.15).

On the other hand, at higher levels (>500 nM) S100B starts to have toxic effects on neurons, again in a RAGE-mediated manner, by increasing the production of reactive oxygen species (ROS) and enhances Aβ neurotoxicity [76]. Some studies found that even at concentrations normally thought to be protective to neurons, S100B might turn neurotoxic in ROS overproduction presence [77]. Nevertheless, it has been reported that S100B in even higher levels like 5μM, S100B adopt other functions such as promotion of neuronal survival via RAGE-dependent activation via NF-κB pathway (figure 1.15).

The observation of high concentrations presence of S100B in several brain pathological conditions including Alzheimer's disease and Down syndrome and in aging brain, leads to the idea that S100B could be involved in pathogenesis of neurodegeneration and brain inflammatory diseases. This idea was conceived by the observations of astrocytosis and axonal growth found in the hippocampus of S100B transgenic mice model and also the neuronal cytoskeletal and behavioral signs of altered aging processes detected in the same brains. In this mice model was also detected the loss of dendritic and synaptic markers and increase of apoptotic markers [78, 79].

As already outlined, the effects of S100B on neurons vary depending on the concentration and the context (microenvironment). This protein can have a protective role on neurons at concentrations up to a

few nanomolar and turning prejudicial at high concentrations or above a critical threshold of ROS production in neurons or nearby immune system cells (like microglia or astrocytes). Therefore, it can be possible that baseline levels of extracellular S100B in the normal brain and increased S100B levels in the aging brain and/or initial stages of brain insults, may have a beneficial effect on neurons [80].

Regarding Alzheimer's disease, the proinflammatory protein S100B is highly up-regulated and may rise the susceptibility to pathologic processes characterized by S100B overproduction. Indeed, the neurite growth-promoting effects of S100B have been proposed to be involved in evolution of Aβ deposits from benign to a pathogenic neuritic forms, as present in AD [81]. Also, there are evidences suggesting that high levels of S100B cause glycogen synthase kinase 3 β (GSK3β)-dependent hyperphosphorylation of Tau protein via RAGE-dependent activation of c-Jun N-terminal kinase (JNK) and upregulation of Dickoff-1, a activator of GSK3β in human neural stem cells (figure 1.15) [82]. It is known that hyperphosphorylated Tau is the major component of NFTs, a hallmark of AD. Also, in some studies was observed that S100B increases APP levels in neuronal cultures and that the levels of S100B elevates, in a mouse model of AD brains, and precedes the appearance of Aβ plaques. These findings can represent a mechanistic link between S100B overexpression in AD brains and overproduction of S100B in reactive astrocytes in proximity of NFTs [83, 84].

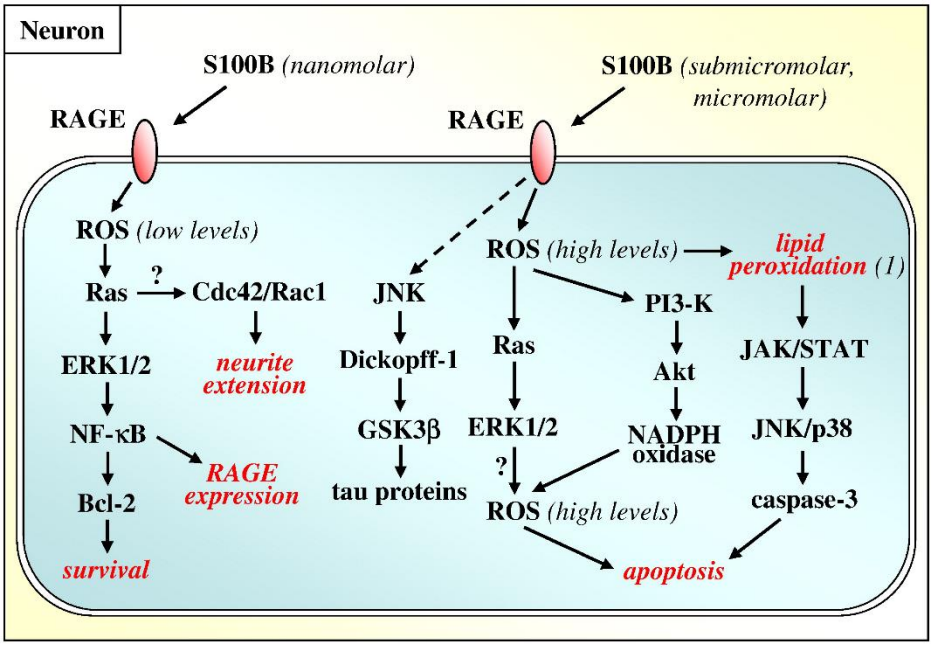


**Figure 1.15: Schematic model of extracellular effects of S100B on neurons**. In low S100B concentrations, NF-κB pathway is activated leading to neurons survival, on contrary when S100B is at high concentrations Dickopff-1, JNK and ERK pathways are activated and leads to neuron apoptosis and disease progression. Extracted from [80].

Also, S100B was found to be a suppressor of Aβ aggregation and toxicity *in vitro*, by physically interacting with Aβ, possibly by switching the Aβ disordered conformation to a α-helical conformer locking aggregation. This interaction and consequent function seem to be favored by $Ca^{2+}$. Moreover, in the same study, S100B protects the cells from Aβ toxicity, rescuing cell viability and decreasing the apoptosis in human neuroblastoma cell culture [64]. S100B can also be up taken into neurons [85]. Other studies revealed the intercellular co-localization of S100B and Tau NFTs [86, 87], through immunohistochemical assessment of AD patients brain tissue. These findings were essential for this project development.

## 1.3 Protein structural analysis and biophysical techniques

### 1.3.1 Circular dichroism spectroscopy

Circular dichroism (CD) spectroscopy is a technique which provides structural information about biomolecules with absorbing chromophores which cause selective deviation of circularly polarized light; the fact that light is left or right deviated correlates with the structure chromophore within the biomolecule under study (for a technical review on CD see [88]).

Protein CD is one of the most useful methods to investigate protein structure, folding and stability. ~~G~~In proteins, the chromophores of interest include the peptide bond (absorption below 240 nm), aromatic amino acid side chains (absorption in the range 260 to 320 nm) and disulphide bonds (weak broad absorption bands centered around 260 nm). To study the secondary structure the absorption wavelength needs to be below 240nm once it is due to the peptide bond absorption. So, the different types of secondary structure in proteins will result in characteristic CD spectra in the far ultraviolet (UV) (figure 1.16 - A). It can be extracted the estimation of α-helical content of peptides and proteins by using the values of CD signals at 208nm and 222nm and β-sheet content by using around 217-220nm, and with this evaluate structural contents and changes by following these wavelengths progression [89]. So, structural changes can be followed by CD spectra alterations that give us new information about protein structure and mechanisms.

To evaluate tertiary structure of proteins, the spectra should be recorded in near UV region 260-320, and this contribution arrives mainly by aromatic amino acids. Tryptophan show a peak close to 290nm with fine structure between 290-305nm, tyrosine peak between 275-282nm, with a shoulder at longer wavelengths and phenylalanine shows weak and sharp bands between 255-270nm (figure 1.16 - B). The shape and magnitude of near UV CD spectrum can inform about the type of amino acids present, protein motility, nature of the environment and their spatial disposition, once that all these factors alter the spectrum. So, near UV CD spectra of proteins provides a "fingerprint" of a tertiary structure of each protein that can be used to compare between others.

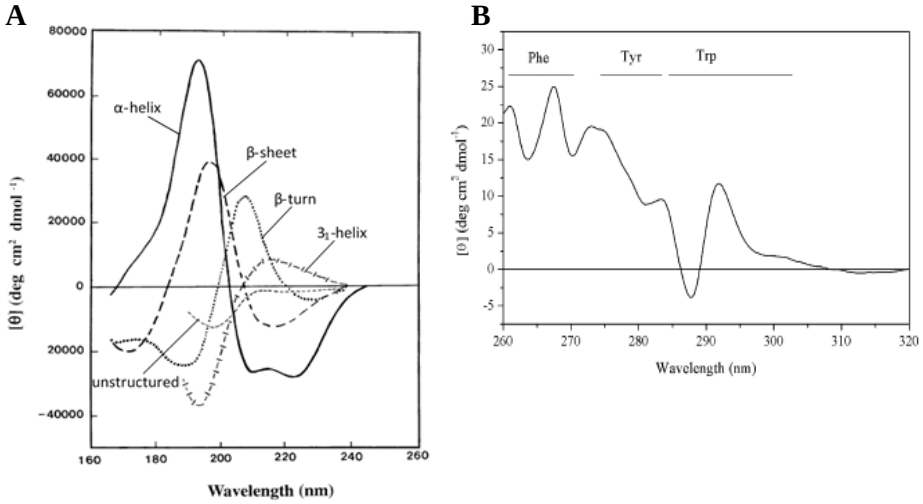


**Figure 1.16: Far and near UV CD spectra of protein analysis. A** – Far-UV CD spectra of typical types of secondary structure. Solid line, α-helix; long dashed line, anti-parallel β-sheet; dotted line, type I β-turn; cross dashed line, extended $3_1$-helix; short dashed line, unstructured. **B** – Near-UV CD spectrum of a dehydroquinase sample. The wavelengths ranges correspond to signals from the amino acids side chains as indicated. Extracted from [88].

CD is a highly sensitive method to monitor protein-protein and protein-ligand interactions. Indeed, interactions can be detected and quantitated by evaluation subtle conformation and structural changes occurring during the binding process.

### 1.3.2 Attenuated total reflectance Fourier transform infrared spectroscopy

Protein infrared spectroscopy is a useful method to characterize protein structure and conformational variations. The infrared spectra of a protein exhibit 5 characteristic bands where 3 of them are known as amide bands and these are the most used in IR protein studies. The amide I band, which has the strongest absorption of infrared light, is found between 1600 and 1700 $cm^{-1}$ (figure 1.17). It is primarily caused by stretching vibrations of C=O coupled weakly with C−N stretch and N−H bending. The exact band position is determined by the backbone conformation and the hydrogen bonding pattern within the protein molecule [90]. The amide II band ranges between 1500–1600 $cm^{-1}$ and is mainly derived from the C−N stretch along with N−H in-plane bending. Lastly, the amide III band is found between 1200–1300 $cm^{-1}$. The vibrations responsible for this band are a complex mix of N−H bending and C−N stretching along with deformation vibrations of C−H and N−H (figure 1.17) [90].

Although all three bands can be useful to elucidate the secondary structure of a protein, the amide I band is the most sensitive to structural changes and is the most commonly used in secondary structure analysis. The features responsible for the structural sensitivity of the amide I band include hydrogen bonding and coupling between transition dipoles, both inter and intra molecular, which will influence the protein and IR light interaction [91]. Further analysis of the amide I band is essential to obtain the types and quantities of secondary structure present on sample. This can be attained through Fourier deconvolution and second derivative, curve fitting and spectral subtraction, for example [92]. Overall, α-helical structures have a band peak at wavenumbers 1650–1658 $cm^{-1}$, β-sheet structures tend to have bands between 1620 and 1640 $cm^{-1}$ and between 1670 and 1695 $cm^{-1}$ and random coil structures occur at around 1644 $cm^{-1}$ (figure 1.17 - inset) [91].

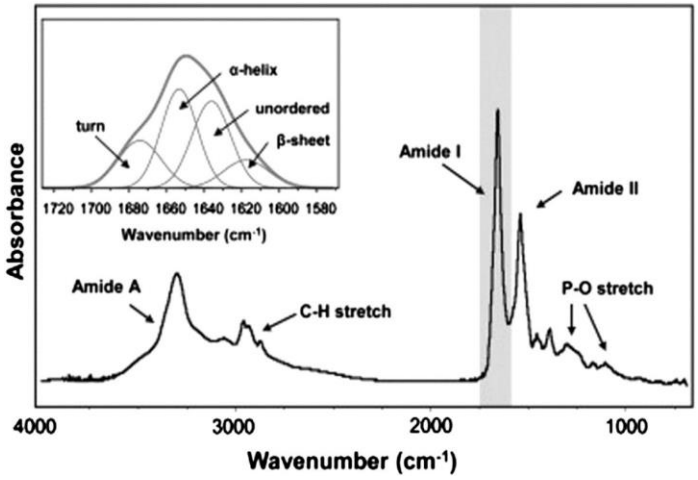


**Figure 1.17: FTIR typical spectrum of a protein.** FTIR spectrum of a protein with highlighted zone corresponding to the amide I band (~1650$cm^{-1}$), with high absorbance signal. Amide II band (~1540$cm^{-1}$) has also high absorbance in proteins spectra. Inset: Expanded view of amide I band (grey zone) with secondary structure components deconvolved. Extracted from [93].

The study of protein samples in aqueous solution is challenging since there is overlap of the water bending mode with the amide I band at 1600 $cm^{-1}$, but this could be overcome using $D_2O$. However, this can affect the native secondary structure of the protein. Moreover, the current FTIR spectrometers allow for accurate subtraction of the water band, promoting even further the technical difficulties resolution [94]. Attenuated total reflectance-FTIR (ATR-FTIR) has been shown to be useful for studying the secondary structure and other properties of proteins at modest concentrations in aqueous environments.

### 1.3.3 Atomic force microscopy

Atomic force microscopy (AFM) is a bioimaging method which allows to characterize the topography of biomolecules and cells, and it is particularly useful to characterize protein aggregates and amyloid fibrils [95]. In AFM, in simple terms, a flexible cantilever with a sharp tip probes a surface on which the biomolecule of interest has been deposited, and from tip–sample interaction force a three-dimensional representation of the surface can be obtained (figure 1.18, A). AFM imaging can thus can provide a nanometer-resolution image of amyloid fibrils (figure 1.18, B) including the contour length, width, height, periodicity or high-order assembly of single protofilaments into mature fibrils [96].

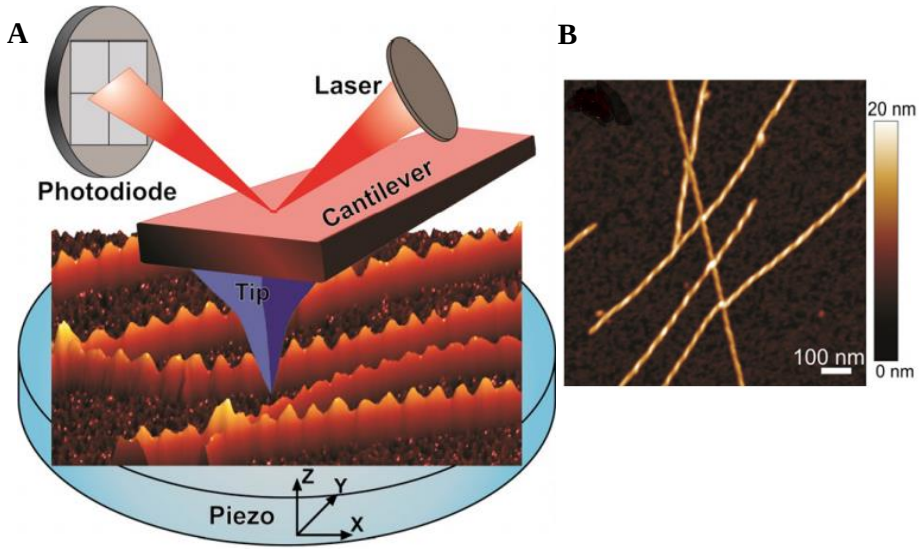


**Figure 1.18: Schematic examples of AFM operating principle and bioimaging**. **A** - Schematic representation of the operating principle of AFM. **B** - AFM image of amyloid fibrils in a twisted ribbon conformation. Extracted from [96].

### 1.3.4 Fluorescence spectroscopy

Fluorescence spectroscopy is one of the current and most powerful methods to study protein folding, dynamics, assembly, and interactions, as well as membrane structure. It has been successfully applied to investigate the complex mechanisms of protein aggregation including amyloid fibril formation, as well as their dynamic structures. Almost all proteins have natural fluorophores like tyrosine, phenylalanine and tryptophan residues that have intrinsic fluorescence, which allow study of changes in protein conformation

by exposure or hiding from the solvent. Also, site-specific labeling with external fluorophores is easily attainable by mutagenesis (insertion of fluorescent amino acids or proteins) and chemical modifications (with reactive fluorophores). Fluorescence spectroscopy only requires a small amount of material (pM–nM range) and has a high signal-to-noise ratio [97].

Tryptophan has the highest quantum yield and its emission maximum is sensitive to the polarity of its environment. Thus, tryptophan is a frequently used intrinsic fluorescent probe in studying protein folding and dynamics. The $\lambda_{max}$(absortion) is 280nm and the $\lambda_{max}$(emission) of a buried tryptophan is around 335nm, whereas fully solvent exposed has $\lambda_{max}$(emission) around 355nm [97].

Thioflavin-T (ThT) and 1-anilinonaphthalene-8-sulfonic acid (ANS) (figure 1.19, A) are commonly used as non-covalent extrinsic fluorescent probes in studies of protein folding and amyloid fibril formation. The ANS is used to detect the presence of hydrophobic patches since its quantum yield is increased up to 100 times upon binding to hydrophobic regions of a protein. Once that the intermediary species, like partially unfolded protein or molten globes, have exposed hydrophobic regions, ANS is widely used to detect and characterize protein-folding intermediates. The binding of ANS is result in a blue shift of the emission maximum (from ~530 nm to ~475 nm) [98].

Thioflavin-T (ThT) is among the most widely used amyloid dye in the present, however when it was discovered it was described as a potent fluorescent marker of amyloid in histology since it was observed selectively localized to amyloid deposits [99]. ThT when in presence of amyloid structures has enhanced fluorescence and this feature takes place because of the organization of ThT molecules bound to fibrils aligned parallel to the long axis of the fiber, thanks to the contribution of cross-β-sheet structure, that can sterically "lock" the bound dye, leading to an enhancement of ThT fluorescence (figure 1.19, A) [100].

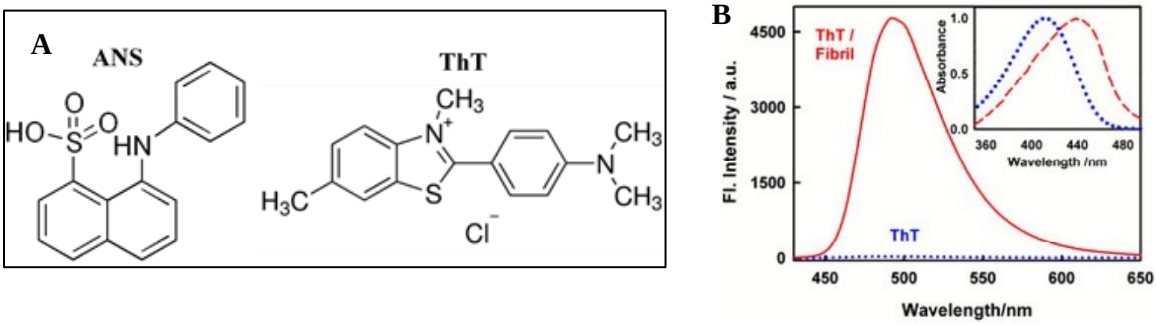


**Figure 1.19: Fluorophores structure and ThT fluorescence spectrum**. **A** – Extrinsic non-covalent fluorophores ANS and ThT chemical structures. **B** - Steady-state fluorescence spectrum of ThT in aqueous solution (dotted blue) and in insulin amyloid fibril (solid red). Inset: Normalized ground-state absorption spectra of ThT in same conditions. Extracted from [101].

This dye can have a generalized use through all the protein that generate amyloid fibrils, despite their distinct amino acid sequences, what strongly suggest that ThT recognizes a structural feature common among fibrils. Its binding is specific demonstrating a great shift of excitation maximum (from 385 to 450nm) (figure 1.19, B - inset) and the emission maximum (from 445 to 482nm), and ThT fluorescence originated is from dye that is bound to the amyloid structures [102]. The several orders of magnitude (10-500 fold) of increasing in ThT fluorescence intensity upon fibril binding makes it an excellent sensitive and efficient reporter (figure 1.19, B).

## 1.4 Objectives

Tau hyperphosphorylation and aggregation in the brain are hallmark features in Alzheimer's disease (AD). The S100B pro-inflammatory cytokine, an abundant brain protein which is upregulated in AD, promotes APP overexpression, modulates Aβ aggregation and promotes Tau hyperphosphorylation. However, no clear mechanistic relationship between S100B and Tau have so far been established. This work aimed at i) investigating a possible interaction involving these two proteins; ii) testing if the interaction between S100B and Tau would influence Tau aggregation; and iii) determine if binding of calcium or zinc to S100B would influence the interaction with Tau and its aggregation. Specific objectives included:

- Recombinant expression and purification of highly pure homodimeric human S100B and optimization of the purification procedure of monomeric human Tau protein, through bacterial expression and chromatographic purification with biochemical characterization;
- Analysis of the interaction between S100B and Tau and testing the influence of calcium and zinc binding to S100B on the Tau-S100B crosstalk, through biochemical and biophysical methods (circular dichroism);
- Determine the optimal conditions for Tau aggregation kinetics and investigate the effect of S100B in the apo, Ca- and Zn- bound states, using thioflavin-T fluorescence spectroscopy;
- Characterize the morphology of Tau aggregates using AFM bioimaging.

The work reported in this dissertation was carried out at the 'FCUL Protein Folding and Misfolding Laboratory' (http://folding.fc.ul.pt/) which is affiliated to BioISI – Biosystems & Integrative Sciences Institute and is located at the Chemistry and Biochemistry Department (C8 building FCUL campus) at the Faculdade de Ciências da Universidade de Lisboa. The AFM measurements and analysis described in results were performed by collaborators Dr. Ana Carapeto and Prof. Mário Rodrigues at the BioISI Magnetic Nanosystems Group at Department of Physics, also at FCUL (see acknowledgments).

# II. MATERIALS AND METHODS

## 2.1 Protein expression and purification

### 2.1.1 hTau441 expression and purification

Expression and purification of recombinant full length human Tau (hTau441) was adapted and optimized from that described in [103]. To obtain the overexpression of proteins, BL21(DE3) competent *Escherichia coli* (Lucigen) cells were transformed with 1µL of the plasmid pET15b-Tau recombinant T7 expression kindly provided by I. Landrieu (University of Lille, France), encoding the longest isoform of human Tau (441 amino acid residues). For transformation, cells were treated by heat shock (incubating on ice for 30 minutes, following by 45 seconds at 42°C and then incubation on ice for 5 minutes). 900µL of Expression Recovery Medium (lactose minus, Lucigen) were added and incubated at 37°C shaking at 250 rpm for 1 hour. The transformed cells were plated in Luria-Bertani solid (LA) medium with 100µg/mL ampicillin (Nzytech) and incubated overnight at 37°C. One isolated colony was selected and used to inoculate 100mL of Luria-Bertani (LB) medium with 100µg/mL ampicillin and was incubated at 37°C with shaking at 150rpm. After overnight incubation, 20mL of culture was added to 500mL of M9 medium containing 100µg/mL of ampicillin at 37°C, 150rpm. When $OD_{600nm}$ = 1 expression was induced with 0.4mM of IPTG and further incubated (37°C, 150rpm) for 3 hours.

Cells were recovered by centrifugation (Beckman Coulter Avanti J30I, with JA-14) at 8000rpm (10000g), 4°C for 10 minutes and stored at -20°C. The cells pellet was thawed and resuspended in buffer A (50mM Tris-HCl (Nzytech) pH 6.5 and 1mM EDTA (Sigma-Aldrich)), DNAse (PanReac, Applichem), 1mM phenylmethanesulfonyl fluoride (PMSF, Roth) and freshly supplemented with cOmplete™ EDTA-free protease inhibitor cocktail 1x (1 tablet, Roche). Bacterial cells were disrupted using high-pressure French Press homogenizer at 20000 psi, following centrifugation (Beckman Coulter Avanti J30I, with JA-25.50) at 20000rpm (48000g) at 4°C for 1 hour to remove insoluble material. The bacterial cell extract was heated for 15 minutes at 75°C in a water bath and then again centrifuged (Beckman Coulter Avanti J30I, with JA-25.50) at 20000rpm, 4°C for 1 hour to remove precipitated proteins. After every centrifugation 1mM PMSF was added to the supernatant.

Next, cation-exchange (CEX) chromatography was performed in a 20mL bed ($V_c$) column (Hiprep SP Fast-Flow, GE Healthcare) using a fast protein liquid chromatography (FPLC) ÄKTA purifier UPC 10 system (GE Healthcare). Flow rate was set to 2mL/min for column equilibration in buffer A (50mM Tris-HCl pH 6.5 and 1mM EDTA). 20mL of heat-treated Tau extract was loaded, collecting 5mL fractions and allowing complete elution of unbound protein fraction. When the absorbance at 280 nm returns to baseline values, a linear gradient of 2 $V_c$ up to 1M NaCl is set, using Buffer B (Buffer A + 1M NaCl). Eluted fractions (10µl) obtained during the CEX elution were analyzed by SDS-PAGE and those containing Tau (eluted at ~0.5M NaCl) were pooled into a single fraction. The buffer of this Tau containing faction was -exchanged through successive washing with buffer A in an Amicon centrifuge filter (Millipore, Merk) with a cut-off of 3kDa, and concentrated to around 10 mL (4-5x the initial volume). Tau samples were aliquoted, labelled and stored at -20°C. Frozen fractions were then lyophilized and stored at -20°C.

A size exclusion chromatography (SEC) was then performed in a S200 column (GE Healthcare) mounted in a FPLC ÄKTA purifier UPC 10 system (GE Healthcare), with a prior treatment of the lyophilized samples with 500µL containing 7.6M urea (Sigma-Aldrich) and 50mM dithiothreitol (DTT, Applichem) following 1 hour incubation at room temperature. The sample was injected (500µL loop) and eluted at 0.5mL/min with 50mM Tris-HCl pH 7.4, pooling 0.5 mL fractions. All samples were centrifuged (14800rpm for 5 minutes) in a benchtop microcentrifuge before injection into column to remove particles in suspension. All buffers were passed through Chelex resin (Bio-Rad) to remove contaminant trace metal ions. The band corresponding monomeric Tau was aliquoted and lyophilized as described above. Tau concentration was determined spectrophotometrically using $\varepsilon_{hTau441}^{280nm}$ =7550 $M^{-1}cm^{-1}$.

### 2.1.2 S100B expression and purification

S100B was expressed and purified using a previously established protocol [104]. To overexpress S100B, BL21 – Gold (DE3) competent *Escherichia coli* (Stratagen) cells were transformed with 1µL of the plasmid pGEMEX-2 – S100B encoding the wild-type human S100B protein. Cells were then treated by heat shock (incubating on ice for 30 minutes, following by 20 seconds at 42°C and incubation on ice for 2 minutes). 900µL of LB were added and incubated (37°C at 250rpm) for 1 hour. The cells transformed in plaques with LA medium containing 100µg/mL ampicillin (Nzytech) were grown overnight at 37°C. From one isolated colony it was inoculated 100mL of LB medium with 100µg/mL ampicillin at 37°C, 150rpm, overnight. 10mL of the overnight growth was added to 500mL of LB medium containing 100µg/mL of ampicillin at 37°C, 150rpm. When $OD_{600nm}$ = 0.6 - 1 it was induced with 1mM of IPTG and incubated at 37°C, 150rpm overnight. Cells were recovered by centrifugation (Beckman Coulter J2-21, with JA-14 rotor) at 8000rpm (10000g), 4°C for 10 minutes and stored at -20°C.

Cells pellet was thawed and resuspended with resuspension buffer (50mM Tris-HCl (nzytech) pH 7.4 and 5mM $MgCl_2$ (USB), DNAse (PanReac), 0.5mM phenylmethanesulfonyl fluoride (PMSF, Roth). Bacterial cells were disrupted using high-pressure French Press homogenizer at 20000 psi and centrifuged (in a 45Ti rotor, Beckman) at 42000rpm (204000g), 4°C for 45min to remove insoluble material. The supernatant was diluted 2x its volume with phenylsepharose buffer A (50mM Tris-HCl pH 7.4 and 5mM $CaCl_2$) and it was left in slow agitation overnight. The PhenylSepharose 6 prepacked column (HiPrep Phenyl Fast-Flow, GE Healthcare) mounted in a ÄKTA purifier UPC 10 system (GE Healthcare) was equilibrated with the same buffer and column loading was performed using a superloop. The elution of S100B was done by buffer switch to phenylsepharose buffer B (50 mM tris pH 7.4, 10 mM EDTA).

Apo form of S100B dimer was obtained through sample incubation at 37°C for 2 hours with a 300-fold excess of DTT and 0.5 mM EDTA (Sigma-Aldrich) and elution in a Superdex S75 (GE Healthcare) with 20 mM Tris-HCl pH 7.4 and 150 mM NaCl buffer. All samples were centrifuged (14800rpm for 5 minutes) in a benchtop microcentrifuge before injection into column to remove particles in suspension. All buffers were passed through Chelex resin (Bio-Rad) to remove contaminant trace metal ions. The peak corresponding to dimer was collected and concentrated with an Amicon centrifuge filter with a 3KDa cutoff and stored at -20°C. and the concentration was calculated from molar extinction coefficient for S100B dimer concentration was determined spectrophotometrically using $\varepsilon_{hTau441}^{280nm} = 2980$ $M^{-1}cm^{-1}$.

## 2.2 hTau441 monomer isolation analysis

### 2.2.1 hTau441 monomer isolation – Size exclusion chromatography

1mg of pure lyophilized hTau441 samples were resuspended in four different conditions: 50mM Tris-HCl pH 7.4 (nzytech) water chelex (Chelex resin, Bio-Rad); 7M guanidine hydrochloride (Sigma-Aldrich); 8M urea (Sigma-Aldrich); 7.6M urea and 50mM dithiothreitol (DTT, Applichem). Solutions (final volume of 500µL), were incubated for 1 hour at room temperature. After that, the samples were injected in a Superdex 200 column (GE Healthcare) mounted in a FPLC ÄKTA purifier UPC 10 system (GE Healthcare). The samples were eluted at 0.5mL/min and collected 500µL aliquots with 50mM Tris-HCl pH 7.4 water chelex as running buffer, as above.

### 2.2.2 Steady-state thioflavin-T fluorescence - hTau441 monomer isolation analysis

After the hTau441 monomer isolation analysis treatments, the protein concentration was determined spectrophotometrically as above. Monomeric hTau441 was diluted to a final concentration of 2µM and was subsequent added 5µM thioflavin-T (ThT, Sigma–Aldrich) with 50mM Tris-HCl (nzytech) pH 7.4 buffer, to a final volume of 400µL. The measurement was performed in a Jasco FP-8200 Spectrofluorimeter (Jasco) using a fluorescence cuvette with a 10x2mm (Hellma, 104.002F-QS) light path. The excitation wavelength was 440nm and the emission spectra was record between 450-600nm with 5 spectra accumulations.

## 2.3 S100B:Tau size exclusion chromatography binding assay

The size exclusion chromatography (SEC) was performed in a Superdex S200 Tricorn (GE Healthcare) column mounted in a FPLC ÄKTA purifier UPC 10 system (GE Healthcare) with an injection volume of 500µL at a flow of 0.5mL/min with 50mM Tris-HCl (nzytech) pH 7.4 water chelex (Chelex resin, Bio-Rad) as running buffer. The samples were prepared with a final concentration of 4µM for each protein and a 4x concentration for each metal ions (16µM): $CaCl_2$ (Fluka) and $ZnCl_2$ (Merk). After adding all compounds of the mixture let incubate overnight at 4°C. The hTau441 sample for this SEC was readily used after Tau monomer isolation (see hTau441 expression and purification). All samples were centrifuged at 14800rpm for 5 minutes (Microcentrifuge PRISM) before injection into column.

## 2.4 Circular dichroism spectroscopy

Circular dichroism (CD) spectroscopy was performed in Jasco CD spectropolarimeter (Jasco J-1500) with 50mM Tris-HCl (nzytech) pH 7.4 with water chelex (Chelex resin, Bio-Rad) and to a final volume of 200µL. CD samples were prepared to have a protein concentration of 0.1mg/mL (limit of detection of CD spectrometer) as 1x concentration and knowing that S100B (21.4 kDa) at 5µM is at around 0.1mg/mL, all the samples were prepared in ratio to 5µM as 1x concentration. The hTau441 sample for CD measurement was readily used after Tau monomer isolation (see hTau441 expression and purification) and added to sample mixture where it stayed 30 minutes incubating on ice. The baseline was done using 50mM Tris-HCl

pH 7.4 water chelex. 200µL samples were measured in CD far-UV cuvettes with a 0.1cm of optical pathway (Hellma) programmed to measure with a wavelength range from 200 to 260nm, 8 accumulations, 0.5nm of data pitch, 1nm bandwidth, 100nm/min of scanspeed and a programmed temperature of Peltier-controlled thermostated cell support, of 20°C. If the high tension (HT) voltage values were equal to or above 600 V, there are not enough photons being sampled by the photomultiplier tube to measure a reliable or valid CD signal, so these data points were discarded [105].

### 2.5 Attenuated total reflection - Fourier-transform infrared spectroscopy

Fourier-transform infrared spectroscopy was performed in a Bruker Tensor FTIR instrument equipped with an attenuated total reflection cell (Harrick) (ATR-FTIR) in order to assess secondary structure of protein samples. The final volume used was 40µL and S100B was used at 40µM, however hTau441 was used within a concentration range (4-40µM). Metal ions like $CaCl_2$ (Fluka) and $ZnCl_2$ (Merk) were 4x more concentrated than S100B, that is, 160µM. The hTau441 sample for FTIR measurements was readily used after Tau monomer isolation (see hTau441 expression and purification). After the compounds mixture the samples incubated for 30 minutes on ice. The baseline was done using 50mM Tris-HCl (Nzytech) pH 7.4 water chelex (Chelex resin, Bio-Rad) plus the metal ion used ($CaCl_2$ or $ZnCl_2$) in the experiment. 20µL sample were analysed. The spectra were obtained from 4000 to 900 $cm^{-1}$, with a 4$cm^{-1}$ resolution and a 120 sample scans.

### 2.6 hTau441 aggregation kinetics

hTau441 aggregation assays followed by Thioflavin-T (ThT, Sigma–Aldrich) fluorescence were performed in a FluoSTAR OPTIMA (BMG Labtech) microplate fluorimeter. Half-area 96-well polyethylene glycol-coated black polystyrene microplates (nonbinding surface) (Corning, ref. 3881) with a clear-bottom in order to allow the bottom-reading measurement were used. The microplates were sealed with transparent foil to avoid evaporation. hTau441 used in these experiments was readily used after hTau441 monomer isolation (see hTau441 expression and purification) and its experimental concentrations varied between 0.5 to 50 µM. S100B protein concentration used in these experiments was 0.5x, 1x or 4x the concentration of hTau441. The concentration of heparin (heparin sodium salt from porcine, Sigma–Aldrich), that allowed the *in vitro* enhanced aggregation of hTau441, with best effect was 0.5mg/mL. The concentration of DTT (Applichem), a powerful reductant that allowed the maintenance of a higher monomer population of hTau441, was 1mM [47]. The NaCl (Nzytech) concentration was first assessed and then was fixed to 50mM in all subsequent experiments [47]. The concentration of PMSF (Roth), a protease inhibitor that reduced the formation of hTau441 fragments, used in these experiments was of 1mM. The reporter dye, ThT, was used at 75µM and the metal ions ($CaCl_2$ (Fluka) and $ZnCl_2$ (Merk)), when added, were used in a final concentration of 1.1mM. All samples were prepared using 50mM Tris-HCl (nzytech) pH 7.4 water chelex (Chelex resin, Bio-Rad).

Samples were analysed with an excitation filter of 440nm and an emission of 480nm with a gain of 1000 and aggregation was performed at a 37°C with an orbital shaking at 600rpm for 300 seconds before each measurement.

## 2.7 Analysis of aggregation kinetic data

The hTau441 heparin-induction fibrilization follows a typical amyloid growth curve that is described with an initial lag phase (nucleation reaction), followed by a growth phase (elongation reaction) and ending with a plateau phase (equilibrium). Several parameters can be obtained from a growth curve such as time of lag phase ($t_{lag}$) and apparent reaction rate ($K_{app}$), and these values are calculated from the sigmoidal fitting of the experimental data points by the equation (Equation 2.1) [106]:

$$Y = (y_i + m_i x) + \frac{(v_f + m_i x)}{\left(1 + exp^{-\left(x - \frac{X_0}{\tau}\right)}\right)} \qquad \text{(Equation 2.1)}$$

Where $Y$ is fluorescence intensity, $x$ is the time, $X_0$it is $t_{50}$. Lag phase time is calculated by $t_{lag} = X_0 - 2\tau$ and the apparent reaction velocity is calculated by $K_{app} = 1\tau$.

## 2.8 AFM bioimaging

Aggregated Tau samples were deposited on the surface of freshly cleaved mica (Agar Scientific) for 30 min, washed 3 times with 500 µL of deionized filtered water, to remove unwanted contaminants, and dried with a nitrogen source and then subjected to AFM analysis. The samples were prepared from end time points of the aggregation kinetic obtained in distinct conditions. The volume applied on mica was 20 µL with a final concentration between 0.5 – 1.0 µM of initial protein concentration. The AFM measurements and analysis were performed by collaborators at the BioISI Magnetic Nanosystems Group / Department of Physics, also at FCUL (see acknowledgments).

# III. RESULTS AND DISCUSSION

## 3.1 Purification of recombinant human Tau441

### 3.1.1 Purification of human hTau441

The recombinant full-length human Tau (hTau441) expression was performed using a plasmid with the gene encoding for the longest human isoform of the protein (441 amino acids). This plasmid was transferred to *E. coli* allowing the expression of hTau441 after bacterial induction. The bacterial growth was done in minimal medium (M9 medium) in order to minimize the formation of hTau441 fragments, once that this protein is very sensitive to proteases and the use of nutrient-rich medium prone this event.

After bacterial lysis, the soluble protein extract was incubated at 75°C for 15 minutes, to precipitate contaminant proteins, taking advantage of the high thermal stability of hTau441, which remains soluble. Cation exchange chromatography was then employed to purify hTau441 (figure 3.1 – A). The hTau441 containing fraction elutes at ≈ 0.5 M NaCl (peak 5) as determined from SDS-PAGE analysis of eluting bands (figure 3.1 – B, lane 5). hTau441 migrates as an apparent 66 kDa band (MW 45.9 kDa), a known characteristic of intrinsically disordered proteins whose extended conformations and high mobility increase the hydrodynamic radius of the conformational ensembles resulting in abnormal electrophoretic migrations [103]. Fraction 5 contains semi-purified hTau441 still with some smaller fragments resulting from self-proteolysis. At this stage the typical yield is 14mg of partly purified hTau441 per liter of culture.

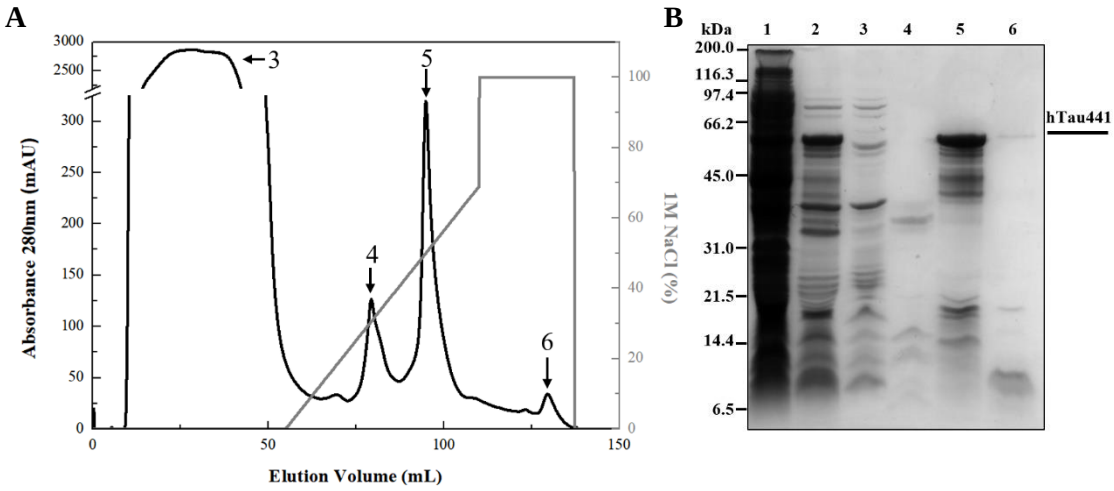


**Figure 3.1: Purification hTau441 cation exchange chromatogram and SDS-PAGE analysis. A –** Size exclusion chromatogram (HiPrep SP Fast-Flow column): 3 – Unbound fraction; 4 – First elution peak after buffer switching program start; 5 – Second elution peak (elution of hTau441); 6 – Last elution peak. **B –** SDS-PAGE gel of first set of purifications steps: 1 – Soluble protein extract; 2 – Supernatant after heating at 75°C (injected in SP FF column); 3 – Unbound fraction; 4 – First elution peak after buffer switching program start; 5 – Second elution peak (elution of hTau441); 6 – Last elution peak.

### 3.1.2 Optimizing the purification of monomeric hTau441

Subsequent studies require a homogenous preparation of pure monomeric hTau441. In order to minimize hTau441 fragmentation we have resuspended the semi-purified lyophilized hTau441 fraction form the previous step in four different buffer systems containing with different strong chaotropic agents and reductant: 50mM Tris-HCl pH7.4; 7M GndHCl; 8M Urea; 7.6M Urea and 50mM DTT. Samples were incubated during 1 hour at room temperature and subsequently resolved in SEC (Fig 3.2, A). Eluted fractions were tested for amyloidogenicity as inferred from their thioflavin-T (ThT) fluorescence emission (figure 3.2, B).

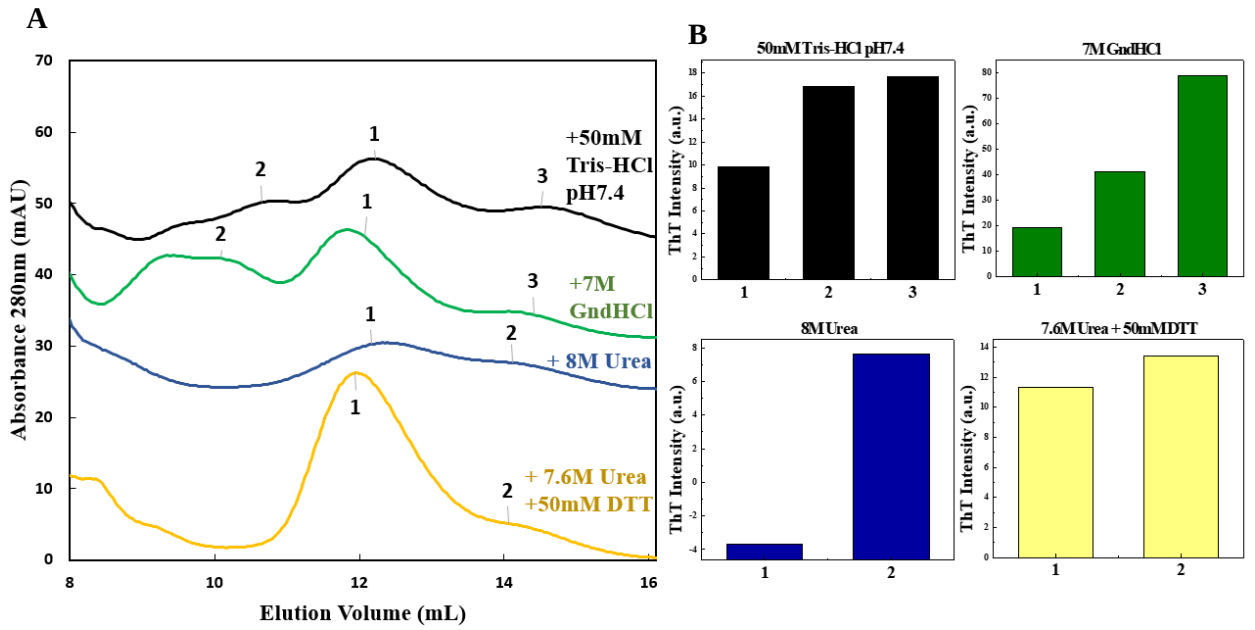


**Figure 3.2: hTau441 monomer isolation assessment. A –** SEC chromatograms of 1mg of hTau441 resuspended in 4 different conditions; **B** – Thioflavin-T fluorescence of samples, resuspended in 4 different conditions, after elution from SEC; Excitation wavelength = 440nm and emission wavelength = 495nm. Conditions of resuspension of 1mg hTau441: 50mM Tris-HCl pH7.4 (black); 7M GndHCl (green); 8M Urea (blue); 7.6M Urea + 50mM DTT (yellow). The numbers in chromatogram are the peaks selected for ThT fluorescence that correspond to the columns number.

It can be observed that the peak eluting around 12.5mL (figure 3.2, A peaks 1) has always the lowest ThT fluorescence (figure 3.2, B) when compared to the other peaks of the same chromatogram, meaning this is the least amyloidogenic hTau441 species regardless of treatment. The best condition of resuspension is the combined use of 7.6M urea and 50mM DTT (figure 3.2), once this treatment originates the lowest relative quantity of other protein peaks, as well as maintaining the lower amyloidogenicity of main peak.

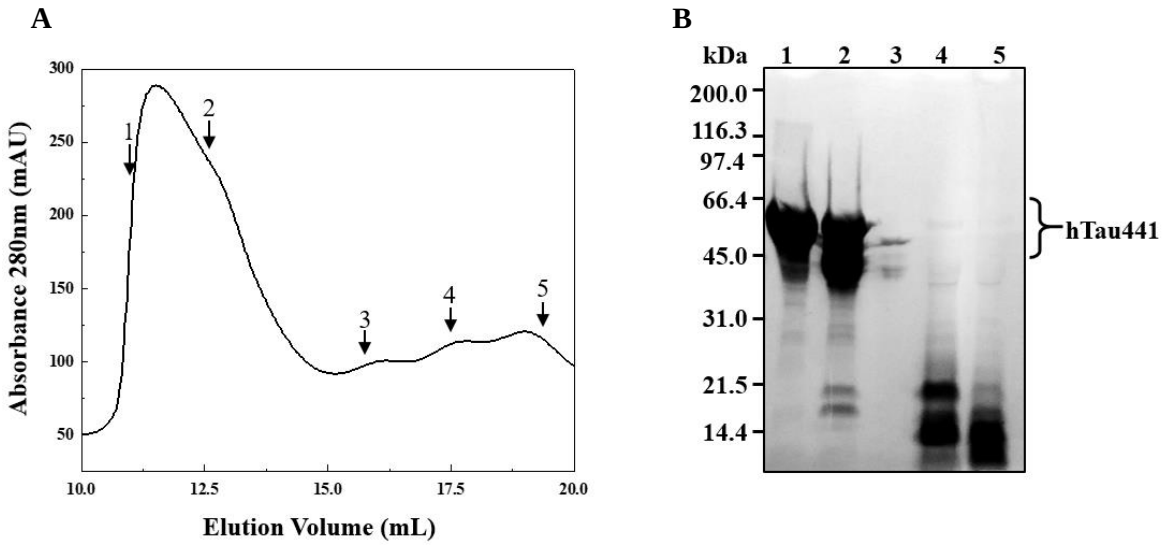


**Figure 3.3: SEC chromatogram and SDS-PAGE gel of hTau441 monomer isolation. A –** SEC chromatogram of treated hTau441 sample with 7.6M urea and 50mM DTT; **B** - Samples of the peaks were run on an SDS-PAGE gel. The numbers of peaks in the chromatogram correspond to the samples analyzed in SDS.

For the purification of the monomer a combined treatment of 7.6M urea and 50mM DTT was performed two times before each experiment using hTau441. One after the cation exchange chromatography and other before hTau441 experimental use, always lyophilizing between these purification steps. The resulting chromatogram and SDS analysis (figure 3.3) allow the selection of the peak containing monomeric hTau441. The final yield of this highly purified hTau441 monomer is 4mg per liter of culture.

## 3.2 Recombinant human S100B dimer purification

### 3.2.1 S100B expression and purification

Human S100B was expressed overnight in *E. coli*. The purification first step after bacterial lysis, took advantage of $Ca^{2+}$-binding sites of S100B that allow the protein structure rearrangement and exposure of hydrophobic regions capable of interacting with PhenylSepharose 6 prepacked column [104]. So, first the soluble protein extract was diluted in a buffer containing $Ca^{2+}$ and then an affinity chromatography was performed. S100B was eluted by switching the elution buffer to one containing EDTA, instead of $Ca^{2+}$. By chelating this metal ion, it was promoted the S100B detach of the resin and its consequent elution (figure 3.4). As can be seen in SDS-PAGE gel (figure 3.4 – B) (before the 6.5kDa protein marker, MW(S100B) = 10.7kDa) S100B is more purified than the injected extract.

After recovered all assay tubes corresponding to S100B elution peak it was assessed the final yield of 46.6mg of S100B per liter of culture. The S100B samples were frozen at -20°C until apo S100B preparation.

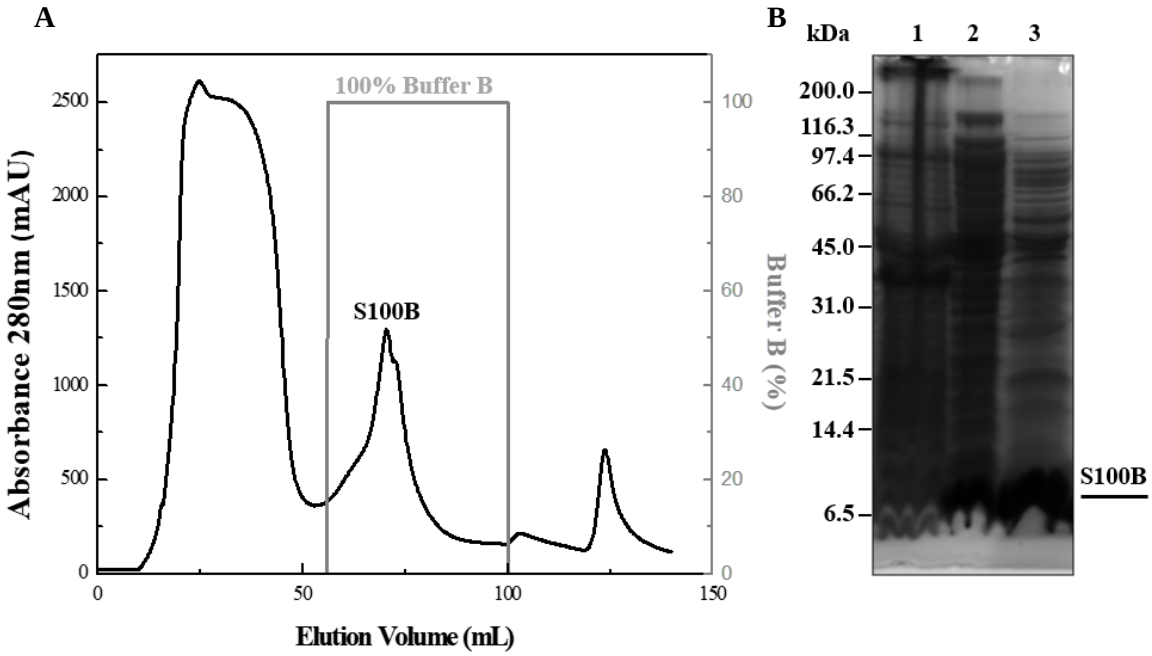


**Figure 3.4: Purification S100B affinity chromatogram and SDS-PAGE analysis. A –** S100B purification by affinity chromatography eluting after the buffer switching allowing the S100B detach of the column. **B –** SDS-PAGE gel of samples during the S100B purification: 1 – Sample of pellet after bacterial lysis; 2 – Sample of supernatant after bacterial lysis (injected in column); 3 – S100B peak (collected fraction).

### 3.2.2 Apo S100B preparation

Once that S100B homodimer is able to bind metal ions such as $Ca^{2+}$ and $Zn^{2+}$, and that binding induce conformational changes and increase of binding ability to others protein partners [65, 107], it was necessary to prepare an apo S100B dimer [64]. To achieve this, S100B samples were prepared by incubation at 37°C for 2 hours with a 300-fold excess of dithiothreitol (DTT) and 0.5 mM EDTA, to chelate all the metal ions and breach the protein disulfide links. Then a size exclusion chromatography (SEC) was performed using a Superdex 75 column (figure 3.5 – A), to eliminate DTT and EDTA, as well as some protein contaminants (figure 3.5 – B). Tubes corresponding to apo S100B dimer (Figure 3.5 – A, S100B dimer peak) were recovered and stored until use at -20°C.

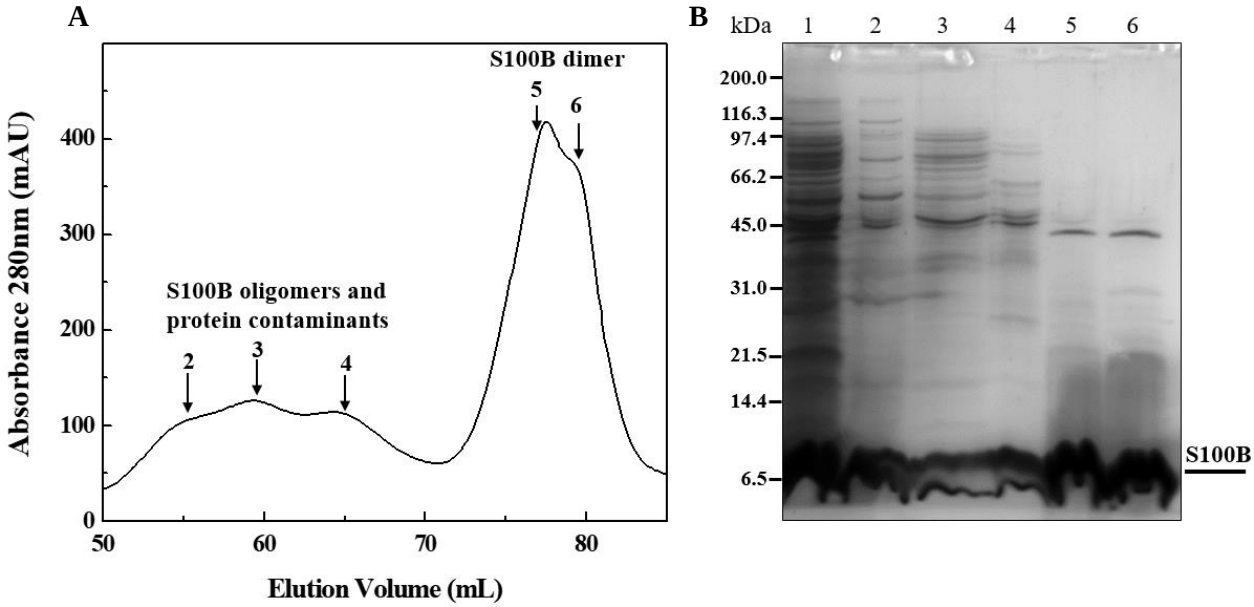


**Figure 3.5: Apo S100B dimer preparation and SDS-PAGE analysis. A –** SEC in a Superdex 75 column of S100B after apo preparation treatment. The numbers correspond to the peaks analyzed in SDS-PAGE gel. **B –** SDS-PAGE gel of samples during the apo S100B preparation: 1 – Sample after affinity chromatography (injected in S75); 2 – Sample eluting at 56mL volume; 3 – Sample eluting at 60mL volume; 4 – Sample eluting at 66mL volume; 5 – Sample eluting at 78mL volume; 6 – Sample eluting at 82mL volume.

By analyzing SDS-PAGE gel of S100B apo preparation (figure 3.5, B) (before the 6.5kDa protein marker, MW(S100B) = 10.7kDa), can be concluded that S100B is highly purified (> 90%) (figure 3.5, B lanes 5 and 6) and the presence of other bands has very low intensity compared with S100B band. These bands can be observed because of protein overload in gel well, that should have not sufficient intensity when the amount of protein loaded is lower.

## 3.3 hTau441 and S100B interaction and metal ions effects

Tau and S100B interaction was previously proposed from assays using semi purified protein extracts from Alzheimer's disease (AD) patients brains which suggested that this interaction was zinc-dependent [108-110]. S100B is a protein that binds calcium and zinc ions whose coordination triggers structural modifications and interactions sites [85, 111]. We have used gel filtration, circular dichroism and attenuated total reflection Fourier-transform infrared spectroscopy to assess interactions between S100B and Tau, and to determine the influence of metal ion binding to S100B on the interacting proteins.

### 3.3.1 Assessing formation of a S100B/Tau complex by SEC

To assess if S100B and hTau441 interact, forming a protein complex stable enough to resist size exclusion chromatography (SEC), samples of 4μM of each protein were mixed with $CaCl_2$ and/or $ZnCl_2$ or in absence of metal ions and incubated overnight at 4°C, along with corresponding controls. After incubation the samples were centrifuged and resolved in by SEC (figure 3.6). If a complex would be formed, then we would expect to observe the elution of a band corresponding to a complex with a higher hydrodynamic radius.

In the assay in the absence of added metals, the mixture behaved roughly as sum of the individual proteins. However, there is a higher intensity of bands eluting at lower volumes (higher radii) compatible with larger protein species (figure 3.6, A). In the assay in the presence of $CaCl_2$ condition the result is not similar to the other conditions. It could be due to the condition and be a trustworthy result, or some unexpected event took effect during the chromatography that does not allow the correct visualization of the phenomenon that actually happened (figure 3.6, B). Anyway, this experimental condition should be repeated. In the assay in the presence of $ZnCl_2$ the chromatogram obtained is very similar with the apo condition. First it seems that the mixture chromatogram results roughly as the sum of the individual proteins, but there is present higher intensity of bands eluting also at lower volumes, like in the prior explanation (figure 3.6, C). In the presence of both metal ions ($CaCl_2$ and $ZnCl_2$) it is possible to observe a more evident (higher intensity) of bands eluting at lower volumes, as well as a "consumption" of S100B control peak, that may be present in a possible interaction when hTau441 and these ions are present.

We tried to evaluate the integration of the obtained bands, that could have helped in quantitative protein analysis, however the range of concentrations is small to use in this analysis, making it susceptible to perturbances of the chromatography. We also tried to evaluate the presence of hTau441 and S100B in the eluted peaks with lower volumes, that were compatible with larger protein species, through SDS-PAGE. Unfortunately, protein concentration was probably very low to have distinct bands. These analyses could be done, however it is necessary a set of experimental optimizations.

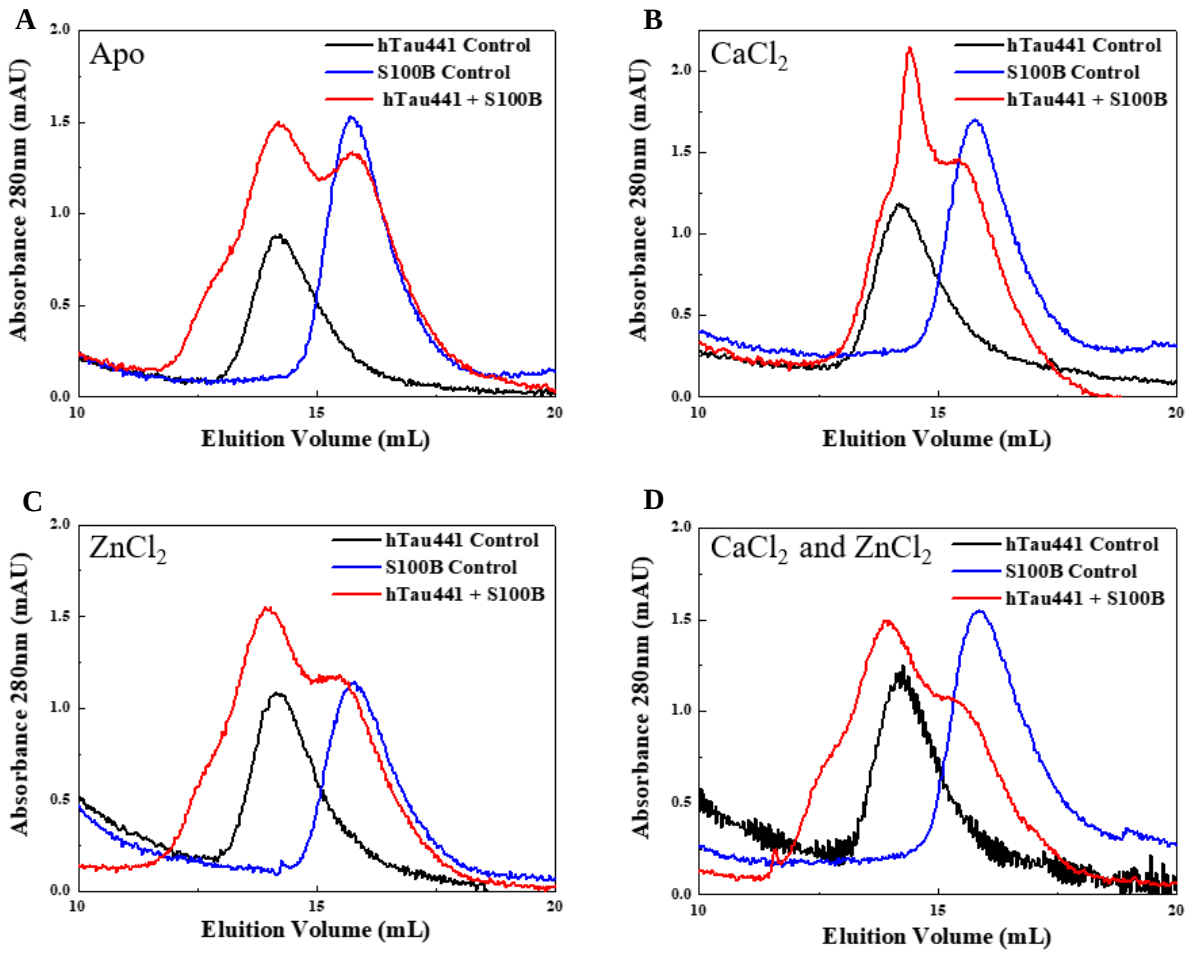


**Figure 3.6: Size exclusion chromatograms from SEC assay of S100B with hTau441 in absence of metals ion and presence of $CaCl_2$ and/or $ZnCl_2$.** Size exclusion chromatograms from SEC assay to follow the protein complex formation between S100B (4µM) and hTau441 (4µM) in absence of metal ions (**A**), $CaCl_2$ (**B**), $ZnCl_2$ (**C**) or both metal ions (**D**) presence. Samples prepared with 50mM Tris-HCl pH 7.4 water chelex to a final concentration of 4µM of each protein and 16µM of each metal ion; hTau441 alone with/without metal ion (black line), S100B alone with/without metal ion (blue line) and hTau441 and S100B with/without metal ion (red line).

### 3.3.2 Far UV circular dichroism monitored binding titration

To evaluate conformational changes arising upon interaction of hTau441 with S100B, we carried out titration experiments monitored by far ultraviolet circular dichroism (far UV-CD) spectroscopy. It is known that the far UV-CD spectrum of S100B is typical of an α-helical protein, with two minima negative bands at 208nm and 222nm. hTau441 has a far UV-CD spectrum of a typical random coil protein, with a negative band at 200nm (figure 3.7, A-C). Again, we carried out experiments in the apo and metal bound states.

The data from CD signal at 222nm of hTau441 titration in S100B presence (figure 3.7, D-F) was calculated from spectra values subtracted with hTau441 alone, at same wavelength, once that hTau441 had a contribution to the signal itself. The behavior of apo and 4x$ZnCl_2$ treatments have a similar profile, with a change of the CD signal at 222nm only with a higher ratio hTau441/S100B, when compared to 4x$CaCl_2$ treatment, that change with a much lower ratio.

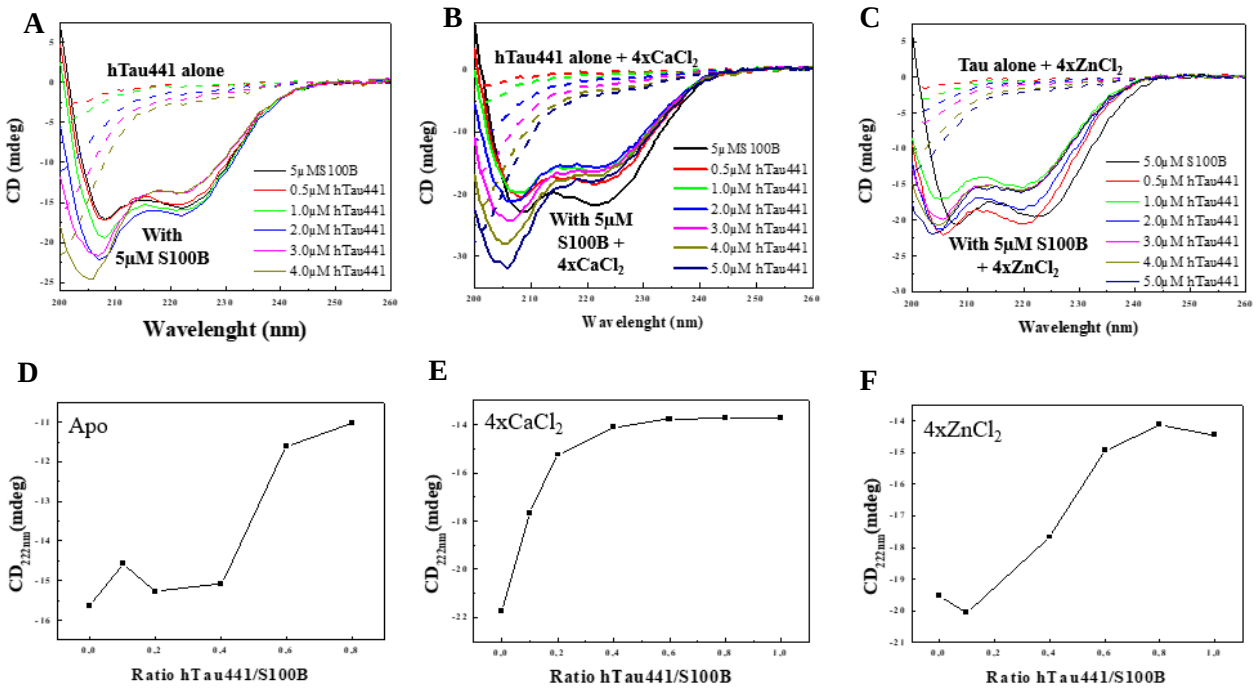


**Figure 3.7: Far UV circular dichroism of S100B titration with hTau441 in absence of ion metals and presence of $CaCl_2$ or $ZnCl_2$. A-C –** Far UV-CD spectra of hTau441 alone (dashed line) and hTau441 titration in 5µM S100B presence (solid line), in apo conditions (**A**), 4x$CaCl_2$ presence (**B**) and 4x$ZnCl_2$ presence (**C**); **D-F –** CD signal at 222nm of hTau441 titration in S100B presence, in apo conditions (**D**), 4xCaCl2 presence (**E**) and 4xZnCl2 presence (**F**). Samples were incubated for 30 minutes on ice before measurement. hTau441 concentrations used were 0.5µM (red), 1µM (green), 2µM (blue), 3µM (pink), 4µM (dark yellow) and 5µM (dark blue). The S100B sample (black solid line) was at a constant concentration of 5µM.

The hTau441 protein does not have gain of structure when interact with S100B in apo condition, in the presence of 4x$CaCl_2$ or 4x$ZnCl_2$ as seen for other proteins like p53 or A-beta peptide (Aβ) [64, 112] (figure 3.7, A-C). On the contrary it appears to have a contribution in loss or relaxation of S100B α-helical structure, once that the CD signal at 222nm seems to rise in presence of higher ratios of hTau441/S100B and in all metal ions presence or absence conditions (figure 3.7, D-F). However, it is promoted by $CaCl_2$ (figure 3.7, E) when compared with remaining conditions.

These observations can represent a possible binding of these proteins that can be followed by loss or relaxation of S100B α-helical structure (figure 3.7, A-C). This event is promoted by the presence of calcium, possibly by improving the binding of hTau441 and S100B.

### 3.3.3 ATR-FTIR monitored binding titration

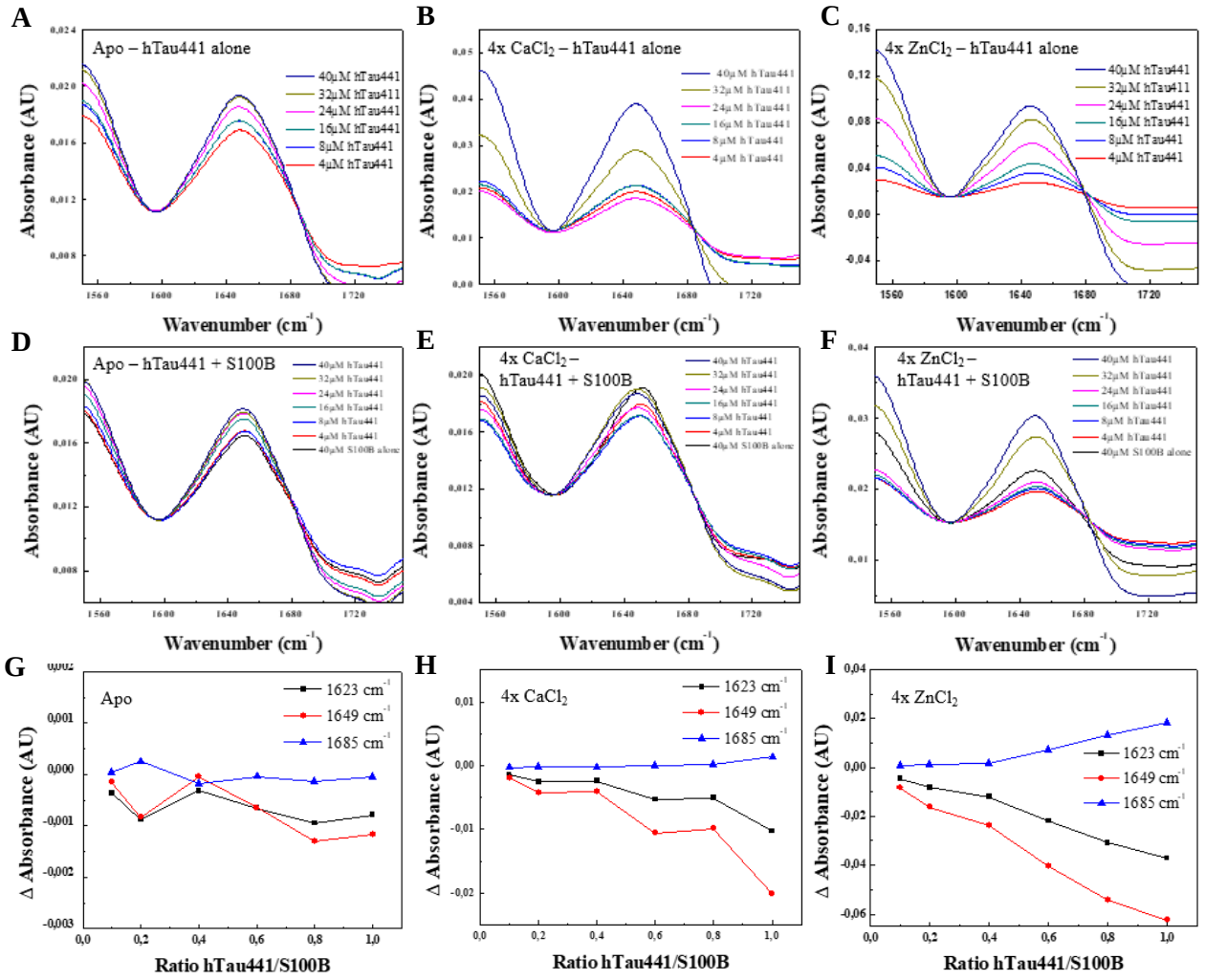


**Figure 3.8: ATR-FTIR of S100B titration with hTau441 in absence of ion metals and presence of $CaCl_2$ or $ZnCl_2$. A-C –** ATR-FTIR spectra (amide I band) of hTau441 alone, in apo conditions (**A**), 4x$CaCl_2$ presence (**B**) and 4x$ZnCl_2$ presence (**C**); **D-F** – ATR-FTIR spectra (amide I band) of hTau441 titration in 40μM S100B presence (black line), in apo conditions (**D**), 4x$CaCl_2$ presence (**E**) and 4x$ZnCl_2$ presence (**F**); **G-I –** Titration of hTau441 in S100B presence followed by 1623, 1649 and 1685 $cm^{-1}$ wavelengths variation. The plots values represent the difference between hTau441 with S100B spectra and hTau441 alone spectra, at those wavelengths, in apo conditions (**G**), 4xCaCl2 presence (**H**) and 4xZnCl2 presence (**F**). Samples were incubated for 30 minutes on ice before measurement. hTau441 concentrations: 4μM (red), 8μM (blue), 16μM (dark cyan), 24μM (magenta), 32μM (dark yellow) and 40μM (dark blue). The S100B sample (black line) was at a constant concentration of 40μM. Metal ions concentration 160μM.

We have also studied the S100B:hTau441 interactions using ATR-FTIR. Using this method, it is possible to distinct α-helical from β-sheet structures through amide I band analysis (that results from the C=O stretching vibrations of the peptide bond), however is more difficult to distinct α-helical from random coil structure, once they have a more overlapped absorbance FTIR spectra.

Protein secondary structure identification, by ATR-FTIR spectroscopy, of samples in aqueous solution, the amide I band (1600-1700$cm^{-1}$) of α-helix is around 1650 $cm^{-1}$ (S100B) and of unstructured conformation is around 1640 $cm^{-1}$ (native Tau) and of β-sheet is at ~1630 $cm^{-1}$ as well as ~1685 $cm^{-1}$ [113].

After spectra acquisition, the data was normalized to one wavelength point (around 1600 $cm^{-1}$) (figure 3.8, A-F). Then, to follow the gain and loss of protein secondary structure, spectra values of hTau441 with S100B (figure 3.8, D-F) were subtracted with spectra values of hTau441 alone (figure 3.8, A-C). From these new data, the change of absorbance with the increase of hTau441/S100B ratio was followed through 1623, 1649 and 1685 $cm^{-1}$ wavelength values in the three conditions (apo, $CaCl_2$ and $ZnCl_2$) (figure 3.8, G-I).

In apo condition there is not a significant change in overall secondary structure. It only can be observed an attenuated loss in α-helical/random coil structure ($1649cm^{-1}$), but not a gain of β-sheet when followed by $1685cm^{-1}$ wavelength (figure 3.8, G). In presence of $4xCaCl_2$ it can be observed a greater loss of α-helical/random coil structure with higher hTau441/S100B ratio values, by following the $1649cm^{-1}$ absorbance variation values. However, the β-sheet structure does not vary with the ratio (figure 3.8, H). In presence of $4xZnCl_2$ it can be observed an even greater loss of α-helical/random coil structure as well has a great increase in the β-sheet structure with the ratio increasing (figure 3.8, I). This is probably due to hTau441 structural changes, since its aptitude to aggregate in zinc presence.

These set of results suggests, as similar to CD data, that the loss of S100B structure can be due to interaction with hTau441 protein and that this interaction is promoted by the presence of $Ca^{2+}$.

## 3.4 hTau441 aggregation kinetics analysis

### 3.4.1 hTau441 aggregation induced by heparin

It is known that sulfated glycosaminoglycans can change the conformation of Tau, inducing it to polymerize via the microtubule-binding repeats of individual Tau molecules, resulting in the formation of filaments like those present in AD, without the need for Tau phosphorylation [114].

To assess what is the ideal heparin concentration to induce hTau441 aggregation followed by thioflavin-T (ThT) fluorescence in the experimental conditions, we tested two different concentrations (0.5mg/mL and 1.0mg/mL) within the highly used range in similar experiments [115]. The same conditions were performed with two different heparin concentrations: 0.5 and 1.0 mg/mL. The samples were left for 122 hours at 37°C with 600rpm of orbital agitation. The hTau441 samples also contained 1mM DTT, to maintain a reducing condition allowing a higher hTau441 monomer population [116].

It is observed, with 0.5mg/mL of heparin that the difference from initial point (0h) and the end-time point (122h) was greater than the difference of 1.0mg/mL of heparin conditions (figure 3.9, A). When these samples were applied on a native gel at 10%, that do not denature proteins or dissociate protein interactions, it can be observed the formation of larger aggregates and fibrils, after 122h, with the 0.5mg/mL condition than with 1.0mg/mL of heparin (figure 3.9, B). Moreover, the samples were applied on an SDS-PAGE tris-tricine gel but treated with a loading buffer without dithiothreitol (DTT) it is observed that higher molecular complex are more present with 0.5mg/mL heparin than with 1.0mg/mL heparin (figure 3.9, C lane 4 and 5).

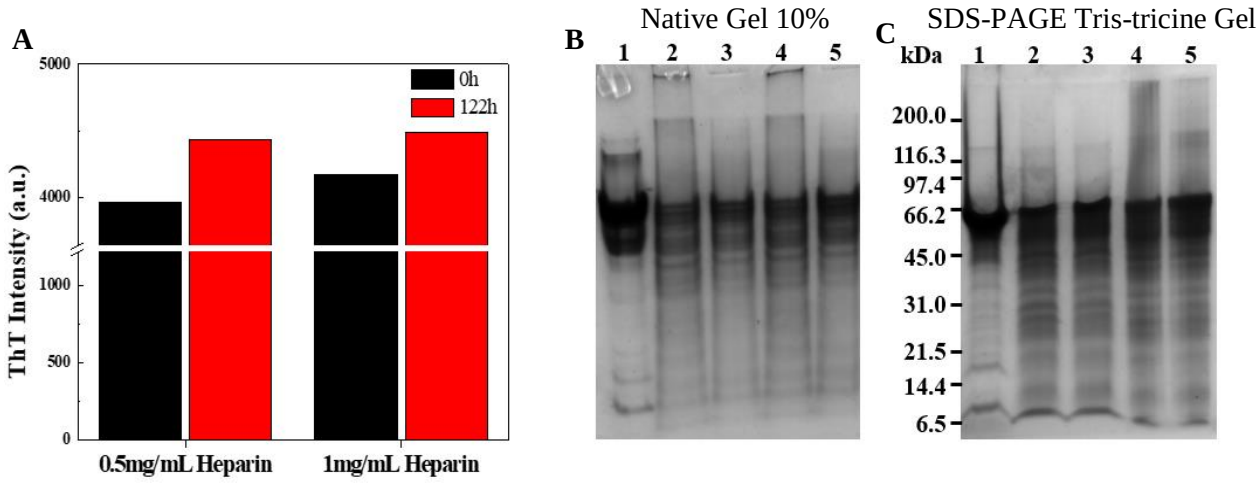


**Figure 3.9: hTau441 heparin-induced aggregation: time zero and end-time point times analysis. A –** ThT intensity of 15µM hTau441 incubation at 37°C for 0h and 122h, with 0.5mg/mL or 1.0mg/mL of heparin; n=3; **B –** Native gel at 10% of end time samples: 1- hTau441 control; 2- 0.5mg/mL heparin end time sample; 3- 1.0mg/mL heparin end time sample; **C** – SDS-PAGE gel of end time samples: 1- hTau441 control; 2- 0.5mg/mL heparin end time sample solubilized in normal loading buffer; 3- 1.0mg/mL heparin end time sample solubilized in normal loading buffer; 4- 0.5mg/mL heparin end time sample solubilized in loading buffer without DTT; 5- 1.0mg/mL heparin end time sample solubilized in loading buffer without DTT. The hTau441 experimental concentration was 15µM also containing 1mM DTT and 75µM ThT. Experimental conditions: 37°C with orbital agitation for 5 min at 600rpm before each measurement with a 440nm excitation wavelength and 480nm emission wavelength.

After this set of experiments the heparin concentration used on subsequent hTau441 aggregation experiments was always 0.5mg/mL.

### 3.4.2 Modulation of hTau441 aggregation by NaCl

Ionic interactions influence hTau441 aggregation, in an optimal concentration range, by stabilization of amino acids charge of the protein, allowing structural changes and exposure of regions that are prone to aggregation. Once that hTau441 is an intrinsically disordered protein (IDP) this effect is even more important to protein-protein interaction and initiation of its aggregation. So, it has been used NaCl to modulate hTau441 aggregation *in vitro* [115, 116]. In order to assess what would it be the best pro-aggregation NaCl concentration, two different hTau441 concentrations (15 and 50µM) were tested in three different conditions: without NaCl, 50mM NaCl and 100mM NaCl (figure 3.10).

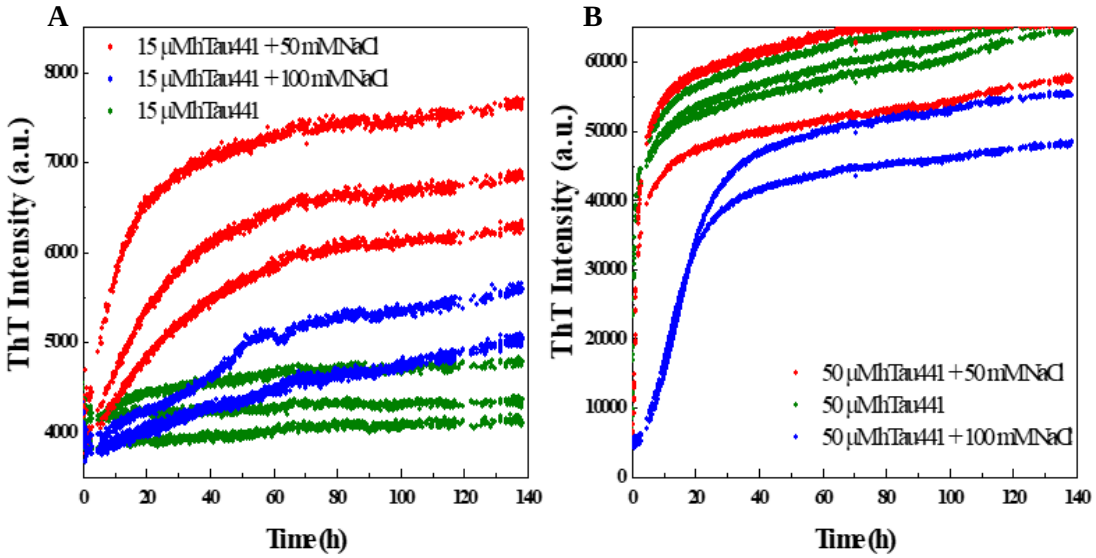


**Figure 3.10: hTau441 aggregation modulated by NaCl.** 15µM (**A**) and 50µM (**B**) hTau441 aggregation with different NaCl concentrations followed by ThT fluorescence. NaCl concentrations: 0µM (green), 50mM (red) and 100mM (blue). The hTau441 experimental sample also contained 1mM DTT, 0.5mg/mL heparin and 75µM ThT. Experimental conditions: 37°C with orbital agitation for 5 min at 600rpm before each measurement with a 440nm excitation wavelength and 480nm emission wavelength.

It is observed that in presence of 50mM NaCl, hTau441 aggregation is faster and that ThT intensity is higher, when compared with other NaCl conditions (figure 3.10). After these observations the NaCl concentration used on subsequent hTau441 aggregation experiments was always 50mM.

### 3.4.3 Modulation of hTau441 aggregation by $CaCl_2$

The presence and homeostasis of metal ions on brain is essential for the normal function and is known that metal dyshomeostasis directly causes neuronal dysfunction, leading to neuronal cell death. Clinical studies have shown elevated levels of copper, iron and zinc ions in post-mortem brain tissues of AD patients [117, 118]. hTau441 aggregation can be modulated by metal ions such as calcium and zinc [52], so we assessed the direct involvement and modulation of these metal ions on hTau441 heparin-induced aggregation in vitro, with optimized conditions.

To assess the calcium kinetic modulation in hTau441 aggregation it was performed the aggregation protocol with different hTau441 concentrations, and in absence or presence of 1.1mM of $CaCl_2$, with the already stablished conditions.

It appears that the lag time (time until the aggregation starts) shifted to lower times with $CaCl_2$ (Figure 3.11 A-B), meaning that the aggregation seems to be promoted by calcium. Estimation of kinetic parameters was performed by fitting to a sigmoidal curve. Results of time of lag phase ($\tau_{lag}$) and reaction rate ($\kappa_{app}$) for all hTau441 alone aggregation conditions are presented in table 3.1.

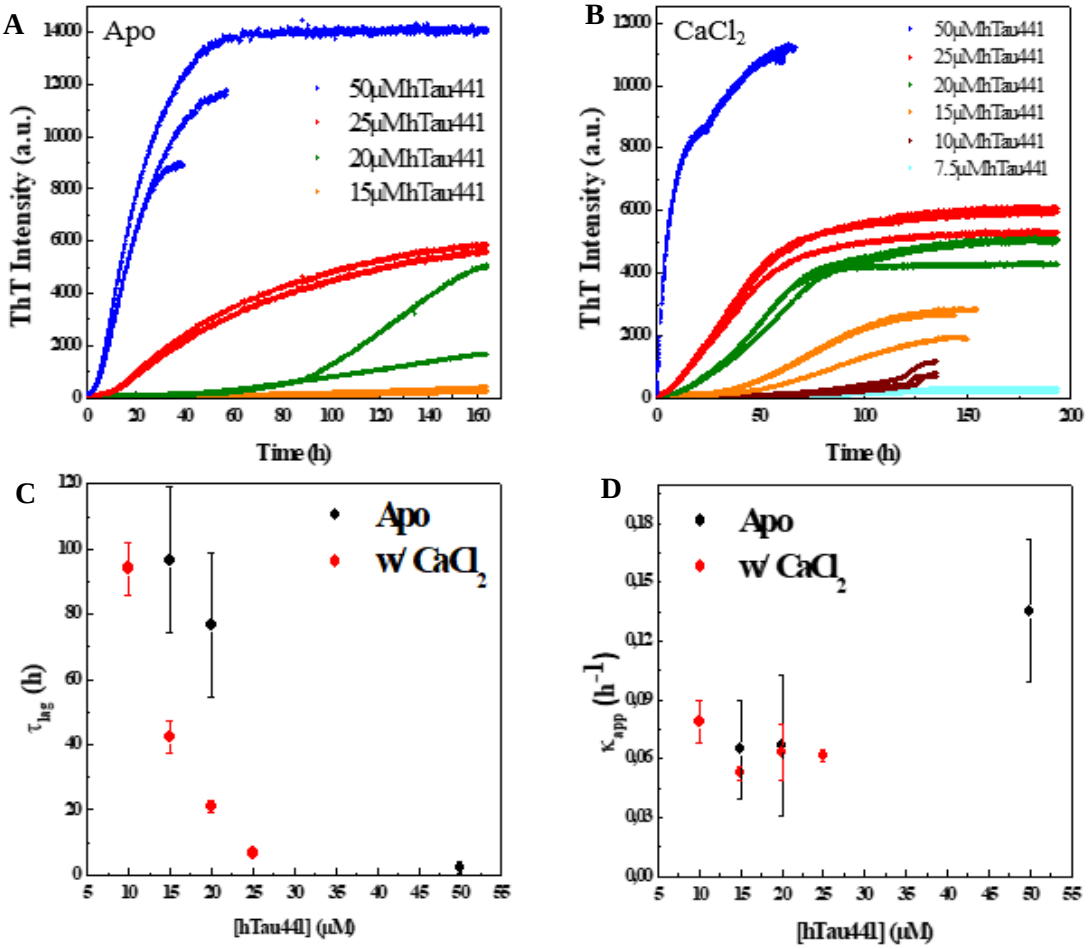


**Figure 3.11: hTau441 aggregation modulated by $CaCl_2$.** hTau441 heparin-induced aggregation in different concentrations (7.5-50µM) on absence (**A**) or presence of $CaCl_2$ (**B**) followed by ThT fluorescence. **C** – Lag time of hTau441 aggregation in absence (black) and presence (red) of 1.1mM $CaCl_2$; n=3. **D** – Apparent reaction rate of hTau441 aggregation in absence (black) and presence (red) of 1.1mM $CaCl_2$; n=3. The hTau441 experimental sample also contained 1mM DTT, 0.5mg/mL heparin, 50mM NaCl, 1mM PMSF and 75µM ThT. Experimental conditions: 37°C with orbital agitation for 5 min at 600rpm before each measurement with a 440nm excitation wavelength and 480nm emission wavelength.

It is observed that the lag time values are much smaller with the $CaCl_2$ presence than in apo condition (Figure 3.11, C). However, the apparent reaction velocity values do not vary when comparing between the absence and presence of calcium (Figure 3.11, D).

### 3.4.4 Modulation of hTau441 aggregation by $ZnCl_2$

Other metal ion that is dysregulated in AD patient brains is zinc [117] and was already showed that affects the hTau441 phosphorylation *in vivo* [54] and regulates its toxicity in an hyperphosphorylation independent fashion [119]. It was also studied the influence of zinc in Tau fragments aggregation both on wild-type as cysteines mutated Tau fragments [55] as well with other Tau constructs [120].

To assess the effect of zinc on hTau441 aggregation we performed aggregation assays at different hTau441 concentrations, and in absence or presence of 1.1mM of $ZnCl_2$, under previously established conditions. In contrast to previous conditions, zinc significantly potentiates the hTau441 aggregation, by lowering the lag time that it cannot even be fully observed in these aggregation curves (figure 3.12), like observed for apo conditions or with calcium (figure 3.12, A-B). This happened in a broad range of hTau441 concentrations (0.5µM to 50µM), demonstrating that these results are part of a consistent event in hTau441 aggregation kinetics upon 1.1mM $ZnCl_2$ condition.

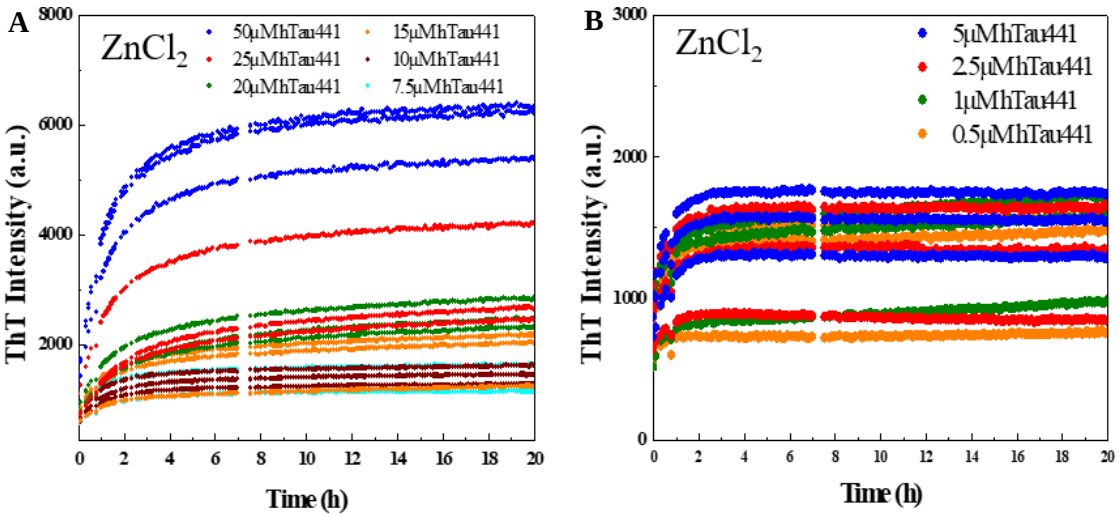


**Figure 3.12: hTau441 aggregation modulated by $ZnCl_2$.** hTau441 heparin-induced aggregation in different concentrations (0.5-50µM) on absence (**A**) or presence of $ZnCl_2$ (**B**) followed by ThT fluorescence. The hTau441 experimental sample also contained 1mM DTT, 0.5mg/mL heparin, 50mM NaCl, 1mM PMSF and 75µM ThT. Experimental conditions: 37°C with orbital agitation for 5 min at 600rpm before each measurement with a 440nm excitation wavelength and 480nm emission wavelength.

**Table 3.1 – hTau441 Aggregation kinetics parameters in absence and presence of metal ions.** Aggregation conditions has previously described. n/a – not available; n=3.

| [hTau441] (µM) | $Ca^{2+}$ | $\tau_{lag}$ (h) | $\kappa_{app}$ ($h^{-1}$) |
|---|---|---|---|
| **50** | − | 2.34 ± 1.64 | 0.14 ± 0.037 |
| | + | n/a | n/a |
| **25** | − | n/a | n/a |
| | + | 6.65 ± 0.33 | 0.06 ± 0.003 |
| **20** | − | 76.64 ± 22.16 | 0.07 ± 0.036 |
| | + | 21.00 ± 1.86 | 0.06 ± 0.014 |
| **15** | − | 96.66 ±22.36 | 0.07 ± 0.025 |
| | + | 42.34 ± 4.76 | 0.05 ± 0.343 |
| **10** | − | n/a | n/a |
| | + | 94.18 ± 8.08 | 0.08 ± 0.011 |

## 3.5 Modulatory effect of hTau441 aggregation kinetics by S100B and metal ions

The interaction of S100B with several metal ions, such as calcium [111], zinc [85] and copper [121] has been already studied. There is a connection between binding of these metal ions with structural changes promoting the interaction of S100B with other proteins [122]. To explore the ability of S100B interaction with hTau441 in different metal ions conditions, it was tested the modulatory effect of S100B on hTau441 heparin-induced kinetic aggregation.

### 3.5.1 Modulation of hTau441 aggregation by S100B

To assess the S100B modulation on hTau441 aggregation it was performed the aggregation reaction *in vitro*, with optimized conditions, in the absence of metal ions (apo condition). The aggregation of 25 µM hTau441 was followed by thioflavin-T (ThT) fluorescence intensity, at four S100B:Tau ratios: 0, 0.5x, 1x and 4x; compared with hTau441 concentration (figure 3.13, A).

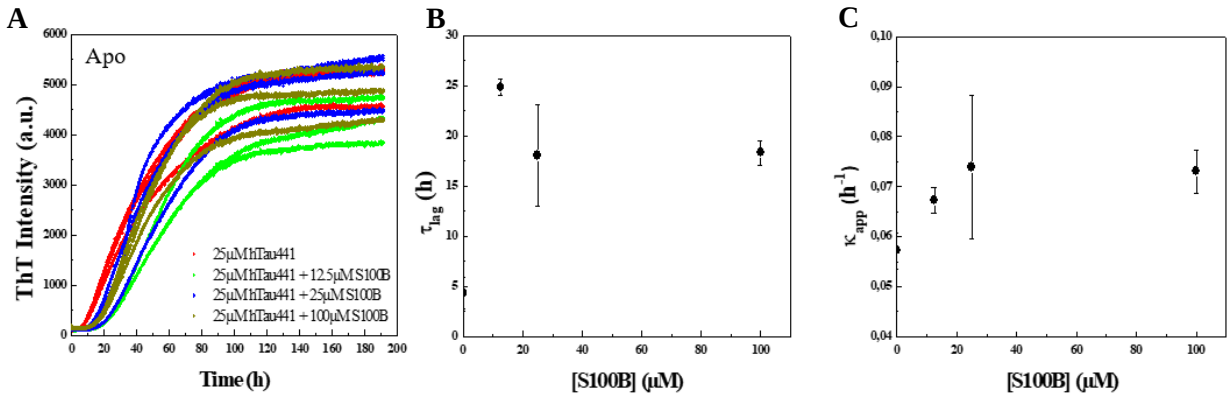


**Figure 3.13: hTau441 aggregation modulated by S100B in apo condition. A –** 25µM hTau441 heparin-induced aggregation curve on absence or presence of 3 different S100B concentrations (12.5, 25 and 100µM), followed by ThT fluorescence. **B** – Lag time of hTau441 aggregation for different S100B concentrations; n=3; **C** – Apparent reaction rate of hTau441 aggregation for different S100B concentrations; n=3. The hTau441 experimental sample also contained 1mM DTT, 0.5mg/mL heparin, 50mM NaCl, 1mM PMSF and 75µM ThT. Experimental conditions: 37°C with orbital agitation for 5 min at 600rpm before each measurement with a 440nm excitation wavelength and 480nm emission wavelength.

It is observed that S100B influences hTau441 aggregation kinetic parameters, in apo conditions, by increasing the aggregation lag time, but not in a concentration-dependent way (figure 3.13, B), and also increasing the aggregation reaction velocity (figure 3.13, C). This suggest that in apo conditions S100B can interact with hTau441 delaying the elongation reaction start point, however the reaction velocity is slightly increased. Results of time of lag phase ($\tau_{lag}$) and reaction rate ($\kappa_{app}$) for all hTau441 aggregation conditions are presented in table 3.2.

### 3.5.2 Modulation of hTau441 aggregation by S100B in the presence of $CaCl_2$

To assess the S100B modulation on hTau441 aggregation we performed aggregation reactions *in vitro*, under optimized conditions, in the presence of 1.1mM calcium ($CaCl_2$ condition). The aggregation of 10µM and 25 µM hTau441 were followed by thioflavin-T (ThT) fluorescence intensity, each one under four different ratios of S100B: 0, 0.5x, 1x and 4x; compared with hTau441 concentration (figure 3.14, A-B).

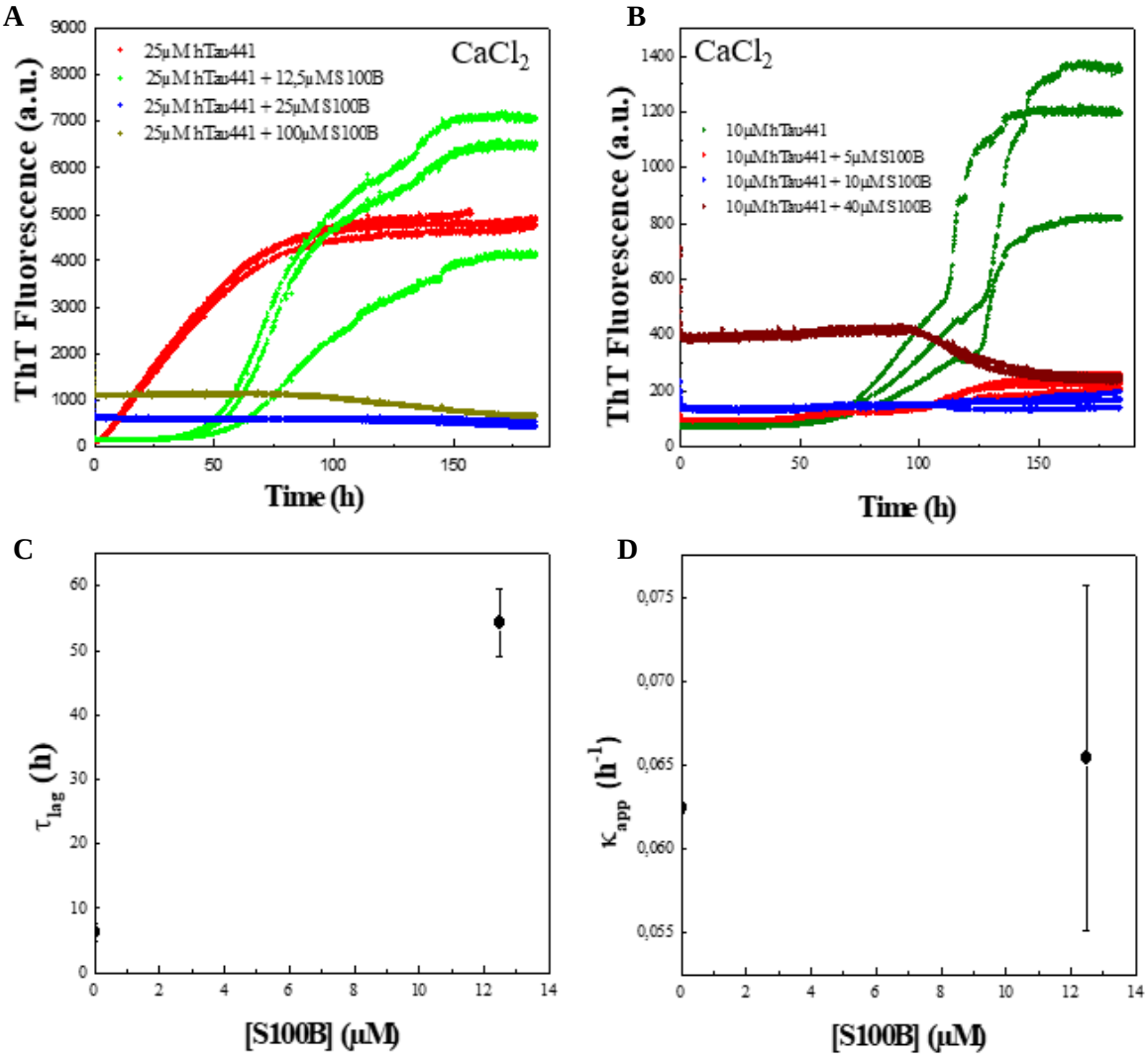


**Figure 3.14: hTau441 aggregation modulated by S100B in $CaCl_2$ presence. A –** 25µM hTau441 heparin-induced aggregation curve, with 1.1mM $CaCl_2$ presence, and on absence or presence of 3 different S100B concentrations (12.5, 25 and 100µM), followed by ThT fluorescence; **B –** 10µM hTau441 heparin-induced aggregation curve, with 1.1mM $CaCl_2$ presence, and on absence or presence of 3 different S100B concentrations (5, 10 and 40µM), followed by ThT fluorescence; **C** – Lag time of 25µM hTau441 aggregation for different S100B concentrations; n=3; **D** – Apparent reaction rate of 25µM hTau441 aggregation for different S100B concentrations; n=3. The hTau441 experimental sample also contained 1mM DTT, 0.5mg/mL heparin, 50mM NaCl, 1mM PMSF and 75µM ThT. Experimental conditions: 37°C with orbital agitation for 5 min at 600rpm before each measurement with a 440nm excitation wavelength and 480nm emission wavelength.

It is observed that S100B influences hTau441 aggregation kinetic parameters, in $CaCl_2$ conditions, by increasing the aggregation lag time to a point of total aggregation inhibition. This happened when S100B reaches equimolar or higher concentration values (figure 3.14, A-C). The aggregation reaction velocity does

not seem to be significantly changed for 25µM hTau441 + 12.5µM S100B (figure 3.14, D), for the rest the velocity is null, once that were totally inhibited (figure 3.14, A-B).

This set of results suggest that in $CaCl_2$ presence, S100B interact with hTau441 delaying the elongation reaction start point to a level of total inhibition. The ratio that allowed total aggregation inhibition was 1:1 and higher, lower ratios only delayed the lag time. This happened for both 25µM and 10µ hTau441 what further get strong the consistency of this event.

### 3.5.3 Modulation of hTau441 aggregation by S100B in the presence of $ZnCl_2$

To assess the S100B modulation on hTau441 aggregation we performed aggregation reactions *in vitro*, under optimized conditions, in the presence of 1.1mM zinc ($ZnCl_2$ condition). The aggregation of 10µM and 25 µM hTau441 were followed by thioflavin-T (ThT) fluorescence intensity, each one under four different ratios of S100B: 0, 0.5x, 1x and 4x; compared with hTau441 concentration (figure 3.15, A-B).

It is observed the same behavior as observed when hTau441 was treated alone with zinc (figure 3.12, A-B), this is, a quick aggregation reaction almost without observable lag phase, for both hTau441 concentrations (figure 3.15, A-B). The only condition where this event does not occur was the 25µM hTau441 treatment with 100µM S100B, that does not aggregate immediately. This might have happened because of S100B zinc chelation as observed in other cases [85].

**Table 3.2 – hTau441 Aggregation kinetics parameters in absence and presence of metal ions and S100B.** hTau441 aggregation conditions used: 25µM hTau441 and 12.5µM of S100B (when S100B is present). n/a – not available; n=3.

| | **Apo** | | **1.1mM $Ca^{2+}$** | | **1.1mM $Zn^{2+}$** | |
|---|---|---|---|---|---|---|
| S100B | – | + | – | + | – | + |
| **$\tau_{lag}$ (h)** | 4.32 ± 1.55 | 24.90 ± 0.84 | 6.30 ± 1.27 | 54.30 ± 5.28 | n/a | n/a |
| **$\kappa_{app}$ ($h^{-1}$)** | 0.057 ± 0.0036 | 0.067 ± 0.0025 | 0.062 ± 0.0003 | 0.065 ± 0.0103 | n/a | n/a |

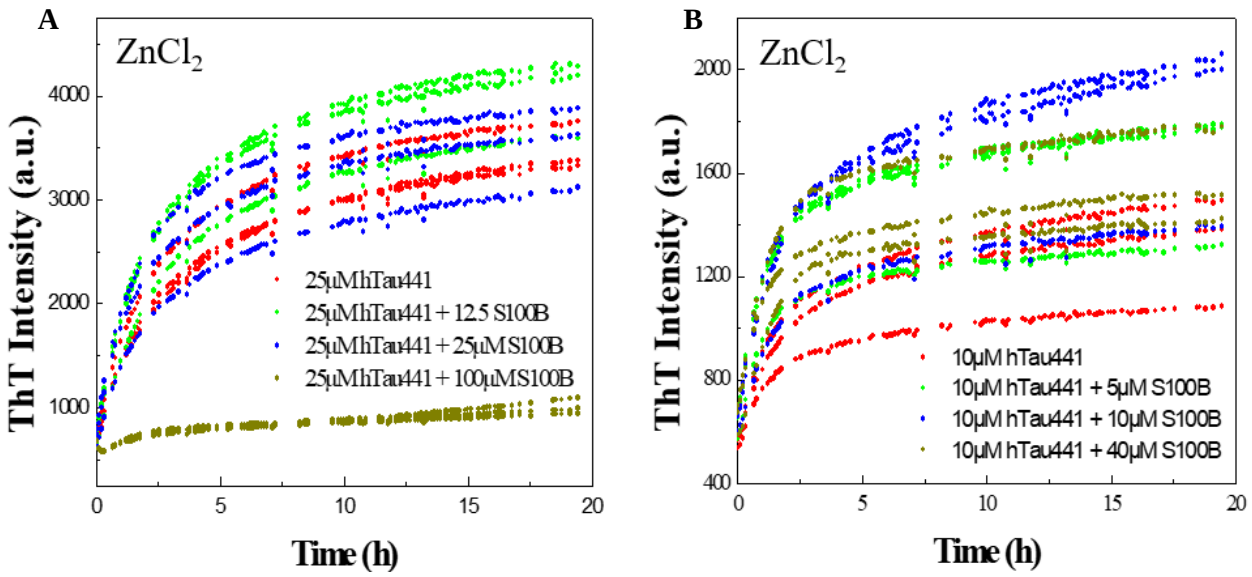


**Figure 3.15: hTau441 aggregation modulated by S100B in the presence of $ZnCl_2$. A –** 25µM hTau441 heparin-induced aggregation curve, with 1.1mM $ZnCl_2$ presence, and on absence or presence of 3 different S100B concentrations (12.5, 25 and 100µM), followed by ThT fluorescence; **B –** 10µM hTau441 heparin-induced aggregation curve, with 1.1mM $ZnCl_2$ presence, and on absence or presence of 3 different S100B concentrations (5, 10 and 40µM), followed by ThT fluorescence. The hTau441 experimental sample also contained 1mM DTT, 0.5mg/mL heparin, 50mM NaCl, 1mM PMSF and 75µM ThT. Experimental conditions: 37°C with orbital agitation for 5 min at 600rpm before each measurement with a 440nm excitation wavelength and 480nm emission wavelength.

## 3.6 hTau441 fibril and aggregates bioimaging by AFM

### 3.6.1 AFM characterization of hTau441 fibrils in the presence of metal ions

To characterize the end time products from hTau441 aggregation assays in different conditions, we used atomic force microscopy (AFM).

Initially, to analyze what type of aggregates/fibrils were formed from hTau441 apo sample as control we used AFM to image the aggregates formed under typical conditions (50µM hTau441 and 100mM NaCl, end point of kinetic trace in figure 3.10, B). AFM showed the formation of amyloid mature fibrils which are heterogenous, consisting of straight and helical fibrils, as previously reported [14] (figure 3.16, A).

We also imaged the samples from 25µM hTau441 aggregation end-time point in the presence of 1.1mM $Ca^{2+}$ (end point of kinetic trace in figure 3.14, A) and in presence of 1.1mM $Zn^{2+}$ (end point of kinetic trace in figure 3.15, A).

The resulting imaging of these three aggregation conditions (apo, $Ca^{2+}$ and $Zn^{2+}$ presence) can be comparable and resulted in structural similar fibrils, being present in all samples several types of fibrils like straight and twisted ribbon (figure 3.16). However, it is worth noting that in sample containing $Zn^{2+}$ (figure 3.16 - C) there was formation of shorter fibrils with low presence of long formed fibrils. This result can have two possible explanations: first, once that the incubation time of this sample was shorter than the others, it maybe had not enough time to elongate properly formed fibrils; second, since $Zn^{2+}$ greatly enhances aggregation velocity, it could have done it by facilitating primary nucleation, originating more nucleation sites and smaller fibrils.

By this set of images is possible to conclude that hTau441 under all the conditions (apo, $Ca^{2+}$ and $Zn^{2+}$ presence) leads to formation of amyloidogenic mature fibrils that are characterized by being structurally heterogenous, consisting of straight and helical fibrils.

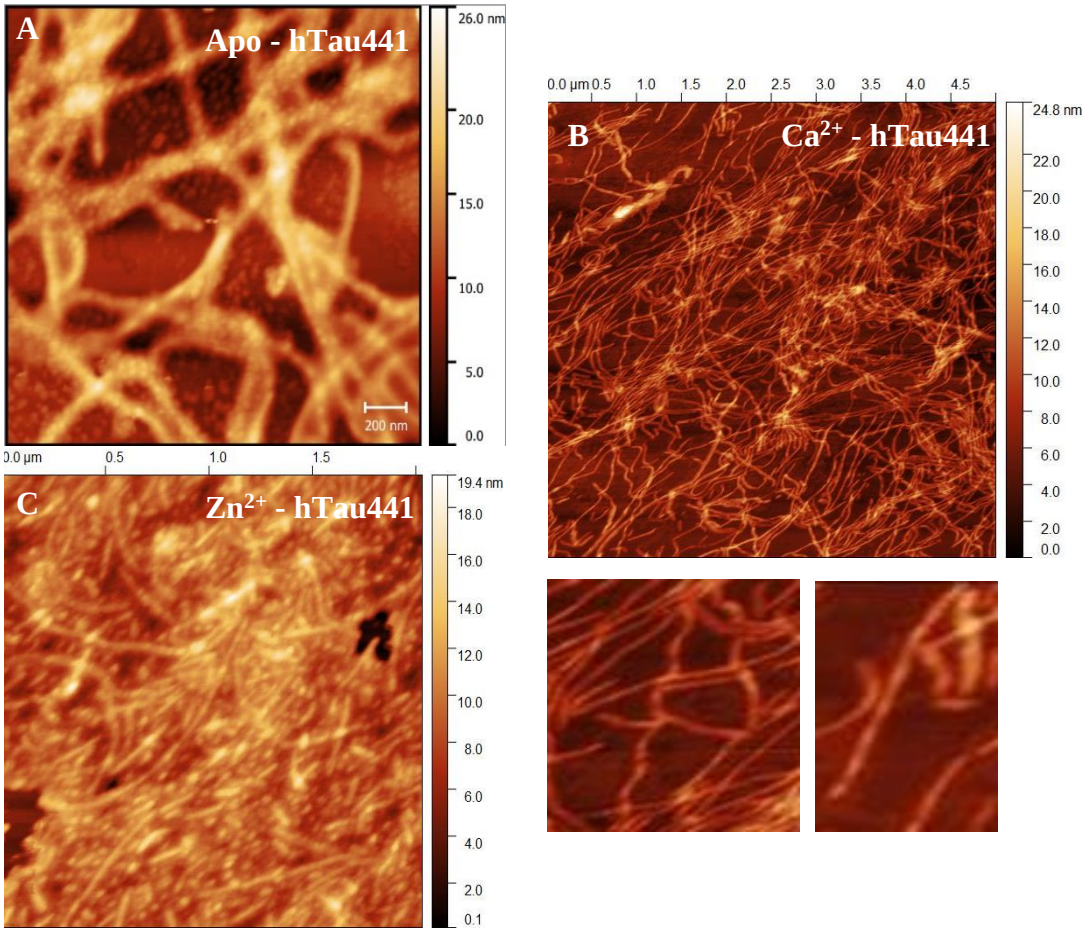


**Figure 3.16: AFM images of end-time points of hTau441 aggregation in apo condition, in the presence of $CaCl_2$ and in $ZnCl_2$.** **A –** AFM of aggregation sample containing 50µM hTau441 with 100mM NaCl and after 140 hours at 37°C with 600 rpm; **B –** AFM of aggregation sample containing 25µM hTau441 with 1.1mM $CaCl_2$ and after 180 hours at 37°C with 600 rpm; **C –** AFM of aggregation sample containing 25µM hTau441 with 1.1mM$ZnaCl_2$ and after 20 hours at 37°C with 600 rpm. Sampling was performed with 20µL of diluted sample ([protein monomer] = 0.5-1 µM) applied on a mica freshly cleaved, during 30 minutes and then washed with distillated water.

### 3.6.2 AFM characterization of hTau441 fibrils in the presence of metal ions and S100B

Since that S100B had an effect in hTau441 aggregation kinetics with metal ions presence like $Zn^{2+}$ and $Ca^{2+}$, AFM bioimaging was performed to the end-time points of hTau441 aggregation in the presence of S100B and metal ions ($Zn^{2+}$ and $Ca^{2+}$).

Bioimaging of the end time point of the sample with the initial conditions of 25µM hTau441, 1.1mM $CaCl_2$ (end point of kinetic trace in figure 3.14) was performed.

These results observations revealed that hTau441 aggregation in presence of S100B and $Ca^{2+}$ does not form hTau441 fibrils (figure 3.17, A) and this is in agreement with what is observed in aggregation results where is not formed ThT reactive species (see figure 3.14). However, in AFM image can be observed the presence of large spherical aggregates (figure 3.17, A) that probably are constituted by S100B, since it is described in the literature that S100B can form these types of structures [66].

So, since that in equimolar concentration of S100B and hTau441 and in presence of $Ca^{2+}$ there is not formed ThT reactive species nor fibrils, it can be concluded that S100B, in these conditions, can inhibit the amyloid aggregation process of hTau441 into fibrils. Together with prior interaction results, we can hypothesize that this inhibition can be achieved by S100B and hTau441 interaction and binding promoted by calcium.

Bioimaging of the end time points of the samples with the initial conditions of 1.1mM $ZnCl_2$ with 25µM S100B and with 100µM S100B (end point of kinetic trace in figure 3.15) were performed (figure 3.17, B and C).

In the presence of $Zn^{2+}$, S100B shows an inability to prevent hTau441 aggregation, since it can be observed the presence of mature fibrils (figure 3.17, B) in the end point samples. These samples are ThT reactive, just like the prior results in the absence of S100B (figure 3.16, C). Moreover, in the condition with 4x more concentration of S100B in comparison with hTau441 (figure 3.17, C), where there was a very subtle change in the ThT fluorescence during time (figure 3.1, A), it can be observed by AFM fibrils formed. However, the number of fibrils it was much less than the prior condition.

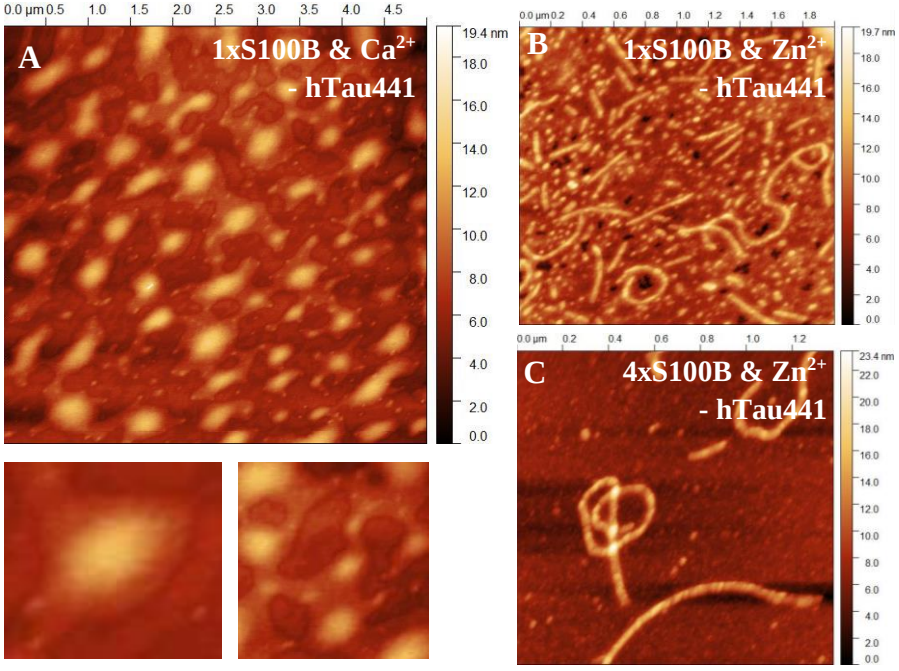


**Figure 3.17: AFM images of end-time points of hTau441 aggregation in the presence of S100B, with $CaCl_2$ and $ZnCl_2$. A –** AFM of aggregation end-time point sample containing 25µM hTau441 and 25µM S100B with 1.1mM $CaCl_2$ and after 180 hours at 37°C with 600 rpm; **B –** AFM of aggregation end-time point sample containing 25µM hTau441 and 25µM S100B with 1.1mM $ZnCl_2$ and after 20 hours at 37°C with 600 rpm; **C –** AFM of aggregation end-time point sample containing 25µM hTau441 and 100µM S100B with 1.1mM $ZnCl_2$ and after 20 hours at 37°C with 600 rpm. Sampling was performed with 20µL of diluted sample ([protein monomer] = 0.5-1 µM) applied on a mica freshly cleaved, during 30 minutes and then washed with distillated water.

Together, these results showed that S100B in $Zn^{2+}$ presence is unable to have the role of hTau441 aggregation inhibitor. This proves that, in these conditions, the metal ions environment is critical for S100B role in hTau441 aggregation modulation.

# IV. CONCLUSIONS

In Alzheimer's disease (AD), the accumulation of highly phosphorylated Tau protein in neurofibrillar tangles is one of hallmark disease features [123]. Moreover, important neuronal components such as pro-inflammatory cytokines and transition metal ion levels are consistently deregulated with aging, which is the most prominent risk factor for AD. In particular, S100B pro-inflammatory cytokine is known to promote hyperphosphorylation of Tau, but no clear mechanistic relationship has been established between the two proteins. This work aim at exploring a possible interaction between S100B and Tau protein and investigating the effects of S100B over Tau aggregation.

Firstly, we optimize the protocol of Tau purification to produce a highly pure and homogeneous solution of monomeric hTau441 to minimize the existence of Tau fragments and to obtain reproducible results in the further assays. The best condition found was to dilute the lyophilized Tau protein in 7.6M urea and 50mM DTT and elute in a size exclusion chromatography and isolate the corresponding peak of monomeric hTau441.

Next, to investigate the relationship between S100B and Tau protein we performed protein-protein interaction assays and aggregation assays with different metal ions, since S100B interaction with other partners are regulated by calcium and zinc [69]. We performed a size exclusion chromatography to assess if hTau441 and S100B could interact and form stable complex. The resulted chromatograms in all the conditions tested (apo, with zinc and/or calcium) were suggestive of a possible interaction but unclear if a complex was formed between the two proteins. Further assays must be performed to be sure that the complex is formed. We then evaluated the conformational changes in the secondary structure arising upon interaction of hTau441 with S100B. Far-UV CD spectra suggested that hTau441 contribute to loss or relaxation of S100B α-helical structure in presence of higher ratios of hTau441/S100B, and it is strongly promoted by $CaCl_2$. In the presence of $Zn^{2+}$ there is also a shift of the 222nm band to lower wavelength values, suggesting an increase in β-sheet structure. To support these results, in ATR-FTIR spectra was also possible to observe a substantial loss of α-helical/random coil structure at higher hTau441/S100B ratios, in the presence of $CaCl_2$. In the presence of $ZnCl_2$ we can observed an even greater loss of α-helical/random coil structure, as well as, an increase in the β-sheet structure content. Altogether these results suggest a possible interaction between Tau and S100B that can be promoted by calcium and zinc.

In AD patients, high levels of S100B are positively correlated with positive Tau plaques and S100B was found around and within Tau plaques [86, 87]. Additionally, inhibition of Aβ aggregation by S100B is promoted by calcium binding to S100B [64, 116]. We performed hTau441 aggregation kinetics assays with heparin and salt, since it is already reported as pro-aggregation factors [116] and tested the influence of calcium and zinc on hTau441 aggregation. Calcium and zinc modulate hTau441 aggregation. The presence of calcium decreases the lag phase time up to 3.5 times but do not interfere with the hTau441 apparent aggregation rate. Zinc ions promotes a spontaneous aggregation reaction of hTau441 where no time for nucleation is necessary. By AFM we observed that hTau441 formed fibrils in absence and in the presence of $Zn^{2+}$ and $Ca^{2+}$, and they were structurally identical with a mixture of straight and twisted fibrils. The fibrils were shorter in presence of $Zn^{2+}$, probably due to shorter time of incubation.

The presence of S100B modulates Tau aggregation: in apo conditions a delay up to 5 times in the lag phase of Tau aggregation was observed; in the presence of calcium it was also observed a decrease in

the lag phase at substoichiometric ratios of S100B:Tau and a complete inhibition of hTau441 aggregation at equimolar ratio. Indeed, by AFM no fibrils were observed in the presence of $Ca^{2+}$ and equimolar protein ratio of S100B, supporting the inhibitor role of S100B over Tau aggregation in the presence of calcium.

Altogether, the results of this study contributed to the understanding of the role of S100B and metal ions on the biochemistry of Tau aggregation. The results in this thesis give a hint on a possible interaction between S100B and Tau protein that therefore impact Tau aggregation, inhibiting the formation of fibrils in a calcium dependent fashion. In a near future it would be interesting to further characterize the complex formed between hTau441 and S100B in presence of neurometal ions by other techniques, such as fluorescence molecules and Förster resonance energy transfer (FRET) effects, as well as test other Tau isoforms and fragments that are key players on Tau aggregation into neurofibrillary tangles. Would be of great interest to perform cellular (for example, neuronal cells) toxicity and survival experiments with hTau441 monomers, oligomers, and fibrils and understand the impact of S100B and metal ions.

# V. BIBLIOGRAPHY


1. Rachakonda, V., T.H. Pan, and W.D. Le, *Biomarkers of neurodegenerative disorders: how good are they?* Cell Res, 2004. **14**(5): p. 347-58.
2. Gomez-Isla, T., et al., *Profound loss of layer II entorhinal cortex neurons occurs in very mild Alzheimer's disease.* J Neurosci, 1996. **16**(14): p. 4491-500.
3. Harvey, P.D., *Clinical applications of neuropsychological assessment.* Dialogues Clin Neurosci, 2012. **14**(1): p. 91-9.
4. Masters, C.L., et al., *Alzheimer's disease.* Nat Rev Dis Primers, 2015. **1**: p. 15056.
5. Hardy, J. and D.J. Selkoe, *The amyloid hypothesis of Alzheimer's disease: progress and problems on the road to therapeutics.* Science, 2002. **297**(5580): p. 353-6.
6. el-Agnaf, O.M. and G.B. Irvine, *Aggregation and neurotoxicity of alpha-synuclein and related peptides.* Biochem Soc Trans, 2002. **30**(4): p. 559-65.
7. Bachurin, S.O., E.V. Bovina, and A.A. Ustyugov, *Drugs in Clinical Trials for Alzheimer's Disease: The Major Trends.* Med Res Rev, 2017. **37**(5): p. 1186-1225.
8. Himmler, A., et al., *Tau consists of a set of proteins with repeated C-terminal microtubule-binding domains and variable N-terminal domains.* Mol Cell Biol, 1989. **9**(4): p. 1381-8.
9. Goedert, M., et al., *Multiple isoforms of human microtubule-associated protein tau: sequences and localization in neurofibrillary tangles of Alzheimer's disease.* Neuron, 1989. **3**(4): p. 519-26.
10. Liu, F. and C.X. Gong, *Tau exon 10 alternative splicing and tauopathies.* Mol Neurodegener, 2008. **3**: p. 8.
11. Wang, Y. and E. Mandelkow, *Tau in physiology and pathology.* Nat Rev Neurosci, 2016. **17**(1): p. 5-21.
12. Jeganathan, S., et al., *Global hairpin folding of tau in solution.* Biochemistry, 2006. **45**(7): p. 2283-93.
13. Bukar Maina, M., Y.K. Al-Hilaly, and L.C. Serpell, *Nuclear Tau and Its Potential Role in Alzheimer's Disease.* Biomolecules, 2016. **6**(1): p. 9.
14. Fitzpatrick, A.W.P., et al., *Cryo-EM structures of tau filaments from Alzheimer's disease.* Nature, 2017. **547**(7662): p. 185-190.
15. Weingarten, M.D., et al., *A protein factor essential for microtubule assembly.* Proc Natl Acad Sci U S A, 1975. **72**(5): p. 1858-62.
16. Terwel, D., I. Dewachter, and F. Van Leuven, *Axonal transport, tau protein, and neurodegeneration in Alzheimer's disease.* Neuromolecular Med, 2002. **2**(2): p. 151-65.
17. Rodriguez-Martin, T., et al., *Tau phosphorylation affects its axonal transport and degradation.* Neurobiol Aging, 2013. **34**(9): p. 2146-57.
18. Reynolds, C.H., et al., *Phosphorylation regulates tau interactions with Src homology 3 domains of phosphatidylinositol 3-kinase, phospholipase Cgamma1, Grb2, and Src family kinases.* J Biol Chem, 2008. **283**(26): p. 18177-86.
19. Souter, S. and G. Lee, *Tubulin-independent tau in Alzheimer's disease and cancer: implications for disease pathogenesis and treatment.* Curr Alzheimer Res, 2010. **7**(8): p. 697-707.
20. Dent, E.W. and F.B. Gertler, *Cytoskeletal dynamics and transport in growth cone motility and axon guidance.* Neuron, 2003. **40**(2): p. 209-27.
21. Guzik, B.W. and L.S. Goldstein, *Microtubule-dependent transport in neurons: steps towards an understanding of regulation, function and dysfunction.* Curr Opin Cell Biol, 2004. **16**(4): p. 443-50.
22. Binder, L.I., A. Frankfurter, and L.I. Rebhun, *The distribution of tau in the mammalian central nervous system.* J Cell Biol, 1985. **101**(4): p. 1371-8.
23. Papasozomenos, S.C. and L.I. Binder, *Phosphorylation determines two distinct species of Tau in the central nervous system.* Cell Motil Cytoskeleton, 1987. **8**(3): p. 210-26.
24. Butner, K.A. and M.W. Kirschner, *Tau protein binds to microtubules through a flexible array of distributed weak sites.* J Cell Biol, 1991. **115**(3): p. 717-30.

25. Khatoon, S., I. Grundke-Iqbal, and K. Iqbal, *Brain levels of microtubule-associated protein tau are elevated in Alzheimer's disease: a radioimmuno-slot-blot assay for nanograms of the protein.* J Neurochem, 1992. **59**(2): p. 750-3.
26. Ackmann, M., H. Wiech, and E. Mandelkow, *Nonsaturable binding indicates clustering of tau on the microtubule surface in a paired helical filament-like conformation.* J Biol Chem, 2000. **275**(39): p. 30335-43.
27. Kellogg, E.H., et al., *Near-atomic model of microtubule-tau interactions.* Science, 2018. **360**(6394): p. 1242-1246.
28. Wang, Y., et al., *A novel tau transcript in cultured human neuroblastoma cells expressing nuclear tau.* J Cell Biol, 1993. **121**(2): p. 257-67.
29. Sultan, A., et al., *Nuclear tau, a key player in neuronal DNA protection.* J Biol Chem, 2011. **286**(6): p. 4566-75.
30. Andorfer, C., et al., *Cell-cycle reentry and cell death in transgenic mice expressing nonmutant human tau isoforms.* J Neurosci, 2005. **25**(22): p. 5446-54.
31. Lindwall, G. and R.D. Cole, *Phosphorylation affects the ability of tau protein to promote microtubule assembly.* J Biol Chem, 1984. **259**(8): p. 5301-5.
32. Alonso, A.C., et al., *Role of abnormally phosphorylated tau in the breakdown of microtubules in Alzheimer disease.* Proc Natl Acad Sci U S A, 1994. **91**(12): p. 5562-6.
33. Kopke, E., et al., *Microtubule-associated protein tau. Abnormal phosphorylation of a non-paired helical filament pool in Alzheimer disease.* J Biol Chem, 1993. **268**(32): p. 24374-84.
34. Grundke-Iqbal, I., et al., *Abnormal phosphorylation of the microtubule-associated protein tau (tau) in Alzheimer cytoskeletal pathology.* Proc Natl Acad Sci U S A, 1986. **83**(13): p. 4913-7.
35. Trinczek, B., et al., *Domains of tau protein, differential phosphorylation, and dynamic instability of microtubules.* Mol Biol Cell, 1995. **6**(12): p. 1887-902.
36. Johnson, G.V. and W.H. Stoothoff, *Tau phosphorylation in neuronal cell function and dysfunction.* J Cell Sci, 2004. **117**(Pt 24): p. 5721-9.
37. Hutton, M., et al., *Association of missense and 5'-splice-site mutations in tau with the inherited dementia FTDP-17.* Nature, 1998. **393**(6686): p. 702-5.
38. Goedert, M. and R. Jakes, *Mutations causing neurodegenerative tauopathies.* Biochim Biophys Acta, 2005. **1739**(2-3): p. 240-50.
39. Wolfe, M.S., *Tau mutations in neurodegenerative diseases.* J Biol Chem, 2009. **284**(10): p. 6021-5.
40. Nicholl, D.J., et al., *An English kindred with a novel recessive tauopathy and respiratory failure.* Ann Neurol, 2003. **54**(5): p. 682-6.
41. Pickering-Brown, S.M., et al., *Frontotemporal dementia with Pick-type histology associated with Q336R mutation in the tau gene.* Brain, 2004. **127**(Pt 6): p. 1415-26.
42. Momeni, P., et al., *Clinical and pathological features of an Alzheimer's disease patient with the MAPT Delta K280 mutation.* Neurobiol Aging, 2009. **30**(3): p. 388-93.
43. Braak, H., et al., *Occurrence of neuropil threads in the senile human brain and in Alzheimer's disease: a third location of paired helical filaments outside of neurofibrillary tangles and neuritic plaques.* Neurosci Lett, 1986. **65**(3): p. 351-5.
44. von Bergen, M., et al., *Assembly of tau protein into Alzheimer paired helical filaments depends on a local sequence motif ((306)VQIVYK(311)) forming beta structure.* Proc Natl Acad Sci U S A, 2000. **97**(10): p. 5129-34.
45. Khlistunova, I., et al., *Inducible expression of Tau repeat domain in cell models of tauopathy: aggregation is toxic to cells but can be reversed by inhibitor drugs.* J Biol Chem, 2006. **281**(2): p. 1205-14.
46. Kadavath, H., et al., *Tau stabilizes microtubules by binding at the interface between tubulin heterodimers.* Proc Natl Acad Sci U S A, 2015. **112**(24): p. 7501-6.

47. Ramachandran, G. and J.B. Udgaonkar, *Understanding the Kinetic Roles of the Inducer Heparin and of Rod-like Protofibrils during Amyloid Fibril Formation by Tau Protein.* Journal of Biological Chemistry, 2011. **286**(45): p. 38948-38959.
48. Braak, E., H. Braak, and E.M. Mandelkow, *A sequence of cytoskeleton changes related to the formation of neurofibrillary tangles and neuropil threads.* Acta Neuropathol, 1994. **87**(6): p. 554-67.
49. Nilsson, M.R., *Techniques to study amyloid fibril formation in vitro.* Methods, 2004. **34**(1): p. 151-60.
50. Cohen, S.I., et al., *From macroscopic measurements to microscopic mechanisms of protein aggregation.* J Mol Biol, 2012. **421**(2-3): p. 160-71.
51. Leal, S.S., H.M. Botelho, and C.M. Gomes, *Metal ions as modulators of protein conformation and misfolding in neurodegeneration.* Coordination Chemistry Reviews, 2012. **256**(19-20): p. 2253-2270.
52. Cristovao, J.S., R. Santos, and C.M. Gomes, *Metals and Neuronal Metal Binding Proteins Implicated in Alzheimer's Disease.* Oxid Med Cell Longev, 2016. **2016**: p. 9812178.
53. Yang, D.J., et al., *Cooperative folding of tau peptide by coordination of group IIB metal cations during heparin-induced aggregation.* Biometals, 2012. **25**(2): p. 361-72.
54. Sun, X.Y., et al., *Synaptic released zinc promotes tau hyperphosphorylation by inhibition of protein phosphatase 2A (PP2A).* J Biol Chem, 2012. **287**(14): p. 11174-82.
55. Mo, Z.Y., et al., *Low micromolar zinc accelerates the fibrillization of human tau via bridging of Cys-291 and Cys-322.* J Biol Chem, 2009. **284**(50): p. 34648-57.
56. Yamamoto, A., et al., *Iron (III) induces aggregation of hyperphosphorylated tau and its reduction to iron (II) reverses the aggregation: implications in the formation of neurofibrillary tangles of Alzheimer's disease.* J Neurochem, 2002. **82**(5): p. 1137-47.
57. Zhou, L.X., et al., *Copper (II) modulates in vitro aggregation of a tau peptide.* Peptides, 2007. **28**(11): p. 2229-34.
58. Lei, P., et al., *Motor and cognitive deficits in aged tau knockout mice in two background strains.* Mol Neurodegener, 2014. **9**: p. 29.
59. Labbe, C., et al., *Role for the microtubule-associated protein tau variant p.A152T in risk of alpha-synucleinopathies.* Neurology, 2015. **85**(19): p. 1680-6.
60. Lasagna-Reeves, C.A., et al., *Identification of oligomers at early stages of tau aggregation in Alzheimer's disease.* FASEB J, 2012. **26**(5): p. 1946-59.
61. Mocanu, M.M., et al., *The potential for beta-structure in the repeat domain of tau protein determines aggregation, synaptic decay, neuronal loss, and coassembly with endogenous Tau in inducible mouse models of tauopathy.* J Neurosci, 2008. **28**(3): p. 737-48.
62. Hoover, B.R., et al., *Tau mislocalization to dendritic spines mediates synaptic dysfunction independently of neurodegeneration.* Neuron, 2010. **68**(6): p. 1067-81.
63. Clavaguera, F., et al., *Transmission and spreading of tauopathy in transgenic mouse brain.* Nat Cell Biol, 2009. **11**(7): p. 909-13.
64. Cristovao, J.S., et al., *The neuronal S100B protein is a calcium-tuned suppressor of amyloid-beta aggregation.* Sci Adv, 2018. **4**(6): p. eaaq1702.
65. Charpentier, T.H., et al., *Divalent metal ion complexes of S100B in the absence and presence of pentamidine.* J Mol Biol, 2008. **382**(1): p. 56-73.
66. Carvalho, S.B., et al., *Intrinsically disordered and aggregation prone regions underlie beta-aggregation in S100 proteins.* PLoS One, 2013. **8**(10): p. e76629.
67. Donato, R., *Intracellular and extracellular roles of S100 proteins.* Microsc Res Tech, 2003. **60**(6): p. 540-51.
68. Donato, R., *S100: a multigenic family of calcium-modulated proteins of the EF-hand type with intracellular and extracellular functional roles.* Int J Biochem Cell Biol, 2001. **33**(7): p. 637-68.

69. Ostendorp, T., et al., *The crystal structures of human S100B in the zinc- and calcium-loaded state at three pH values reveal zinc ligand swapping.* Biochimica Et Biophysica Acta-Molecular Cell Research, 2011. **1813**(5): p. 1083-1091.
70. Nardin, P., et al., *S100B content and secretion decrease in astrocytes cultured in high-glucose medium.* Neurochem Int, 2007. **50**(5): p. 774-82.
71. Ostendorp, T., et al., *Structural and functional insights into RAGE activation by multimeric S100B.* EMBO J, 2007. **26**(16): p. 3868-78.
72. Sorci, G., et al., *S100B Protein, A Damage-Associated Molecular Pattern Protein in the Brain and Heart, and Beyond.* Cardiovasc Psychiatry Neurol, 2010. **2010**.
73. Haglid, K.G., et al., *S-100beta stimulates neurite outgrowth in the rat sciatic nerve grafted with acellular muscle transplants.* Brain Res, 1997. **753**(2): p. 196-201.
74. Pichiule, P., et al., *Hypoxia-inducible factor-1 mediates neuronal expression of the receptor for advanced glycation end products following hypoxia/ischemia.* J Biol Chem, 2007. **282**(50): p. 36330-40.
75. Tramontina, F., et al., *Glutamate uptake is stimulated by extracellular S100B in hippocampal astrocytes.* Cell Mol Neurobiol, 2006. **26**(1): p. 81-6.
76. Businaro, R., et al., *S100B protects LAN-5 neuroblastoma cells against Abeta amyloid-induced neurotoxicity via RAGE engagement at low doses but increases Abeta amyloid neurotoxicity at high doses.* J Neurosci Res, 2006. **83**(5): p. 897-906.
77. Bierhaus, A., et al., *Understanding RAGE, the receptor for advanced glycation end products.* J Mol Med (Berl), 2005. **83**(11): p. 876-86.
78. Shapiro, L.A., A. Marks, and P.M. Whitaker-Azmitia, *Increased clusterin expression in old but not young adult S100B transgenic mice: evidence of neuropathological aging in a model of Down Syndrome.* Brain Research, 2004. **1010**(1-2): p. 17-21.
79. Shapiro, L.A. and P.M. Whitaker-Azmitia, *Expression levels of cytoskeletal proteins indicate pathological aging of S100B transgenic mice: an immunohistochemical study of MAP-2, drebrin and GAP-43.* Brain Research, 2004. **1019**(1-2): p. 39-46.
80. Donato, R., et al., *S100B's double life: intracellular regulator and extracellular signal.* Biochim Biophys Acta, 2009. **1793**(6): p. 1008-22.
81. Nordberg, A., *Amyloid imaging in Alzheimer's disease.* Neuropsychologia, 2008. **46**(6): p. 1636-41.
82. Esposito, G., et al., *S100B induces tau protein hyperphosphorylation via Dickopff-1 up-regulation and disrupts the Wnt pathway in human neural stem cells.* J Cell Mol Med, 2008. **12**(3): p. 914-27.
83. Mrak, R.E. and W.S. Griffin, *Trisomy 21 and the brain.* J Neuropathol Exp Neurol, 2004. **63**(7): p. 679-85.
84. Sheng, J.G., et al., *Overexpression of the neuritotrophic cytokine S100beta precedes the appearance of neuritic beta-amyloid plaques in APPV717F mice.* J Neurochem, 2000. **74**(1): p. 295-301.
85. Hagmeyer, S., et al., *Zinc Binding to S100B Affords Regulation of Trace Metal Homeostasis and Excitotoxicity in the Brain.* Front Mol Neurosci, 2017. **10**: p. 456.
86. Sheng, J.G., R.E. Mrak, and W.S. Griffin, *Glial-neuronal interactions in Alzheimer disease: progressive association of IL-1alpha+ microglia and S100beta+ astrocytes with neurofibrillary tangle stages.* J Neuropathol Exp Neurol, 1997. **56**(3): p. 285-90.
87. Sheng, J.G., R.E. Mrak, and W.S. Griffin, *S100 beta protein expression in Alzheimer disease: potential role in the pathogenesis of neuritic plaques.* J Neurosci Res, 1994. **39**(4): p. 398-404.
88. Kelly, S.M., T.J. Jess, and N.C. Price, *How to study proteins by circular dichroism.* Biochim Biophys Acta, 2005. **1751**(2): p. 119-39.
89. Barrow, C.J., et al., *Solution conformations and aggregational properties of synthetic amyloid beta-peptides of Alzheimer's disease. Analysis of circular dichroism spectra.* J Mol Biol, 1992. **225**(4): p. 1075-93.

90. Haris, P.I. and F. Severcan, *FTIR spectroscopic characterization of protein structure in aqueous and non-aqueous media.* Journal of Molecular Catalysis B-Enzymatic, 1999. **7**(1-4): p. 207-221.
91. Surewicz, W.K., H.H. Mantsch, and D. Chapman, *Determination of protein secondary structure by Fourier transform infrared spectroscopy: a critical assessment.* Biochemistry, 1993. **32**(2): p. 389-94.
92. Shashilov, V.A. and I.K. Lednev, *Advanced statistical and numerical methods for spectroscopic characterization of protein structural evolution.* Chem Rev, 2010. **110**(10): p. 5692-713.
93. Sarver, R.W., Jr. and W.C. Krueger, *Protein secondary structure from Fourier transform infrared spectroscopy: a data base analysis.* Anal Biochem, 1991. **194**(1): p. 89-100.
94. Glassford, S.E., B. Byrne, and S.G. Kazarian, *Recent applications of ATR FTIR spectroscopy and imaging to proteins.* Biochim Biophys Acta, 2013. **1834**(12): p. 2849-58.
95. Adamcik, J. and R. Mezzenga, *Proteins Fibrils from a Polymer Physics Perspective.* Macromolecules, 2012. **45**(3): p. 1137-1150.
96. Adamcik, J. and R. Mezzenga, *Study of amyloid fibrils via atomic force microscopy.* Current Opinion in Colloid & Interface Science, 2012. **17**(6): p. 369-376.
97. Munishkina, L.A. and A.L. Fink, *Fluorescence as a method to reveal structures and membrane-interactions of amyloidogenic proteins.* Biochim Biophys Acta, 2007. **1768**(8): p. 1862-85.
98. Royer, C.A., *Probing protein folding and conformational transitions with fluorescence.* Chem Rev, 2006. **106**(5): p. 1769-84.
99. Biancalana, M. and S. Koide, *Molecular mechanism of Thioflavin-T binding to amyloid fibrils.* Biochim Biophys Acta, 2010. **1804**(7): p. 1405-12.
100. Krebs, M.R., E.H. Bromley, and A.M. Donald, *The binding of thioflavin-T to amyloid fibrils: localisation and implications.* J Struct Biol, 2005. **149**(1): p. 30-7.
101. Singh, P.K., A.K. Mora, and S. Nath, *Ultrafast fluorescence spectroscopy reveals a dominant weakly-emissive population of fibril bound thioflavin-T.* Chem Commun (Camb), 2015. **51**(74): p. 14042-5.
102. Naiki, H., et al., *Fluorometric determination of amyloid fibrils in vitro using the fluorescent dye, thioflavin T1.* Anal Biochem, 1989. **177**(2): p. 244-9.
103. Danis, C., et al., *Nuclear Magnetic Resonance Spectroscopy for the Identification of Multiple Phosphorylations of Intrinsically Disordered Proteins.* J Vis Exp, 2016(118).
104. Botelho, H.M., G. Fritz, and C.M. Gomes, *Analysis of S100 oligomers and amyloids.* Methods Mol Biol, 2012. **849**: p. 373-86.
105. DiNitto, J.M. and J.M. Kenney, *Noise characterization in circular dichroism spectroscopy.* Appl Spectrosc, 2012. **66**(2): p. 180-7.
106. Sarell, C.J., S.R. Wilkinson, and J.H. Viles, *Substoichiometric levels of Cu2+ ions accelerate the kinetics of fiber formation and promote cell toxicity of amyloid-{beta} from Alzheimer disease.* J Biol Chem, 2010. **285**(53): p. 41533-40.
107. Wilder, P.T., et al., *Solution structure of zinc- and calcium-bound rat S100B as determined by nuclear magnetic resonance spectroscopy.* Biochemistry, 2005. **44**(15): p. 5690-702.
108. Yu, W.H. and P.E. Fraser, *S100 beta interaction with tau is promoted by zinc and inhibited by hyperphosphorylation in Alzheimer's disease.* Journal of Neuroscience, 2001. **21**(7): p. 2240-2246.
109. Baudier, J., et al., *Comparison of S100b protein with calmodulin: interactions with melittin and microtubule-associated tau proteins and inhibition of phosphorylation of tau proteins by protein kinase C.* Biochemistry, 1987. **26**(10): p. 2886-93.
110. Baudier, J. and R.D. Cole, *Interactions between the Microtubule-Associated Pi-Proteins and S100b Regulate Pi-Phosphorylation by the Ca-2+ Calmodulin-Dependent Protein Kinase-Ii.* Journal of Biological Chemistry, 1988. **263**(12): p. 5876-5883.
111. Schafer, B.W. and C.W. Heizmann, *The S100 family of EF-hand calcium-binding proteins: functions and pathology.* Trends Biochem Sci, 1996. **21**(4): p. 134-40.

112. Rustandi, R.R., D.M. Baldisseri, and D.J. Weber, *Structure of the negative regulatory domain of p53 bound to S100B(betabeta).* Nat Struct Biol, 2000. **7**(7): p. 570-4.
113. Joseph D Combs, C.U.G.a.C.W., *Surface FTIR Techniques to Analyze the Conformation of Proteins/ Peptides in H2O Environment.* Journal of Physical Chemistry & Biophysics, 2016. **6**(1).
114. Hasegawa, M., et al., *Alzheimer-like changes in microtubule-associated protein Tau induced by sulfated glycosaminoglycans. Inhibition of microtubule binding, stimulation of phosphorylation, and filament assembly depend on the degree of sulfation.* J Biol Chem, 1997. **272**(52): p. 33118-24.
115. Barghorn, S. and E. Mandelkow, *Toward a unified scheme for the aggregation of tau into Alzheimer paired helical filaments.* Biochemistry, 2002. **41**(50): p. 14885-14896.
116. Ramachandran, G. and J.B. Udgaonkar, *Understanding the kinetic roles of the inducer heparin and of rod-like protofibrils during amyloid fibril formation by Tau protein.* J Biol Chem, 2011. **286**(45): p. 38948-59.
117. Bush, A.I., *The metal theory of Alzheimer's disease.* J Alzheimers Dis, 2013. **33 Suppl 1**: p. S277-81.
118. Kim, A.C., S. Lim, and Y.K. Kim, *Metal Ion Effects on Abeta and Tau Aggregation.* Int J Mol Sci, 2018. **19**(1).
119. Huang, Y., et al., *Zinc binding directly regulates tau toxicity independent of tau hyperphosphorylation.* Cell Rep, 2014. **8**(3): p. 831-42.
120. Jiji, A.C., et al., *Zn(2+) Interrupts R4-R3 Association Leading to Accelerated Aggregation of Tau Protein.* Chemistry, 2017. **23**(67): p. 16976-16979.
121. Nishikawa, T., et al., *Identification of S100b protein as copper-binding protein and its suppression of copper-induced cell damage.* J Biol Chem, 1997. **272**(37): p. 23037-41.
122. Donato, R., *Functional roles of S100 proteins, calcium-binding proteins of the EF-hand type.* Biochim Biophys Acta, 1999. **1450**(3): p. 191-231.
123. Wang, J., et al., *A systemic view of Alzheimer disease - insights from amyloid-beta metabolism beyond the brain.* Nature Reviews Neurology, 2017. **13**(10): p. 612-623.